

First detection of orbital motion for HD 106906 b: A wide-separation exoplanet on a Planet Nine-like orbit

MEIJI M. NGUYEN,¹ ROBERT J. DE ROSA,² AND PAUL KALAS^{1,3,4}

¹*Department of Astronomy, University of California, Berkeley, CA 94720, USA*

²*European Southern Observatory, Alonso de Córdova 3107, Vitacura, Santiago, Chile*

³*SETI Institute, Carl Sagan Center, 189 Bernardo Ave., Mountain View, CA 94043, USA*

⁴*Institute of Astrophysics, FORTH, GR-71110 Heraklion, Greece*

(Received August 26, 2020; Revised October 8, 2020; Accepted October 10, 2020)

Submitted to AJ

ABSTRACT

HD 106906 is a 15 Myr old short-period (49 days) spectroscopic binary that hosts a wide-separation (737 au) planetary-mass ($\sim 11 M_{\text{Jup}}$) common proper motion companion, HD 106906 b. Additionally, a circumbinary debris disk is resolved at optical and near-infrared wavelengths that exhibits a significant asymmetry at wide separations that may be driven by gravitational perturbations from the planet. In this study we present the first detection of orbital motion of HD 106906 b using Hubble Space Telescope images spanning a 14 yr period. We achieve high astrometric precision by cross-registering the locations of background stars with the Gaia astrometric catalog, providing the subpixel location of HD 106906 that is either saturated or obscured by coronagraphic optical elements. We measure a statistically significant 31.8 ± 7.0 mas eastward motion of the planet between the two most constraining measurements taken in 2004 and 2017. This motion enables a measurement of the inclination between the orbit of the planet and the inner debris disk of either 36^{+27}_{-14} deg or 44^{+27}_{-14} deg, depending on the true orientation of the orbit of the planet. There is a strong negative correlation between periastron and mutual inclination; orbits with smaller periastra are more misaligned with the disk plane. With a periastron of 510^{+480}_{-320} au, HD 106906 b is likely detached from the planetary region within 100 au radius, showing that a Planet Nine-like architecture can be established very early in the evolution of a planetary system.

1. INTRODUCTION

Massive gas giants have been imaged in young stellar systems that still host large circumstellar disks, both at the gaseous protoplanetary disk phase and the later debris disk phase. These planets undoubtedly play a significant role in the dynamical history of these systems, from carving out gaps in protoplanetary disks (e.g., [Keppler et al. 2018](#)) to causing spiral arms, warps, and other perturbations (e.g., [Mouillet et al. 1997](#); [Oh et al. 2016](#)). Perturbations within resolved images of protoplanetary and debris disks have also been used as indirect evidence of the presence of planets (e.g., [ALMA Partnership et al. 2015](#); [Dong et al. 2015](#); [Esposito et al. 2016](#); [Ren et al. 2020](#)), although alternative mechanisms do exist (e.g., [Lorén-Aguilar & Bate 2015](#); [Okuzumi et al. 2016](#)). External perturbers have also been invoked in several examples, either by bound companions (e.g., [Rodríguez et al. 2018](#); [Wagner et al. 2018](#)) or transient encounters with other stars

within the birth cluster (e.g., [Reche et al. 2009](#)). There are very few examples of systems where both the dynamical effect of an external perturber and its orbit can be determined, typically in cases where the perturber is a stellar companion. Finding additional examples will help further our understanding of their influence on the planet formation process.

HD 106906 is a 15 Myr old spectroscopic binary system ([Rodet et al. 2017](#); [De Rosa & Kalas 2019](#)) comprising two similar mass F-type main-sequence stars located in the Lower Centaurus Crux region of the Scorpius–Centaurus OB association 103 pc from the Sun ([Pecaut & Mamajek 2016](#)). An inner planetary system extending to roughly 50 au radius is inferred from a central dust clearing discovered within a near edge-on debris disk directly imaged at infrared wavelengths ([Kalas et al. 2015](#); [Lagrange et al. 2016](#)). Beyond the detected debris disk lies a directly imaged $11 M_{\text{Jup}}$ planet, HD 106906 b, at a projected separation of 737 au ([Bailey et al. 2014](#)). The dynamical evolution of the system is mysterious because the planet’s projected position is ~ 21 deg away from the disk midplane, while the outer disk itself is highly asymmetric at optical wavelengths ([Kalas et al. 2015](#)). Specifi-

cally, the eastern side of the disk is vertically thin and extended to over 550 au radius, while the western side of the disk is vertically thick and radially extended to 370 au radius. Debris disks can be distorted by stellar flybys (e.g., Larwood & Kalas 2001) and De Rosa & Kalas (2019) discovered that HIP 59716 (F5V) and HIP 59721 (G9V) passed within ~ 0.7 pc of HD 106906 2–3 Myr ago in a near coplanar encounter geometry. However, a closest approach distance < 0.05 pc is needed to modify the orbits of either the planet or disk material (Rodet et al. 2019). Theoretical work shows that the planet could gravitationally distort the disk if it has an eccentric orbit inclined to the disk midplane (Jilková & Zwart 2015; Nesvold et al. 2017; Rodet et al. 2017), inviting comparison to how Planet Nine may be aligning the eccentric orbits of detached Kuiper belt objects (KBOs) like Sedna (Trujillo & Sheppard 2014; Batygin & Brown 2016). However, obtaining an empirical measurement for the orbit of HD 106906 b is essential for validating the theoretical models.

In this paper we present an analysis of archival Hubble Space Telescope (HST) observations of the HD 106906 system where we measured significant orbital motion of the HD 106906 b planet over a 14 yr baseline. The observations and initial data analysis are described in Section 2 and our procedure to measure the Gaia sources within each image is described in Section 3. The model we used to estimate the position of the HD 106906 star within each image is described in Section 4, and its application to HD 106906 to precisely measure relative astrometry between the star and planet is described in Section 5. We present the first constraints on the orbit of the planet in Section 6, and discuss these results in Section 7.

2. OBSERVATIONS AND DATA REDUCTION

Four epochs of HST observations of HD 106906 were used in this study; one epoch each using the Advanced Camera for Surveys (ACS) and the Space Telescope Imaging Spectrograph (STIS), and two epochs using the Wide Field Camera 3 (WFC3). A complete observing log is given in Table 1 where the orientation of the detector on the sky and the instrument plate scale are derived from the `ORIENTAT` value and `CD` matrix within the FITS header.

Three sets of images of HD 106906 were taken with ACS on 2004 December 01 (GO-10330, PI Ford) using the coronagraphic mode of the high-resolution channel (HRC) with the F606W filter. The first two sets of exposures (2×0.1041 s and 2×35 s) were acquisition images taken before the star was placed behind the coronagraph (Figure 1). The star was not saturated in the first image, but heavily saturated in the second. The third exposure set (2×1250 s) was taken after a small offset to position the star behind the coronagraphic mask (Figure 2). An image of a PSF reference star (HR 4570, F5V, $V = 6.3$) was obtained on the following orbit with the

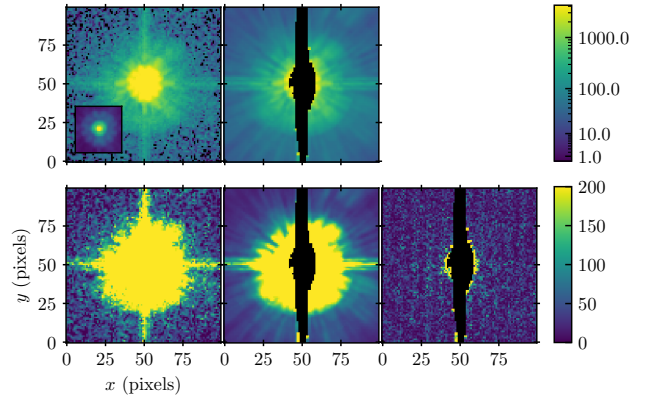


Figure 1. ACS acquisition image of HD 106906 with total exposure times of 0.2082s (left column, image j91711011) and 70s (middle column, image j91711021) taken before the star was moved behind the coronagraphic spot. The inset in the top left panel shows the core of the point spread function (PSF) on a logarithmic scale between the minimum and maximum pixel value. The two images were taken consecutively with no telescope offset. A significant number of saturated pixels are present in the longer exposure (black). The absolute difference between the two images (without translation or scaling) shows no significant residuals beyond the saturated region (bottom right panel).

same instrument configuration except for a slightly reduced exposure time (2×1175 s).

Nine images of HD 106906 were taken with STIS on 2017 February 24 (GO-14670, PI Kalas) using the 50CORON aperture and the “Clear” filter (Figure 3). The star was observed at three different telescope orientations at which three images were obtained; two 350 s exposures near the $1.75''$ width position and one 60 s exposure near the $1.0''$ width position, both on occulter wedge B that was used to block the starlight. The same PSF reference star was observed between the first and second telescope orientations at the same positions on the occulting wedge but with shorter exposure times (100 and 12 s) given the relative brightness of the two stars.

HD 106906 has been observed twice with WFC3; on 2016 January 29 and 2018 June 7 (both under GO-14241, PI Apai; Figure 4). The instrument configuration and observing strategy was similar for both epochs. The observations were taken using the IRSUB256 aperture. At both epochs groups of 10 image sets were taken at each of two orientations, cycling through each filter (f127m, f139m, f153m) with the tenth image set being an additional f127m observation. For the 2016 epoch only 20 image sets were taken, while in 2018 the cycle was repeated three times resulting in 60 image sets, 30 per telescope orientation. Integration times were the same for both epochs, 2×66.4 s, 3×88.4 s, and 3×66.4 s for the three filters, except for the last f127m image set in each cycle, which was 3×66.4 s.

Table 1. Observation Log

Date	Instrument	Filter	Pivot Wavelength (nm)	Frames	Exposure Time (s)	ORIENTAT ^a (deg)	Plate Scale ^b (mas px ⁻¹)	Proposal
2004 Dec 1	ACS	F606W	588.6	1	2×0.1041	80.95	25.00	GO-10330
				1	2×35			
				1	2×1250			
2016 Jan 29	WFC3	F127M	1274	8	2×66.4 ^c	−165.50, 162.50	128.25	GO-14241
		F139M	1384	6	3×88.4			
		F153M	1532	6	3×66.4			
2017 Feb 24	STIS	Clear	5739	9	350.0 ^d	−84.84, −69.94, −54.94	50.77	GO-14670
2018 Jun 7	WFC3	F127M	1274	28	2×66.4 ^c	−58.50, −33.50	128.25	GO-14241
		F139M	1384	21	3×88.4			
		F153M	1532	21	3×66.4			

Notes.

^aThe position angle of the y -axis of the detector on the sky. The position angle of north on the detector is $\theta_N = -\text{ORIENTAT}$.

^bThe plate scale within the FITS header are equivalent in the x and y directions ($p_x = p_y$).

^cLast image at each orientation was 3×66.4 s.

^dLast image at each orientation was 60.0 s.

2.1. Reduction and PSF subtraction

All of the reduced observations were obtained from the Mikulski Archive for Space Telescopes.¹ The data had been processed automatically by the observatory pipeline, including the typical corrections for the dark current, flat field, and, most crucially, the geometric distortion to account for anamorphism in the detector of each instrument. For the ACS and WFC3 frames we used the combined “drizzled” image (“_drz”), whereas for STIS we used the individual reduced frames after the distortion correction had been applied (“_sx2”).

We performed additional postprocessing to subtract the PSF of HD 106906. For the ACS observations we used the PSF of the reference star HR 4570 as a model for the PSF of HD 106906. Although this reference star was also observed with STIS, a background star near HR 4570 was in close proximity to HD 106906 b in several images when the two datasets were aligned, potentially biasing the companion astrometry. We instead used observations of HD 106906 taken at different telescope orientations as a reference PSF. This was also done for the WFC3 observations as no reference star was observed. For each image we optimized the PSF subtraction by shifting and scaling the reference PSF

to minimize the residuals within an annulus surrounding HD 106906. The inner and outer radii were set at 50 and 100 pixels for ACS, 30 and 80 pixels for STIS (excluding regions of the annulus containing the occulting wedge or the bright diffraction spikes of the star), and 15 and 55 pixels for WFC3.

3. POINT-SOURCE ASTROMETRY

HD 106906 is either heavily saturated or occulted by a coronagraphic optical element in all of our images within which HD 106906 b is detected at a high significance. Measuring the precise location of saturated or obscured stars is challenging, typically relying on fitting a model to the saturated PSF (e.g., Vigan et al. 2012) or by measuring the path of the diffraction spikes (e.g., Pueyo et al. 2015). Instead of using these approaches, we used the the Gaia Data Release 2 catalog (Gaia DR2; Gaia Collaboration et al. 2018) sources that were visible within each of our images to determine the pixel position of HD 106906. This technique is independent of assumptions made regarding the behavior of the instrumental PSF at large angular separations when fitting either the wings of a saturated star or the path of the diffraction spikes. Instead, it is limited by the ability to measure the position of unsaturated stars and the precision of the Gaia astrometric catalog.

¹ <https://archive.stsci.edu/hst/>

3.1. Fitting Gaia sources

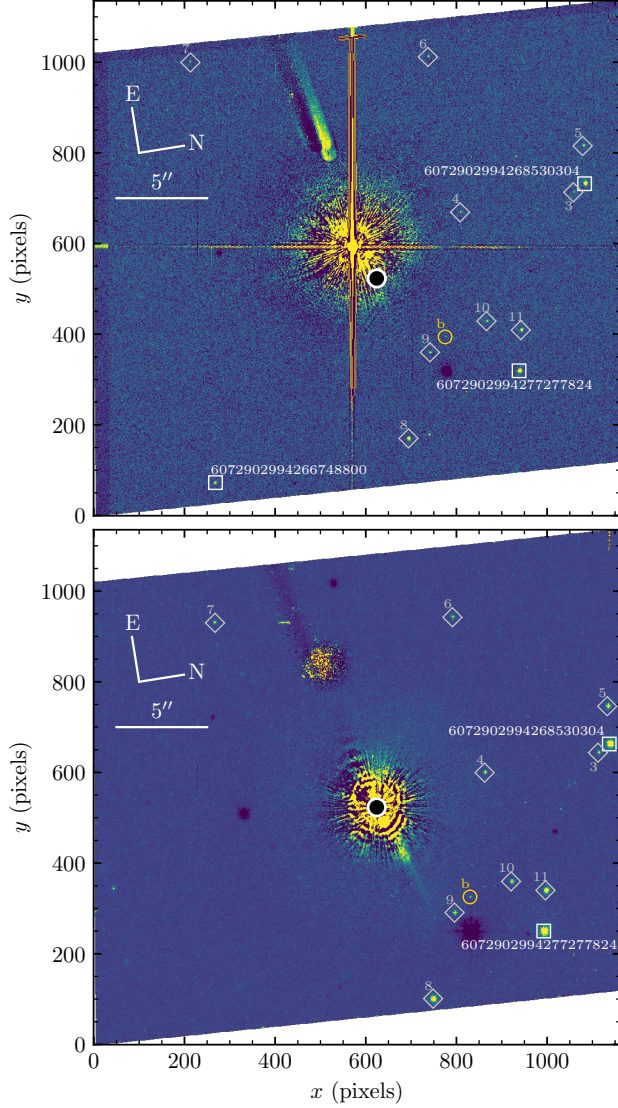


Figure 2. ACS observations of HD 106906 during the acquisition procedure (top, image j91711021) and after the star had been positioned behind the coronagraphic spot (bottom, image j91711031). The position of the coronagraphic spot is indicated (black circle). Background stars within the Gaia DR2 catalog are indicated (white squares), as well as the additional sources used in our alignment procedure that were below the sensitivity limit of the Gaia DR2 catalog (gray diamonds). The location of HD 106906 b is indicated with a yellow circle, but is only detected at a high significance in the coronagraphic image.

We queried the Gaia DR2 catalog for all sources within $120''$ of HD 106906 that had measurements of their position (α , δ), proper motion² (μ_{α^*} , μ_{δ}), and parallax (π), including HD 106906 itself. We applied a small correction to the astrometry of HD 106906 necessary due to the measured off-

² We use the notation $\alpha^* = \alpha \cos \delta$.

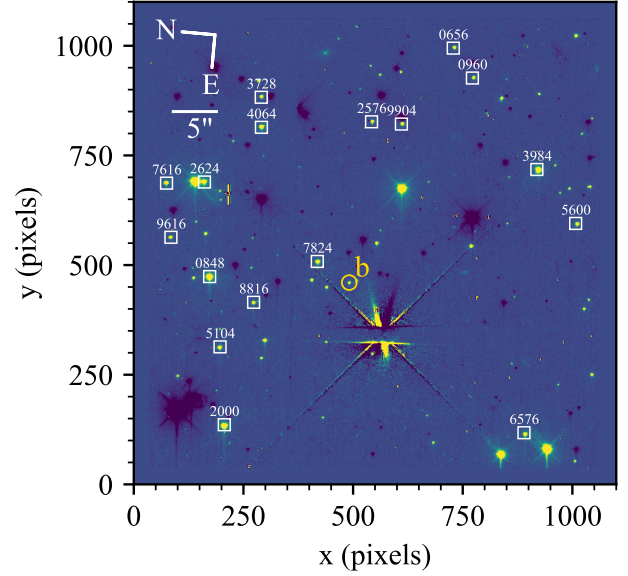


Figure 3. Example STIS (od9t01010) image of HD 106906. Background sources from the Gaia DR2 catalog are indicated (white squares) and uniquely identified using the last four digits of their catalog ID number. The position of HD 106906 b is indicated with a yellow circle.

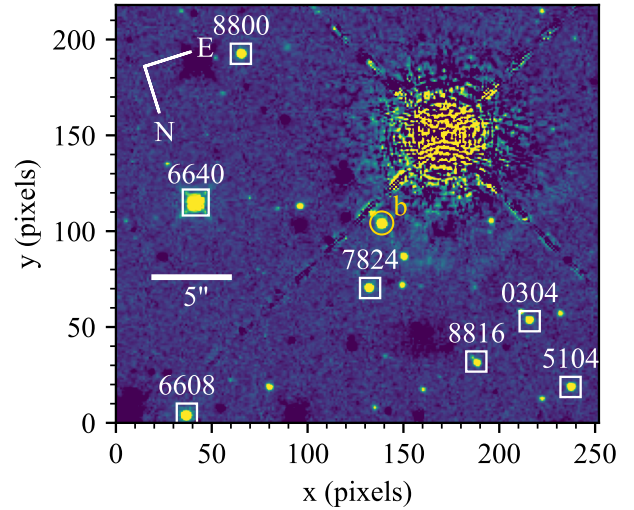


Figure 4. Example 2016 WFC3 (icytb0011) image of HD 106906. Background sources from the Gaia DR2 catalog are indicated (white squares) and uniquely identified using the last four digits of their catalog ID number. The position of HD 106906 b is indicated with a yellow circle.

set between the ICRS and the Gaia DR2 bright star reference frames (Lindgren 2019, 2020), and a small correction to the astrometric uncertainties (Arenou et al. 2018). We excluded Gaia sources that either fell outside of the instrument field of view, were obscured by the coronagraphic optical el-

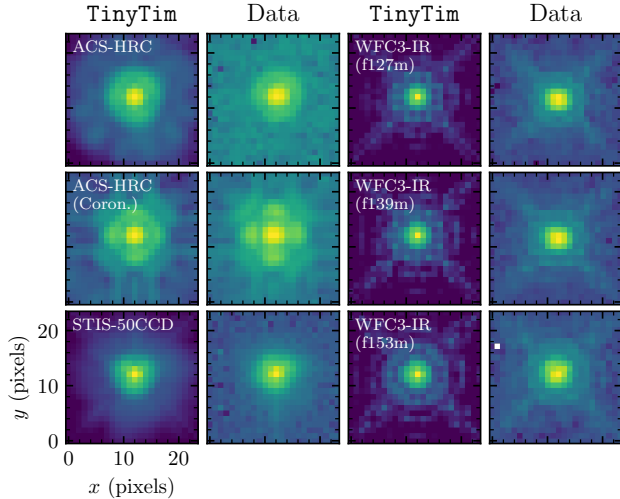


Figure 5. *TinyTim* PSFs (first and third columns) and representative examples extracted from the ACS, STIS, and WFC3 observations (second and fourth columns). The simulated PSFs are noiseless and were created assuming no telescope jitter or defocus.

ements, were contaminated by the diffraction spikes of HD 106906, or were too close to a bad pixel that could not be reliably corrected. Sources with count rates exceeding the linearity limit were also excluded. One source (Gaia DR2 6072902994265468544) was rejected for being a close binary that may have biased the fitting procedure.

After applying these cuts we were left with either two or three useful sources for ACS, between 15 and 21 useful sources for STIS, and between five and seven useful sources for WFC3. For each background star, we extracted an 11-by-11 pixel (approximately $5\lambda/D$ for ACS and $10\lambda/D$ for WFC3 and STIS) data stamp centered on the predicted position of the star and iteratively fit a 2D symmetric Gaussian using a Levenberg–Marquardt least-squares fitting algorithm. A constant offset was not fit as the background was subtracted by the PSF subtraction procedure described previously. We used the same algorithm to measure the coordinates of HD 106906 b within each image, the additional sources not within Gaia used to align the ACS images (see Section 4), and HD 106906 in the first acquisition image taken with ACS where the star is not saturated (see Section 5). The measured pixel positions for each background star in each image, and their propagated tangent plane offsets relative to HD 106906 using the model described in Section 4, are given in Table C1.

3.2. Astrometric uncertainties

We used an injection and recovery framework to assess the uncertainty of the measurements of each background star and HD 106906 b in each image. We used *TinyTim* (Krist et al. 2011) to generate synthetic PSFs for each instrument config-

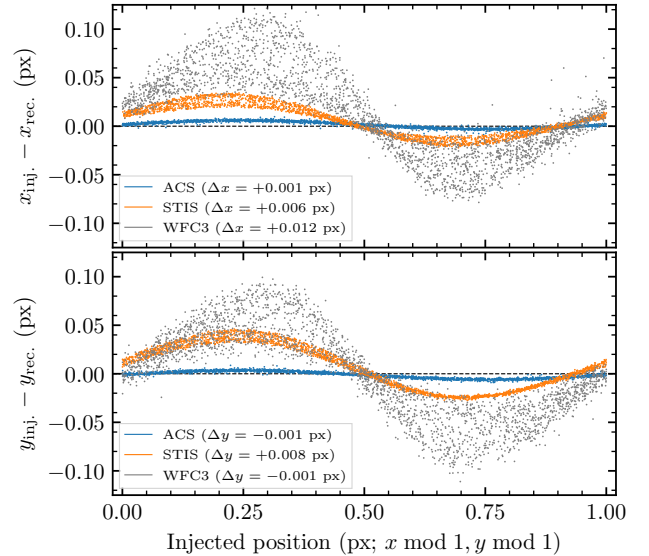


Figure 6. Difference between injected and recovered position in x (top) and y (bottom) as a function of the subpixel position of the injected PSF ($x \bmod 1, y \bmod 1$) for one source within one image of the ACS (blue), STIS (orange), and WFC3 (f153m, gray) datasets. The median offset for each instrument is given in the figure legend.

uration. The objective here was not to perfectly match the PSF of the stars within each image, rather it was to use a reasonably good approximation of the PSF to estimate the precision and accuracy of our Gaussian model. Oversampled PSFs were generated using the spectrum of a K7V star without any focus despace or jitter applied. The resulting PSFs were a reasonable approximation of the observations (Figure 5).

Five thousand injections were performed per source at random locations within an annulus surrounding the source. The width of the annulus was five pixels, with a central radius of 20 pixels for ACS and STIS and 15 pixels for WFC3. The oversampled PSF was shifted by cubic interpolation to the subpixel position of the injection, pixelated to match the sampling of the detector, normalized to have a flux within 10% of the source being tested, and added into the image. The injected PSF was fit using the Gaussian model described previously.

This analysis revealed three sources of error; a random error associated with the signal-to-noise ratio of the injected source and two systematic errors, one associated with the asymmetry of the PSF and the other with the subpixel position of the injected source. The asymmetry of the *TinyTim* PSF was accounted for by adding a small correction to the recovered pixel position, estimated from a Gaussian fit to a 10 times oversampled *TinyTim* PSF generated for each instrument configuration. This offset ($\Delta x = x_{\text{injected}} - x_{\text{recovered}}$) was estimated to be $\Delta x = -0.008$ px and $\Delta y = -0.012$ px for the unocculted ACS PSF, $\Delta x = -0.006$ px and $\Delta y =$

-0.031 px for the occulted ACS PSF, $\Delta x = -0.054$ px and $\Delta y = -0.047$ px for the STIS PSF, and $\Delta x = -0.013$ px and $\Delta y = 0.0$ px for the WFC3/IR PSF. The systematic error associated with the subpixel position of the injected source is demonstrated in Figure 6, after applying the correction due to the asymmetry of the instrument PSF. This effect was not seen at a significant level for the ACS PSF as this instrument is not undersampled. These results were not sensitive to the choice of spectral type used to construct the `TinyTim` PSF. We repeated the experiment for spectral types between K4 and M3, a probable range of spectral types for the distant background objects based on the small subset with effective temperatures reported in the Gaia catalogue, and the values of the derived systematic and random errors were not significantly different.

We accounted for the random error attributed to the signal-to-noise ratio and this remaining systematic error by conservatively adopting the 95th percentile of the absolute value of the difference between the injected and recovered position as our 1σ uncertainty. These uncertainties (σ_x, σ_y) were calculated separately in the x and y directions. Our preliminary fits of the positions of the STIS background stars yielded $\chi^2_\nu \sim 2$, indicating that our uncertainties were slightly underestimated. We combined in quadrature the uncertainties estimated for each source with an additional uncertainty of 0.05 px, leading to $\chi^2_\nu \sim 1$ for these data.

4. ASTROMETRIC MODEL

4.1. Epoch propagation

We propagated the astrometric measurements for each source from the Gaia reference epoch (2015.5) to the epoch of the observation using a Monte Carlo approach. We started by generating 10^5 random draws for each of the five astrometric parameters from a multivariate Gaussian distribution created from the catalog values, uncertainties, and covariances. These random draws were then propagated from 2015.5 to the appropriate epoch using a rigorous coordinate transformation accounting for perspective effects (Butkevich & Lindgren 2014). We adopted a radial velocity of 12.18 ± 0.15 km s $^{-1}$ for HD 106906, while assuming zero radial velocity for the background stars. These stars are likely so distant that their radial velocity has negligible effect on the coordinate propagation. The propagated spherical coordinates of each source (α, δ) were then transformed into tangent plane offsets relative to the propagated position of HD 106906 (α_0, δ_0) following Bedin & Fontanive (2018) as

$$\begin{aligned} \xi_{\text{sky}} &= \frac{\cos \delta \sin(\alpha - \alpha_0)}{\sin \delta_0 \sin \delta + \cos \delta_0 \cos \delta \cos(\alpha - \alpha_0)} \\ &\quad + (\pi P_\alpha - \pi_0 P_{\alpha,0}), \\ \eta_{\text{sky}} &= \frac{\cos \delta_0 \sin \delta - \sin \delta_0 \cos \delta \cos(\alpha - \alpha_0)}{\sin \delta_0 \sin \delta + \cos \delta_0 \cos \delta \cos(\alpha - \alpha_0)} \\ &\quad + (\pi P_\delta - \pi_0 P_{\delta,0}). \end{aligned} \quad (1)$$

The additional terms for both ξ_{sky} and η_{sky} account for the nonzero parallax of both HD 106906 (π_0) and the background stars (π). The parallax factors in the α^* and δ directions ($P_{\alpha,0}, P_{\delta,0}$ for HD 106906 and P_α, P_δ for each source) were calculated from the Euclidean coordinates of the Earth relative to the solar system barycenter ($X_\oplus, Y_\oplus, Z_\oplus$) at the epoch of the observation,

$$\begin{aligned} P_\alpha &= X_\oplus \sin \alpha - Y_\oplus \cos \alpha, \\ P_\delta &= X_\oplus \cos \alpha \sin \delta + Y_\oplus \sin \alpha \sin \delta - Z_\oplus \cos \delta. \end{aligned} \quad (2)$$

This process resulted in 10^5 values for both ξ_{sky} and η_{sky} for each of the background stars at each epoch. We adopted the mean of these draws as the tangent plane offset, and calculated the covariance between them to account for correlated uncertainties within the Gaia catalogue. The tangent plane offset and associated correlation coefficient for each source at each epoch is given in Table C1.

4.2. Converting to detector coordinates

The tangent plane offsets ($\xi_{\text{sky}}, \eta_{\text{sky}}$) were converted to detector coordinates (ξ, η) using the five parameters within our model—the pixel position of HD 106906 (x_0, y_0), and the pixel scale (p_x, p_y) and the position angle of north (θ_N) on the detector—as

$$\begin{bmatrix} \xi \\ \eta \end{bmatrix} = \left(\mathbf{R} \begin{bmatrix} \xi_{\text{sky}} \\ \eta_{\text{sky}} \end{bmatrix} \right) \begin{bmatrix} 1/p_x \\ 1/p_y \end{bmatrix} + \begin{bmatrix} x_0 \\ y_0 \end{bmatrix}, \quad (3)$$

and \mathbf{R} the rotation matrix

$$\mathbf{R} = \begin{bmatrix} -\cos \theta_N & \sin \theta_N \\ \sin \theta_N & \cos \theta_N \end{bmatrix}, \quad (4)$$

to rotate and scale the tangent plane offsets to match the orientation and pixel scale of the detector. The rotation matrix has a nonstandard form to account for the flip in the x -axis when transforming between detector and sky coordinates. We also rotated and scaled the covariance matrix

$$\mathbf{C}_{\xi\eta} = (\mathbf{R}\mathbf{C}_{\xi\eta,\text{sky}}\mathbf{R}^T) \circ \mathbf{S}, \quad (5)$$

where \circ represents an element-wise multiplication. The scaling matrix \mathbf{S} is defined as

$$\mathbf{S} = \begin{bmatrix} 1/p_x^2 & 1/p_x p_y \\ 1/p_x p_y & 1/p_y^2 \end{bmatrix}. \quad (6)$$

4.3. Goodness of fit

The predicted position of a background star (ξ, η) was compared to the measured pixel position (x, y) and adopted uncertainty (σ_x, σ_y) to determine a goodness of fit χ^2 for a given set of model parameters as

$$\chi^2 = \vec{r}^T \mathbf{C}^{-1} \vec{r} \quad (7)$$

where \vec{r} is the residual vector

$$\vec{r} = \begin{bmatrix} \xi - x \\ \eta - y \end{bmatrix}, \quad (8)$$

and \mathbf{C} is the covariance matrix created from the combination of $\mathbf{C}_{\xi\eta}$ and a covariance matrix describing the uncertainty on the measured pixel position of the background star, assumed to be completely uncorrelated

$$\mathbf{C} = \mathbf{C}_{\xi\eta} + \begin{bmatrix} \sigma_x^2 & 0 \\ 0 & \sigma_y^2 \end{bmatrix}. \quad (9)$$

For the STIS measurements, σ_x and σ_y here are the quadratic sum of the measurement uncertainty and the 0.05 px error inflation term described in Section 3.2.

4.4. Specifics for ACS

There are only two Gaia sources within the coronagraphic ACS image, severely limiting our ability to constrain the location of HD 106906. Instead, we used the three Gaia sources within the second acquisition image to determine the star location in this image ($x_0^{\text{acq}}, y_0^{\text{acq}}$) and measured the offset between the acquisition and coronagraphic image using the 11 sources common to both images, yielding the location of the star in the coronagraphic image ($x_0^{\text{coro}}, y_0^{\text{coro}}$). The star position in the acquisition image was fit using the procedure described previously. The offset between the two images was determined by adding three additional parameters to our model; a counterclockwise rotation ($\Delta\theta$) about $(0, 0)$, and a subsequent translation ($\Delta x, \Delta y$) to align the 11 stars common to both images. The goodness of fit for this alignment step was calculated as

$$\chi_{\text{align}}^2 = \vec{r}^T \mathbf{C}^{-1} \vec{r} \quad (10)$$

where

$$\begin{aligned} \vec{r} &= \mathbf{R} \begin{bmatrix} x^{\text{acq}} \\ y^{\text{acq}} \end{bmatrix} + \begin{bmatrix} \Delta x - x^{\text{coro}} \\ \Delta y - y^{\text{coro}} \end{bmatrix}, \\ \mathbf{C} &= \mathbf{R} \mathbf{C}^{\text{acq}} \mathbf{R}^T + \mathbf{C}^{\text{coro}}, \\ \mathbf{R} &= \begin{bmatrix} \cos \Delta\theta & -\sin \Delta\theta \\ \sin \Delta\theta & \cos \Delta\theta \end{bmatrix}. \end{aligned} \quad (11)$$

where $x^{\text{acq}}, y^{\text{acq}}$ and $x^{\text{coro}}, y^{\text{coro}}$ are the pixel position of the background star in the acquisition and coronagraphic image, and \mathbf{C}^{acq} and \mathbf{C}^{coro} are the corresponding covariance matrices. As previously, the measurements were assumed to be uncorrelated and these were used here for completeness. The goodness of fit for a given set of parameters was calculated from the χ^2 of the fit of the Gaia sources in the acquisition image and χ_{align}^2 as

$$\chi^2 = \sum_i^{n_{\text{gaia}}} \chi_{\text{Gaia},i}^2 + \sum_j^{n_{\text{align}}} \chi_{\text{align},j}^2 \quad (12)$$

for the $n_{\text{gaia}} = 3$ Gaia sources in the acquisition image and the $n_{\text{align}} = 11$ sources common to both images. With either the best-fit parameters, or their posterior distributions, the pixel position of HD 106906 in the coronagraphic image can be calculated as

$$\begin{bmatrix} x_0^{\text{coro}} \\ y_0^{\text{coro}} \end{bmatrix} = \begin{bmatrix} \cos \Delta\theta & -\sin \Delta\theta \\ \sin \Delta\theta & \cos \Delta\theta \end{bmatrix} \begin{bmatrix} x_0^{\text{acq}} \\ y_0^{\text{acq}} \end{bmatrix} + \begin{bmatrix} \Delta x \\ \Delta y \end{bmatrix}. \quad (13)$$

5. APPLICATION TO HD 106906

We considered four variants of the model described in Section 4 to determine the position of HD 106906 in each of our images. The first only had the coordinates of HD 106906 (x_0, y_0) as free parameters, using the pixel scale and detector orientation given within the FITS header. The remaining three variants had various combinations of the position angle of north on the detector (θ_N) and the pixel scales along the x - and y -axes of the detector (p_x, p_y) as free parameters to explore the effects of varying the instrument calibration values (model 1: $x_0 y_0$, model 2: $x_0 y_0 \theta_N$, model 3: $x_0 y_0 p_x p_y$, model 4: $x_0 y_0 \theta_N p_x p_y$).

As described in Section 4, only two Gaia sources were present within the deep ACS observation in which the planet was visible due to the small field of view of the instrument (Figure 2, top panel). A third source was visible when the star was offset slightly from the coronagraphic mask for the acquisition images (Figure 2, bottom panel). To include this third star in our analysis we modified the model to simultaneously fit both the position of HD 106906 in the acquisition image and the translation and rotation between the acquisition and coronagraphic images using the two Gaia sources and nine additional sources not within the Gaia catalog that are common to both images.

5.1. Model selection and parameter estimation

We used a maximum likelihood estimation to find the best fit parameters for each of the four variants of our model when applied to each image. The complexity of the model adopted for each epoch was justified by comparing the average value of the Bayesian information criterion (BIC) for each variant of the model (Fig A1). The BIC is a metric that reduces overfitting by penalizing the excessive use of free parameters in a model. For both ACS and WFC3 we found small values of ΔBIC ranging from 0.5 to 6.6 when comparing the more complex models to the two-parameter model, suggesting that the improvement in χ^2 was not sufficient to justify the additional parameters. For the STIS observations we found a large ΔBIC of 1352 when comparing the two-parameter and five-parameter models, indicating that the significant improvement in the goodness of fit justifies the use of the additional parameters for this model. This large improvement in the quality of the fit was due to a systematic error of the position angle of north reported in the FITS header for the

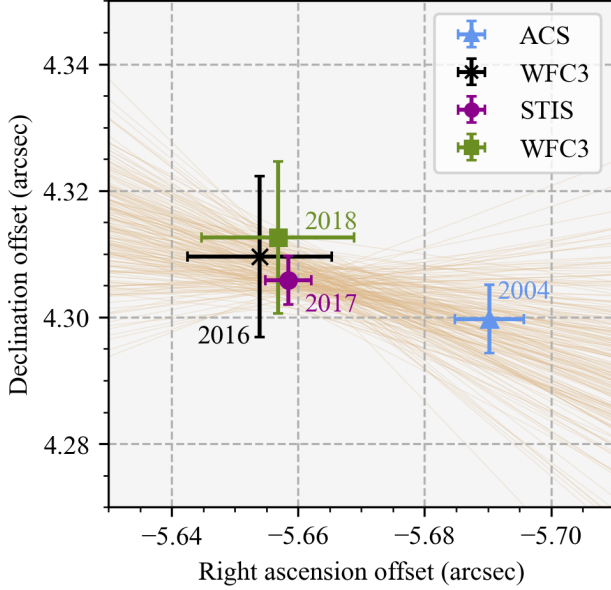


Figure 7. Measured relative astrometry for HD 106906 b using ACS (blue triangle, 2004), STIS (red circle, 2017), and the f153m filter for WFC3 (black cross, 2016; green square, 2018; the f127m and f139m filters were excluded from this figure for visual clarity). Sample orbit fit tracks drawn from the orbital parameter posteriors are overlotted in brown.

STIS observations (incorrect by $0^{\circ}.077$ for these data; see Appendix B).

We used the affine-invariant Markov Chain Monte Carlo ensemble sampler `emcee` (Foreman-Mackey et al. 2013) to sample the posterior distributions of the fitted parameters. We used uniform bounded priors on all free parameters, excluding nonphysical plate scales and limiting the orientation between 0 and 2π . We initialized 50 walkers near the maximum likelihood and advanced them for 1500 steps. The first 500 steps of each chain was discarded as a “burn-in” where the walker positions are still a function of their initial positions. The values and corresponding uncertainties for the fitted parameters for each image of each epoch are given in Tables C2, C3, C4, and C5 of the Appendix.

5.2. Relative astrometry

Relative astrometry between the star and planet was calculated by combining the posterior distributions for the pixel coordinate of the star with the measured pixel position and uncertainty of the planet. This was converted into a sky separation and position angle using the detector plate scales and orientation. The final astrometry for each epoch (and filter for WFC3) was calculated using a weighted mean of the measurements ($x_i \pm \sigma_i$) from each image. For each offset ($\Delta\alpha^*$, $\Delta\delta$) the weighted mean \bar{x} and corresponding uncertainty $\bar{\sigma}$ were calculated as $\bar{x} = \sum_i w_i x_i / \sum_i w_i$ and

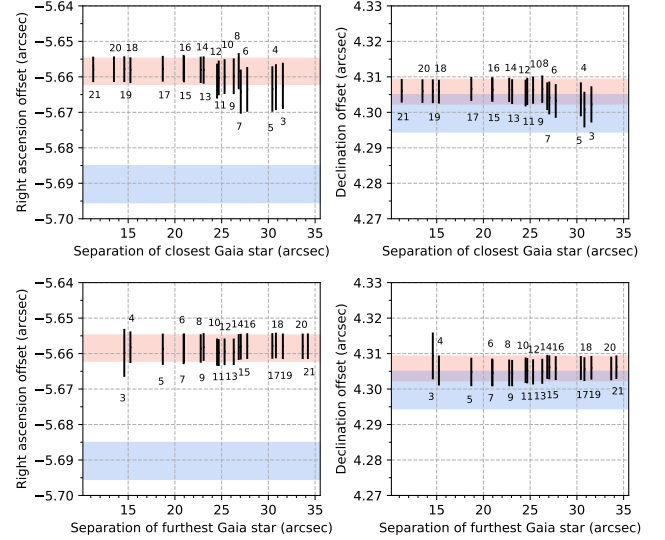


Figure 8. Measured companion astrometry for STIS image od9t03020, where the number of Gaia sources included in the measurement is being iteratively changed by removing either the closest source from HD 106906 (top row) or the furthest source from HD 106906 (bottom row). The numeric labels correspond to the number of Gaia sources included in the data point next to it. The final measured position and 1σ uncertainty for STIS (highlighted in red) and ACS (highlighted in blue) are shown for comparison.

$\bar{\sigma} = \sqrt{\sum_i \sigma_i^2 w_i / \sum_i w_i}$ where $w_i = 1/\sigma_i^2$, under the assumption that the measurements were not independent.

For the ACS observations we used the measurement of the star position in the first acquisition image as a prior for the location in the second under the assumption that there was no telescope motion between these images (Figure 1). We calculated a maximum offset between the two acquisition images of 0.2 px; larger offsets produced significant residuals when the two images were subtracted. We fit the ACS data with and without this prior and find consistent relative astrometry (Table C2), and we adopted the measurements derived from the fit using this prior as our final relative astrometry for the ACS epoch. The final astrometric measurements from each epoch are given in Table 2, and plotted in Figure 7. Our relative astrometric measurements derived from the ACS and WFC3 observations are consistent with previous measurements (Bailey et al. 2014; Zhou et al. 2020), with reduced uncertainties.

5.3. Testing for Gaia systematics

We performed several experiments to gauge the consistency of our astrometry and search for potential biases, specifically testing to determine if the brightness of HD 106906 is biasing the measured Gaia astrometry of the nearby faint sources. The experiments we performed were all variations on using subsets of the available Gaia sources to obtain our final astrometry. In one experiment using the STIS

Table 2. Relative astrometry between HD 106906 and HD 106906 b.

UT Date	MJD	Instrument	$\Delta\alpha^*$ (arcsec)	$\Delta\delta$ (arcsec)	ρ (arcsec)	θ (deg)
2004-12-01	53340.7	ACS	-5.6903 ± 0.0054	4.2997 ± 0.0054	7.1321 ± 0.0054	307.076 ± 0.043
2016-01-29	57416.9	WFC3 (f127m)	-5.6563 ± 0.0196	4.3128 ± 0.0159	7.1130 ± 0.0183	307.325 ± 0.140
2016-01-29	57416.9	WFC3 (f139m)	-5.6581 ± 0.0172	4.3152 ± 0.0145	7.1158 ± 0.0163	307.331 ± 0.125
2016-01-29	57416.9	WFC3 (f153m)	-5.6539 ± 0.0127	4.3096 ± 0.0114	7.1091 ± 0.0123	307.316 ± 0.096
2017-02-24	57808.8	STIS	-5.6585 ± 0.0039	4.3058 ± 0.0037	7.1104 ± 0.0038	307.270 ± 0.030
2018-06-07	58276.1	WFC3 (f127m)	-5.6565 ± 0.0175	4.3086 ± 0.0179	7.1106 ± 0.0176	307.296 ± 0.143
2018-06-07	58276.1	WFC3 (f139m)	-5.6573 ± 0.0157	4.3091 ± 0.0159	7.1115 ± 0.0158	307.296 ± 0.128
2018-06-07	58276.1	WFC3 (f153m)	-5.6568 ± 0.0120	4.3126 ± 0.0120	7.1133 ± 0.0120	307.321 ± 0.097

frames, we limited our analysis to the same three Gaia background sources visible in the ACS observation to see if there was a small sample selection bias affecting the ACS astrometry. We did not uncover any significant bias in limiting our analysis to just these three stars. The measurement remained within 1σ of the STIS astrometry that used all Gaia sources, albeit with an increased uncertainty due to the smaller number of stars used.

In another experiment, we iteratively fit our model for the location of HD 106906, removing the closest star with each iteration until there were only three Gaia stars left. This experiment showed no obvious systematics, with the measured positions remaining around the same value (Figure 8, top row). The uncertainty on each measurement scaled as a function of the decreasing number of sources used. We also tried this same experiment but in the reverse direction, iteratively fitting our model by removing the farthest star from HD 106906 with each iteration. This analysis yielded the same result, with no significant change in the relative astrometry as a function of exclusion radius (Figure 8, bottom row).

We also conducted experiments to test the effect of a poor PSF subtraction on the ACS epoch where the background stars used to cross-register with the Gaia catalogue are within the wings of the PSF of HD 106906, significantly closer than for the STIS epoch. We found that the final relative astrometry was insensitive to errors of the scaling of the reference star of 10%, and of relative shifts between the two stars of 1 pixel, both relative to the best-fit scaling factor and offsets found using the method described in Section 2.1. Errors of this magnitude produced PSF-subtracted images with significant residuals relative to the best-fit solution suggesting that the scaling and offsets were determined to a far greater accuracy.

6. RESULTS

We detected a statistically significant 31.8 ± 7.0 mas eastward motion of the planet relative to the host star between

the 2004 ACS and 2017 STIS epochs (Figure 7). We significantly reduced the uncertainty on the ACS measurement relative to previous attempts (Bailey et al. 2014) and made a more modest improvement over previous WFC3 astrometry (Zhou et al. 2020). The main source of improvement was our usage of Gaia to cross-register background sources in order to indirectly triangulate the position of the primary star. Previous attempts tried to directly fit the PSF of the primary but were typically limited by occultation or saturation effects. The STIS measurement has not previously been published, and is consistent with the WFC3 measurements taken at a similar epoch.

6.1. Orbital motion

We fitted the measured astrometry with a Keplerian orbit using the Orbits for the Impatient (OFTI; Blunt et al. 2017) algorithm that is part of the `orbitize` software package (Blunt et al. 2019). OFTI uses a rejection-sampling algorithm to efficiently generate Bayesian posterior distributions of the orbital parameters. We fitted the following parameters: (1) semi-major axis, (2) eccentricity, (3) inclination, (4) argument of periastron, (5) position angle of the ascending node (where the companion has a positive radial velocity moving away from the observer), (6) epoch of periastron passage in units of the orbital period relative to MJD 58849 (2020), (7) parallax, and (8) system mass. The corresponding Bayesian priors placed on each parameter were (1) log uniform, (2) uniform, (3) sine, (4) uniform, (5) uniform, (6) uniform, (7) Gaussian (9.6774 ± 0.0429 mas), and (8) Gaussian ($2.71 \pm 0.14 M_{\odot}$).

A random selection of orbits drawn from the posterior distributions is plotted in Figure 9, showing the plausible orbital trajectories relative to the resolved debris disk. The median and 1σ credible intervals for the orbital elements derived from the 10^7 OFTI samples are given in Table 3. The marginalized distributions and their covariances for a subset of these parameters are shown in Figure 10. We apply

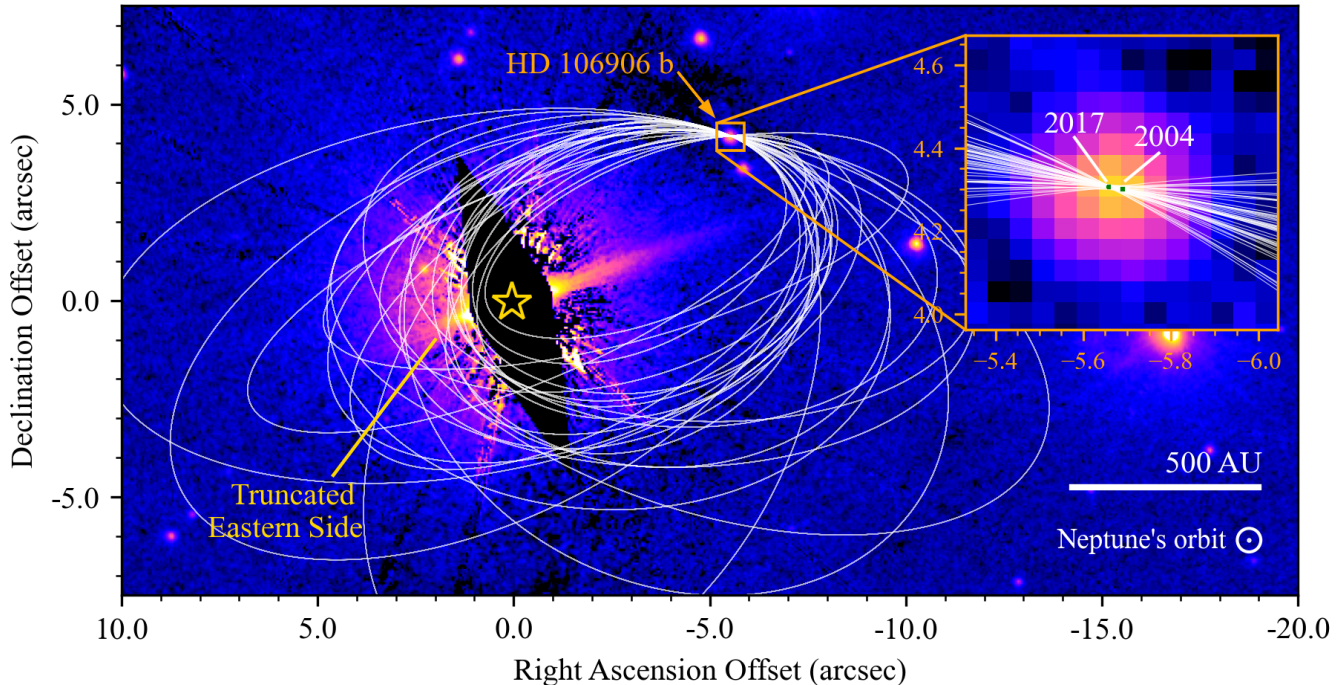


Figure 9. A PSF-subtracted STIS image taken in 2017 of the HD 106906 system showing the nearly edge-on asymmetric debris disk and the planetary-mass companion HD 106906 b (top center; Kalas et al. 2015). The location of the central binary star is denoted by the star symbol. The black region near the star is a region obscured by the occulting wedge of STIS. The cross-like pattern centered on the star is a residual of the imperfect PSF subtraction. Twenty-five orbit tracks sampled randomly from the posterior distributions of the orbital elements are overplotted. The two most constraining astrometric data points from ACS and STIS are inset to highlight our measurements and to indicate the direction of the orbit of the companion. The color scale has been chosen to accentuate the disparity in the visible extension of the eastern side of the disk vs. the western side. The size of Neptune’s orbit is displayed beneath the scale bar for visual comparison.

algebraic transformations to the OFTI samples to additionally derive marginalized distributions for the period using Kepler’s third law, the periastron distance using the relationship $r_{\text{peri}} = a(1 - e)$, and the mutual inclination, i_m , of the plane of the orbit of the companion relative to the debris disk using the formula:

$$\cos i_m = \cos i_{\text{disk}} \cos i_b + \sin i_{\text{disk}} \sin i_b \cos(\Omega_{\text{disk}} - \Omega_b). \quad (14)$$

Because of the ambiguity of Ω_{disk} we calculated i_m for each orbit for the two possible pairs of $(i_{\text{disk}}, \Omega_{\text{disk}})$ that are consistent with the southern part of the disk being behind the star ($i_{\text{disk}} = 85$ deg, $\Omega_{\text{disk}} = 104$ deg and $i_{\text{disk}} = 95$ deg, $\Omega_{\text{disk}} = 284$ deg; Kalas et al. 2015), selecting the smallest value to exclude retrograde orbits.

6.2. Escape velocity

If HD 106906 b is bound to HD 106906, then the three-dimensional velocity of the companion must be lower than the gravitational escape velocity of the system. Radial velocity measurements of HD 106906 b relative to the host star have not yet been made, so we can only calculate a lower limit on the three-dimensional velocity. We estimated the projected linear velocity of the planet by calculat-

ing the instantaneous velocity of the companion at the midpoint of the orbit between the STIS and ACS epochs using the orbital element posterior distributions generated from OFTI. We found a projected velocity of $1.2 \pm 0.2 \text{ km s}^{-1}$, which is $48\% \pm 8\%$ of escape velocity of the system (2.6 km s^{-1}) estimated using a separation of 737 au and a mass of $2.71 M_{\odot}$ (Figure 11). While we cannot use this measurement to definitively conclude that the planet is gravitationally bound to HD 106906, a lower limit greater than the escape velocity would have been definitive evidence that the companion is unbound. Future radial velocity measurements of the planet will be necessary to constrain the three-dimensional relative velocity to demonstrate conclusively that HD 106906 b is gravitationally bound to HD 106906.

6.3. Differential parallax

The difference between the parallax of the star and planet should be negligible if the planet is gravitationally bound, less than $1 \mu\text{as}$ given a 700 au orbit. We used the four astrometric measurements to fit a 10 parameter model for the relative astrometry of HD 106906 b following the procedure outlined by Nguyen et al. (2020). These 10 parameters included the standard five parameters (α , δ , π , μ_{α^*} , and μ_{δ})

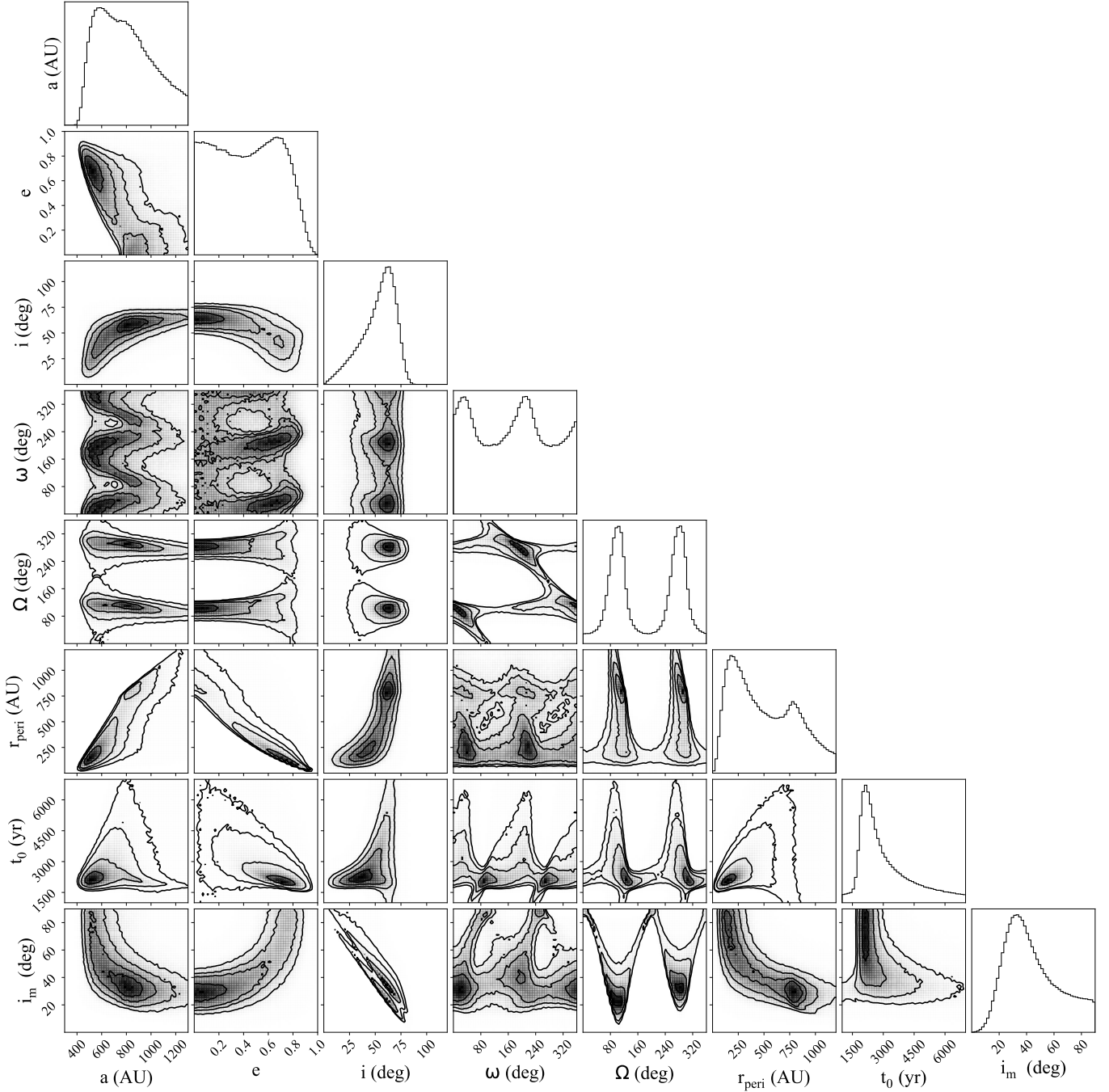
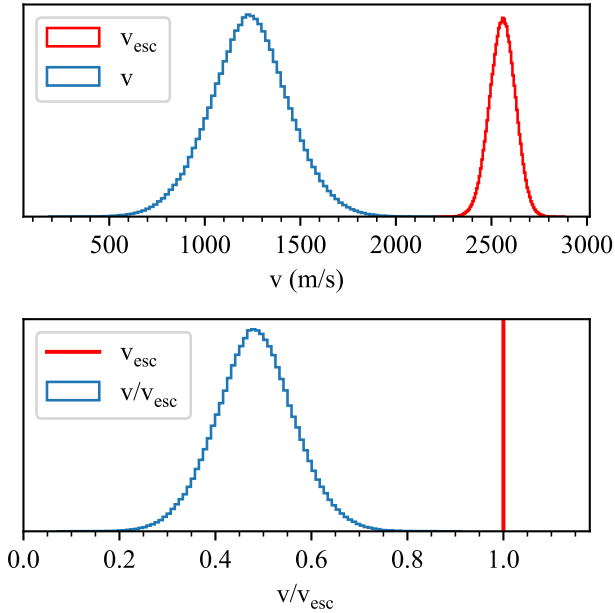
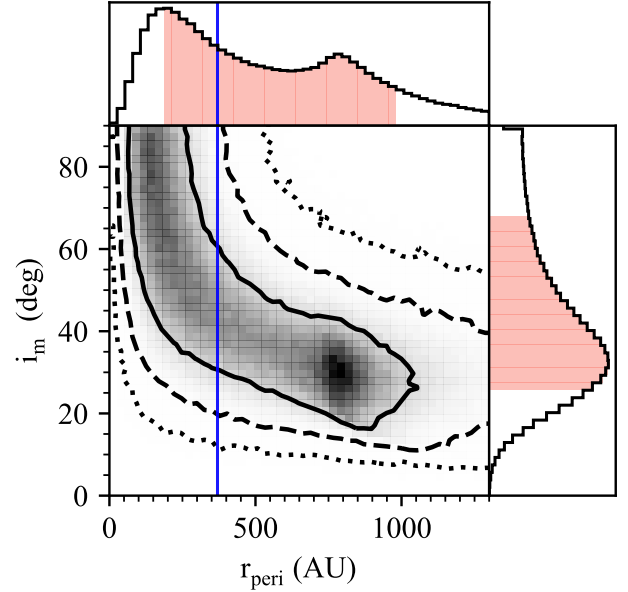


Figure 10. Corner plot showing 2D covariances and 1D marginalized posterior distributions of eight orbital parameters for HD 106906 b derived using the OFTI rejection-sampling algorithm. In order of appearance, the parameters included are (1) semi-major axis, a ; (2) eccentricity, e ; (3) inclination, i ; (4) argument of periastron, ω ; (5) longitude of the ascending node, Ω ; (6) periastron distance, r_{peri} ; (7) epoch of periastron, t_0 ; and (8) mutual inclination, i_m .

Table 3. Orbital elements and derived parameters for HD 106906 b.

Parameter	Unit	Median ($\pm 1\sigma$)
Period (P)	yr	15000^{+17000}_{-6400}
Semi-major axis (a)	au	850^{+560}_{-260}
Periastron distance (r_{peri})	au	510^{+480}_{-320}
Eccentricity (e)	...	$0.44^{+0.28}_{-0.31}$
Inclination (i)	deg	56^{+12}_{-21}
Epoch of periastron ^a (τ)	...	$0.26^{+0.28}_{-0.15}$
Epoch of periastron (t_0)	yr	3200^{+7800}_{-1200}
Parallax (π)	mas	9.677 ± 0.043
System mass (M_{total})	M_{\odot}	2.71 ± 0.14
		Family 1 ^b Family 2 ^c
PA of ascending node (Ω)	deg	99^{+26}_{-28} 279^{+25}_{-29}
Argument of periastron (ω)	deg	356^{+61}_{-86} 176^{+61}_{-87}
Mutual inclination (i_{m})	deg	36^{+27}_{-14} 44^{+27}_{-14}

Notes.^a $\tau = (t_0 - 2020) \bmod P$.^b $10 \leq \Omega < 190$ deg.^c $190 \leq \Omega < 360$ deg or $0 \leq \Omega < 10$ deg.**Figure 11.** Top: projected velocity of HD 106906 b relative to escape velocity of the system. Bottom: projected velocity of HD 106906 b divided by the escape velocity.**Figure 12.** The covariance between the mutual inclination of the inner debris disk and the orbital plane of the planet and the periastron distance of the planet. The corresponding marginalized distributions are also shown. The 1σ credible interval for the marginalized distributions is highlighted in red. The 68th, 95th, and 99.5th percentile contours in the 2D covariance plot are plotted using solid, dashed, and dotted lines, respectively. The sensitivity-limited radius of the observed visible extent of the truncated eastern edge of the HD 106906 debris disk is denoted with a solid blue line.

describing the astrometry of HD 106906 and five parameters ($\Delta\alpha$, $\Delta\delta$, $\Delta\pi$, $\Delta\mu_{\alpha^*}$, and $\Delta\mu_{\delta}$) describing the relative position and motion of HD 106906 b. We used the same MCMC package as previously to sample the posterior distributions of the 10 parameters. We adopted Gaussian priors on the five parameters describing the astrometry of HD 106906 from the Gaia catalog values and uncertainties, and uniform priors for the others. We initialized 256 walkers near the maximum likelihood estimate and advanced them for 2000 steps, discarding the first 800 steps. We measured a differential parallax of $\Delta\pi = 3.66 \pm 5.73$ mas, and a relative proper motion of $\Delta\mu_{\alpha} = 2.78 \pm 0.59$ mas yr⁻¹, $\Delta\mu_{\delta} = 0.77 \pm 0.61$ mas yr⁻¹. Our measurement was not particularly constraining; the differential parallax is consistent with zero but with a large uncertainty. Future astrometric monitoring of the system should greatly improve the uncertainties on this measurement.

7. DISCUSSION

7.1. Is HD 106906 b perturbing the debris disk?

Combining the orbital elements of HD 106906 b presented in Section 6.1 with the orientation and inclination of the debris disk from Kalas et al. (2015) yielded a mutual inclination between the plane of the orbit of the planet and the inner system of either 36^{+27}_{-14} deg or 44^{+27}_{-14} deg (3σ lower limit of

Table 4. Comparison of a selection of orbital elements for HD 106906 and other Solar System bodies.

Param.	Unit	HD 106906	Planet 9	Detached KBOs
		Median ($\pm 1\sigma$)	Range	Range
P	yr	15000^{+17000}_{-6400}	8000–23000	1900–34000
a	au	850^{+560}_{-260}	400–800	160–1000
r_{peri}	au	510^{+480}_{-320}	200–640	40–80
e	...	$0.44^{+0.28}_{-0.31}$	0.2–0.5	0.68–0.95
i_{m}	deg	$36^{+27}_{-14}, 44^{+27}_{-14}$	15–25	4.2–33.5

6 deg or 15 deg), depending on the true orientation of the orbital plane of the planet (Figure 9). We can confidently exclude a coplanar orbit ($3\text{-}\sigma$ lower limit is 13.8 deg or 5.1 deg depending on the value of Ω) as well as a radial trajectory for the companion. The periastron distance and the mutual inclination between the orbital plane and the inner system are highly correlated (Figure 12). Eccentric orbits with periastron distances interior to the sensitivity-limited outer radius of the eastern side of the debris disk (370 au) are highly misaligned with respect to the disk ($i_{\text{m}} \gtrsim 40$ deg), while more circular orbits with larger periastron distances are less misaligned ($i_{\text{m}} \sim 30$ deg).

Previous studies have simulated the dynamical influence of an eccentric and misaligned planetary orbit on the debris disk (Nesvold et al. 2017), assuming a small mutual inclination (~ 10 deg) and a large eccentricity ($e \sim 0.7$), corresponding to a small periastron distance (~ 200 au). These simulations were able to qualitatively reproduce much of the observed morphology of the disk; however a thorough exploration of parameter space for the orbit of the companion is needed in future work. Our results suggest that an eccentricity as large as $e \sim 0.7$ would require a very large mutual inclination of ~ 60 deg. This is larger than the maximum mutual inclination allowed based on the simulation and the lack of an observed vertical extent of the inner debris ring, potentially excluding some of the most eccentric solutions consistent with the astrometry presented in this work. The dynamical effect of a planet on an orbit with a lower eccentricity ($e \sim 0.4$) but a larger mutual inclination ($i_{\text{m}} \sim 30$ deg), also consistent with our astrometric measurements, has not yet been explored.

7.2. A Planet Nine analog?

Table 4 compares our orbit constraints for HD 106906 b against the hypothetical Planet Nine (Batygin et al. 2019) and observations of 15 detached KBOs (Trujillo 2020) demonstrating an approximate commensurability. With age 15 ± 3 Myr, HD 106906 b shows that a Planet Nine-like orbital architecture can be established early, though identifying the

most likely pathway requires future work. One scenario is that the massive planet initially formed in a disk around the eccentric binary star, migrated into an unstable resonance with the stars, pumping the eccentricities and inclinations of the planet, and then the planet’s periastron was raised beyond the central planetary region by passing stars (Rodet et al. 2017; De Rosa & Kalas 2019). If future observations can show that the binary stars, the disk, and HD 106906 b are all moving in a prograde direction, then this pathway would be favored as opposed to an alternate mechanism whereby HD 106906 b was captured from another star or as a free-floating planet. These same pathways are debated for the origin of a hypothetical Planet Nine (Li & Adams 2016). Also compelling is to investigate the theory of how the entire HD 106906 system will evolve in the future. Though there are differences between HD 106906 and the solar system, HD 106906 provides an empirical initial configuration for analytical and numerical experiments to determine how it may resemble the solar system after 4.6 Gyr of evolution.

8. CONCLUSIONS

We have presented the first measurement of the orbital motion of HD 106906 b about its host star. While the orbital period is long ($P \sim 10^4$ yr) a measurement of the trajectory of the planet was sufficient to exclude orbits that are coplanar with the inner debris disk (Kalas et al. 2015; Lagrange et al. 2016)—although this was assumed based on the current position of the planet relative to the inner system—and those that are moving outward in a radial trajectory that might be consistent with a planet in the process of being ejected from the system (e.g., Rodet et al. 2017). The relatively large values for semi-major axis (~ 850 au), eccentricity (~ 0.44) and mutual inclination (~ 40 deg) are comparable to the estimated orbital properties of the hypothetical Planet Nine in our solar system. This suggests that a Planet Nine-like orbital architecture can be established within the first ~ 10 Myr of planet formation and subsequent dynamical evolution. We measured a mutual inclination between HD 106906 b and the resolved debris disk of 36^{+27}_{-14} deg or 44^{+27}_{-14} deg, depending on the true orientation of the planet’s orbit. HD 106906 is one of a small number of systems with an outer massive gas giant (e.g., π Mensae; Damasso et al. 2020; De Rosa et al. 2020; Xuan & Wyatt 2020) or substellar companion (e.g., GQ Lup; Wu et al. 2017) with a significant mutual inclination relative to the inner planet or inferred planetary system. We also measured a strong negative correlation between the periastron distance and the mutual inclination (Figure 12), suggesting that if the planet is indeed responsible for perturbing the disk, it likely has a significant mutual inclination with respect to the plane of the disk.

Previous work simulating the gravitational influence of the planet on the debris disk has shown that an eccentric and

inclined planet external to the disk can reproduce the observed features of the disk (Jílková & Zwart 2015; Nesvold et al. 2017; Rodet et al. 2017). These studies were limited in the range of orbital parameter space they explored due to computational constraints, and they did not overlap with the parameters we estimate from our astrometric measurements. Repeating these simulations with mutual inclinations and eccentricities (or periastron distances) drawn from the locus shown in Figure 12 may help further constrain the range of plausible orbits. It is likely that the most eccentric orbits consistent with the astrometry presented here would result in a significant disruption of the material at the smallest scales (< 100 au) in the inner system, inconsistent with near-infrared observations of the inner dust ring (Kalas et al. 2015; Lagrange et al. 2016). A lower eccentricity, corresponding to a larger periastron distance and smaller mutual inclination, might be sufficient to minimize the impact on the inner dust ring while still perturbing the material seen at wider separations (Kalas et al. 2015).

Additional measurements of the relative astrometry between star and planet would be helpful to confirm the measurement of orbital motion presented here, and to refine the differential parallax measurement attempted in Section 6.3. If such measurements confirmed the results of this study, it is unlikely they would significantly reduce the uncertainties on the orbital parameters unless a significant amount of time had passed. At this point the most useful observation would be a measurement of the radial velocity of the planet; the systemic velocity of the primary has already been measured (De Rosa & Kalas 2019), although to a relatively poor precision of 0.2 km s^{-1} because it is an active, double-lined spectroscopic binary. A significant difference between the two would be conclusive evidence that the planet is not bound to

the star (see Section 6.2), while a small but significant difference can measure the true orientation of the plane of the orbit, leading to a better constraint on the mutual inclination.

ACKNOWLEDGMENTS

We thank Eric Nielsen, Gaspard Duchêne, Lea Hirsch, Thomas Esposito, and Chad Trujillo for discussions relating to this work, as well as the referee for their insightful comments. The authors were supported by NSF AST-1518332, NASA grants NNX15AC89G and NNX15AD95G, as well as HST-GO-14670 through a grant from STScI under NASA contract NAS5-26555. This work benefited from NASA's Nexus for Exoplanet System Science (NExSS) research coordination network sponsored by NASA's Science Mission Directorate. This research made use of the SIMBAD database and the VizieR catalog access tool, both operated at the CDS, Strasbourg, France. This work presents results from the European Space Agency (ESA) space mission Gaia. Gaia data are being processed by the Gaia Data Processing and Analysis Consortium (DPAC). Funding for the DPAC is provided by national institutions, in particular the institutions participating in the Gaia MultiLateral Agreement (MLA). Lastly, this research was based on observations made with the NASA/ESA Hubble Space Telescope, obtained from the data archive at the Space Telescope Science Institute. STScI is operated by the Association of Universities for Research in Astronomy, Inc., under NASA contract NAS 5-26555.

Facilities: HST (ACS, STIS, WFC3).

Software: astropy (Astropy Collaboration et al. 2013), emcee, (Foreman-Mackey et al. 2013), matplotlib (Hunter 2007), orbitize (Blunt et al. 2019), TinyTim (Krist et al. 2011)

REFERENCES

- ALMA Partnership, Brogan, C. L., Pérez, L. M., et al. 2015, *Astrophys. J.*, 808, L3
- Arenou, F., Luri, X., Babusiaux, C., et al. 2018, *A&A*, 616, A17
- Astropy Collaboration, Robitaille, T. P., Tollerud, E. J., et al. 2013, *A&A*, 558, A33, doi: [10.1051/0004-6361/201322068](https://doi.org/10.1051/0004-6361/201322068)
- Bailey, V., Meshkat, T., Reiter, M., et al. 2014, *ApJ*, 780, L4
- Batygin, K., Adams, F. C., Brown, M. E., & Becker, J. C. 2019, *Physics Reports*, 805, 1
- Batygin, K., & Brown, M. E. 2016, *AJ*, 151, 22
- Bedin, L. R., & Fontanive, C. 2018, *MNRAS*, 481, 5339
- Blunt, S., Nielsen, E. L., De Rosa, R. J., et al. 2017, *AJ*, 153, 229
- Blunt, S., Wang, J., Angelo, I., et al. 2019, eprint arXiv:1910.01756
- Butkevich, A. G., & Lindgren, L. 2014, *A&A*, 570, A62
- Damasso, M., Sozzetti, A., Lovis, C., et al. 2020, arXiv, arXiv:2007.06410
- De Rosa, R. J., Dawson, R., & Nielsen, E. L. 2020, *A&A*, 640, A73
- De Rosa, R. J., & Kalas, P. 2019, *AJ*, 157, 125
- Dong, R., Zhu, Z., & Whitney, B. 2015, *Astrophys. J.*, 809, 93
- Esposito, T. M., Fitzgerald, M. P., Graham, J. R., et al. 2016, *AJ*, 152, 85
- Foreman-Mackey, D., Hogg, D. W., Lang, D., & Goodman, J. 2013, *PASP*, 125, 306
- Gaia Collaboration, Brown, A. G. A., Vallenari, A., et al. 2018, *A&A*, 616, A1
- Hunter, J. D. 2007, *Comput. Sci. Eng.*, 9, 90
- Jílková, L., & Zwart, S. P. 2015, *MNRAS*, 451, 804
- Kalas, P. G., Rajan, A., Wang, J. J., et al. 2015, *ApJ*, 814, 32
- Keppler, M., Benisty, M., Müller, A., et al. 2018, *A&A*, 617, A44
- Krist, J. E., Hook, R. N., & Stoehr, F. 2011, in *SPIE Optical Engineering + Applications*, ed. M. A. Kahan (SPIE), 81270J

- Lagrange, A.-M., Langlois, M., Gratton, R., et al. 2016, *A&A*, 586, L8
- Larwood, J. D., & Kalas, P. G. 2001, *MNRAS*, 323, 402, doi: [10.1046/j.1365-8711.2001.04212.x](https://doi.org/10.1046/j.1365-8711.2001.04212.x)
- Li, G., & Adams, F. C. 2016, *Astrophys. J.*, 823, L3
- Lindegren, L. 2019, *A&A*, 633, A1
- . 2020, *A&A*, 637, C5
- Lorén-Aguilar, P., & Bate, M. R. 2015, *MNRAS*, 453, L78
- Mouillet, D., Larwood, J. D., Papaloizou, J. C. B., & Lagrange, A.-M. 1997, *MNRAS*, 292, 896
- Nesvold, E. R., Naoz, S., & Fitzgerald, M. P. 2017, *Astrophys. J.*, 837, L6
- Nguyen, M. M., De Rosa, R. J., Wang, J. J., et al. 2020, *AJ*, 159, 244
- Oh, D., Hashimoto, J., Tamura, M., et al. 2016, *PASJ*, 68, L3
- Okuzumi, S., Momose, M., Sirono, S.-i., Kobayashi, H., & Tanaka, H. 2016, *Astrophys. J.*, 821, 82
- Pecaut, M. J., & Mamajek, E. E. 2016, *MNRAS*, 461, 794
- Pueyo, L., Soummer, R., Hoffmann, J., et al. 2015, *ApJ*, 803, 31
- Reche, R., Beust, H., & Augereau, J. C. 2009, *A&A*, 493, 661, doi: [10.1051/0004-6361:200810419](https://doi.org/10.1051/0004-6361:200810419)
- Ren, B., Dong, R., van Holstein, R. G., et al. 2020, *Astrophys. J.*, 898, L38
- Rodet, L., Beust, H., Bonnefoy, M., et al. 2019, *A&A*, 631, A139, doi: [10.1051/0004-6361/201935728](https://doi.org/10.1051/0004-6361/201935728)
- Rodet, L., Beust, H., Bonnefoy, M., et al. 2017, *A&A*, 602, A12
- Rodriguez, J. E., Loomis, R., Cabrit, S., et al. 2018, *Astrophys. J.*, 859, 150
- Trujillo, C. A. 2020, in *The Trans-Neptunian Solar System* (Elsevier), 79–105
- Trujillo, C. A., & Sheppard, S. S. 2014, *Nature*, 507, 471, doi: [10.1038/nature13156](https://doi.org/10.1038/nature13156)
- Vigan, A., Patience, J., Marois, C., et al. 2012, *A&A*, 544, A9
- Wagner, K., Dong, R., Sheehan, P., et al. 2018, *Astrophys. J.*, 854, 130
- Wu, Y.-L., Sheehan, P. D., Males, J. R., et al. 2017, *ApJ*, 836, 223, doi: [10.3847/1538-4357/aa5b96](https://doi.org/10.3847/1538-4357/aa5b96)
- Xuan, J. W., & Wyatt, M. C. 2020, *MNRAS*, 497, 2096
- Zhou, Y., Apai, D., Bedin, L. R., et al. 2020, *AJ*, 159, 140

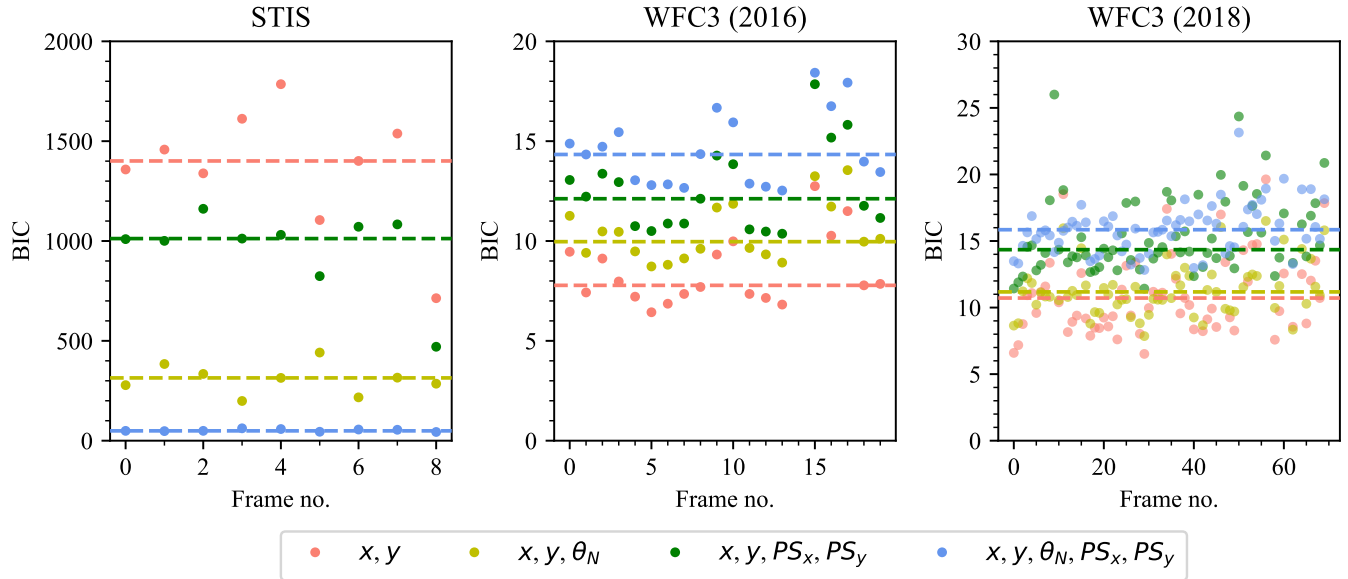


Figure A1. BIC calculated for each frame of the STIS and WFC3 epochs using the four different permutations of free parameters we tested for our astrometric model.

APPENDIX

A. MODEL COMPARISON

We compared the four variants of our astrometric model by computing the BIC for each model applied to each image from the four epochs (Figure A1). A more complex model was only selected if the average ΔBIC exceeded 10, as was the case for the STIS epoch.

B. VERIFYING HST'S ASTROMETRIC CALIBRATION

The significant offset between the derived position angle of north and the value derived from the FITS header for the STIS images prompted us to investigate the astrometric calibration of the three instrument configurations used in this study. We queried the archive for observations using a similar same instrument configuration. We cross-matched with the Gaia DR2 catalog to identify observations with three or more Gaia sources within the instrument field of view. In total, we obtained 1120 ASC/HRC, 1200 STIS/50CCD or STIS/50CORON, and 1113 WFC3/IR reduced datasets from the archive. We used the “_sx2”, “_x2d”, or “_drz” files that are the end product of the observatory pipeline. We used the same algorithm we used for HD 106906 to measure the detector plate scale and orientation. We applied several automatic checks to reject sources that were either saturated or obscured by coronagraphic optical elements, as well as a manual screening of each observation to reject other problematic sources such as close binaries. We also rejected observations with an extremely high number of sources to avoid issues with source blending/confusion and potential Gaia systematic uncertainties in crowded regions.

Our analysis of the ACS/HRC data yielded detector orientation and plate scales that were consistent to within a few hundredths of a degree for the orientation and 0.1% for the plate scales with the calibration values reported in the FITS headers (Figure B1, left column). The WFC3 data also had consistent orientation measurements (Figure B1, right column), but with a 0.02% smaller plate scale in both the x and y directions (~ 128.23 versus 128.25 mas px $^{-1}$). This slight systematic offset of the plate scale is well within the uncertainties of our astrometric measurement of HD 106906 b. For the STIS data we measured a plate scale slightly lower (0.05%) than the nominal value (~ 50.75 versus 50.77 mas px $^{-1}$), and a significant offset between our measurement of the detector orientation and the FITS header values (Figure B1, middle column). This offset is time-dependent, growing steadily at a rate of 0.004 deg yr $^{-1}$. This offset is also seen in observations of the globular cluster NGC 5139, a field that has been regularly observed with almost the same instrument configuration by the STIS instrument team to monitor detector performance. At the time of the HD 106906 observations in early 2017 this offset was approximately $0^\circ.075$, consistent with the average difference between our measured orientation of the STIS images and the FITS header values ($0^\circ.077 \pm 0^\circ.002$). We note that this analysis was only performed with data obtained using the STIS 50CCD and 50CORON apertures; the other apertures were not tested and it cannot be assumed that the results presented here are valid for these other modes.

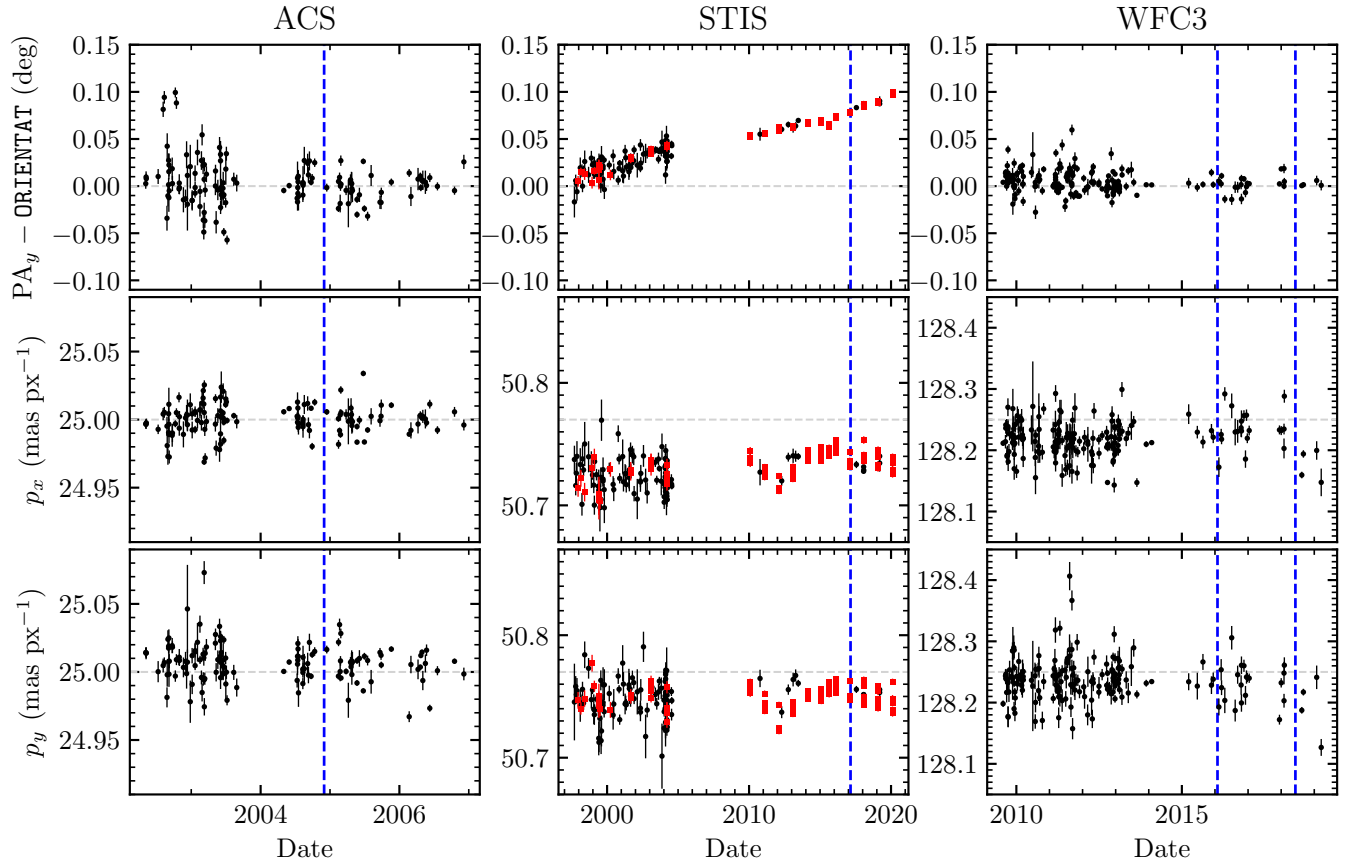


Figure B1. Astrometric calibration of ACS HRC (left), STIS 50CCD/50CORON (middle), and WFC3 IR (right) measured using archival observations with at least 10 Gaia DR2 sources within the field of view as a function of date. Measurements derived from STIS observations of the globular cluster NGC 5139 are highlighted (red points). The top row shows the difference between the derived position angle of the detector y -axis and the ORIENTAT FITS header keyword, while the middle and bottom panels show the plate scales in the x and y directions. The nominal calibration values from the FITS header are denoted by the gray dashed lines. The date of HD 106906 observations are indicated by the vertical dashed blue line.

C. TABLES

Here we tabulate the measured pixel position, tangent plane offset, and associated correlation coefficient for each Gaia catalogue background star for every image in all observing epochs (Table C1). We also present the best fit parameters for the primary star center along with any relevant additional free parameters (e.g. the platescale, position angle of north) for each image in the ACS epoch in Table C2, the STIS epoch in Table C3, the 2016 WFC3 epoch in Table C4, and the 2018 WFC3 epoch in Table C5.

Table C1. Pixel positions and tangent plane offsets for the sources used in this study.

Instrument	Date	Filter	Image	Gaia DR2 Source (607290-)	x (px)	y (px)	ξ (mas)	η (mas)	$\rho_{\xi,\eta}$
ACS	2004-12-01	f606w	j91711021	2994277277824	938.209 ± 0.011	319.208 ± 0.011	-8192.4 ± 6.9	8005.5 ± 7.4	0.350
				2994268530304	1082.825 ± 0.015	731.929 ± 0.013	1433.7 ± 15.1	13213.5 ± 26.9	0.052
				2994266748800	268.371 ± 0.041	72.535 ± 0.042	-11616.7 ± 20.3	-9485.3 ± 13.0	0.203
				(acs-3)	1057.856 ± 0.194	713.013 ± 0.196
				(acs-4)	808.014 ± 0.162	668.929 ± 0.174
				(acs-5)	1078.365 ± 0.060	815.178 ± 0.065
				(acs-6)	737.060 ± 0.196	1011.664 ± 0.198
				(acs-7)	213.164 ± 0.266	999.423 ± 0.265
				(acs-8)	694.153 ± 0.022	170.198 ± 0.022
				(acs-9)	741.553 ± 0.088	359.954 ± 0.095
				(acs-10)	866.120 ± 0.096	428.752 ± 0.106
			(acs-11)	942.057 ± 0.031	409.038 ± 0.033	
			j91711031	2994277277824	992.567 ± 0.006	250.092 ± 0.006	-8192.4 ± 6.9	8005.5 ± 7.4	0.350
				2994268530304	1137.154 ± 0.007	662.783 ± 0.007	1433.7 ± 15.1	13213.5 ± 26.9	0.052
				(acs-3)	1112.256 ± 0.057	643.587 ± 0.068
				(acs-4)	862.152 ± 0.036	599.569 ± 0.036
				(acs-5)	1132.692 ± 0.013	746.046 ± 0.013
				(acs-6)	791.168 ± 0.033	942.434 ± 0.032
				(acs-7)	267.456 ± 0.046	930.048 ± 0.046
				(acs-8)	748.525 ± 0.009	101.038 ± 0.009
				(acs-9)	795.767 ± 0.028	290.816 ± 0.028
				(acs-10)	920.516 ± 0.022	359.599 ± 0.021
(acs-11)	996.384 ± 0.009	339.932 ± 0.009				
STIS	2017-02-24	Clear	od9t01010	2994277277824	419.763 ± 0.058	507.324 ± 0.064	7740.8 ± 1.1	8152.3 ± 1.3	-0.280
				2994277298816	274.109 ± 0.058	414.460 ± 0.065	2369.5 ± 3.3	15076.9 ± 2.1	0.055
				2994265535104	197.442 ± 0.058	312.892 ± 0.064	-3115.6 ± 1.3	18480.8 ± 1.1	-0.259
				2994265496576	890.717 ± 0.058	116.040 ± 0.064	-9858.2 ± 1.3	-17455.6 ± 0.9	-0.163
				3097344752000	206.888 ± 0.058	135.287 ± 0.064	-12055.9 ± 0.4	17180.0 ± 0.4	-0.153
				3196128030848	173.869 ± 0.058	473.199 ± 0.064	4876.9 ± 0.4	20412.8 ± 0.4	-0.158
				3200425179904	611.928 ± 0.058	820.510 ± 0.064	24467.2 ± 1.8	-114.8 ± 1.1	-0.025
				3200426952576	543.808 ± 0.059	825.762 ± 0.065	24416.6 ± 3.2	3347.2 ± 1.8	0.035
				2994266745600	1009.243 ± 0.058	593.332 ± 0.064	14816.1 ± 1.5	-21241.3 ± 1.1	-0.079
				3200426959616	85.678 ± 0.059	562.981 ± 0.065	9012.2 ± 2.7	25287.3 ± 1.9	0.018
				2989964233984	920.849 ± 0.058	716.568 ± 0.064	20640.4 ± 0.4	-16203.9 ± 0.4	-0.153
				3200423962624	162.321 ± 0.058	688.954 ± 0.064	15733.9 ± 1.7	21995.9 ± 0.6	0.107
				3196122664064	292.439 ± 0.058	813.502 ± 0.064	22626.0 ± 0.7	15993.8 ± 0.6	-0.140
				3200423967616	75.862 ± 0.058	686.503 ± 0.064	15206.3 ± 1.0	26352.4 ± 0.8	-0.133
				3200426953728	292.169 ± 0.058	882.159 ± 0.064	26094.8 ± 2.5	16320.3 ± 1.6	-0.022

Table C1 continued

Table C1 (continued)

Instrument	Date	Filter	Image	<i>Gaia</i> DR2 Source (607290-)	x (px)	y (px)	ξ (mas)	η (mas)	$\rho_{\xi,\eta}$
				2994268520960	774.142 ± 0.058	925.229 ± 0.064	30516.8 ± 3.3	-7824.2 ± 1.9	0.083
				3200426950656	730.386 ± 0.058	993.798 ± 0.064	33774.9 ± 3.5	-5300.0 ± 2.1	-0.217
			od9t01020	2994277277824	409.900 ± 0.058	507.380 ± 0.064	7740.8 ± 1.1	8152.3 ± 1.3	-0.280
				2994277298816	264.210 ± 0.058	414.479 ± 0.064	2369.5 ± 3.3	15076.9 ± 2.1	0.052
				2994265535104	187.542 ± 0.058	312.883 ± 0.064	-3115.6 ± 1.3	18480.8 ± 1.1	-0.258
				2994265496576	880.912 ± 0.058	116.021 ± 0.064	-9858.2 ± 1.3	-17455.6 ± 0.9	-0.161
				3097344752000	197.015 ± 0.058	135.232 ± 0.064	-12055.9 ± 0.4	17180.0 ± 0.4	-0.155
				3196128030848	163.951 ± 0.058	473.219 ± 0.064	4876.9 ± 0.4	20412.8 ± 0.4	-0.157
				3200425179904	602.084 ± 0.058	820.605 ± 0.064	24467.2 ± 1.7	-114.8 ± 1.1	-0.024
				3200426952576	533.951 ± 0.058	825.855 ± 0.065	24416.6 ± 3.2	3347.2 ± 1.8	0.037
				2994266745600	999.489 ± 0.058	593.399 ± 0.064	14816.1 ± 1.5	-21241.3 ± 1.1	-0.080
				3200426959616	75.763 ± 0.060	562.998 ± 0.066	9012.2 ± 2.7	25287.3 ± 1.9	0.017
				2989964233984	911.048 ± 0.058	716.650 ± 0.064	20640.4 ± 0.4	-16203.9 ± 0.4	-0.151
				3200423962624	152.422 ± 0.058	689.018 ± 0.064	15733.9 ± 1.7	21995.9 ± 0.6	0.108
				3196122664064	282.578 ± 0.058	813.593 ± 0.064	22626.0 ± 0.7	15993.8 ± 0.6	-0.142
				3200423967616	65.967 ± 0.058	686.580 ± 0.064	15206.3 ± 1.0	26352.4 ± 0.8	-0.134
				3200426953728	282.350 ± 0.058	882.274 ± 0.064	26094.7 ± 2.5	16320.3 ± 1.6	-0.022
				2994268520960	764.321 ± 0.058	925.322 ± 0.064	30516.8 ± 3.3	-7824.2 ± 1.9	0.085
				3200426950656	720.534 ± 0.058	993.900 ± 0.064	33774.9 ± 3.5	-5300.0 ± 2.1	-0.219
			od9t01030	2994277277824	84.621 ± 0.059	509.015 ± 0.065	7740.8 ± 1.1	8152.3 ± 1.3	-0.281
				2994276656640	275.670 ± 0.058	676.128 ± 0.064	17072.3 ± 0.3	-728.4 ± 0.4	-0.185
				2994265496576	555.485 ± 0.059	117.642 ± 0.065	-9858.2 ± 1.3	-17455.6 ± 0.9	-0.164
				2925557175040	605.063 ± 0.058	83.982 ± 0.064	-11336.8 ± 0.3	-20120.4 ± 0.4	-0.189
				3200425179904	276.887 ± 0.059	822.333 ± 0.065	24467.2 ± 1.7	-114.8 ± 1.1	-0.023
				3200426952576	208.831 ± 0.060	827.598 ± 0.066	24416.6 ± 3.2	3347.2 ± 1.8	0.035
				2994266745600	674.328 ± 0.058	595.020 ± 0.064	14816.1 ± 1.5	-21241.3 ± 1.1	-0.079
				2989964233984	585.858 ± 0.058	718.308 ± 0.064	20640.4 ± 0.4	-16203.9 ± 0.4	-0.152
				2925546009088	752.048 ± 0.058	142.723 ± 0.064	-7686.7 ± 0.6	-27266.5 ± 0.5	-0.159
				2994268520960	439.031 ± 0.060	927.050 ± 0.067	30516.8 ± 3.3	-7824.2 ± 1.9	0.084
				2925546004992	901.938 ± 0.062	242.112 ± 0.067	-1959.8 ± 5.2	-34368.3 ± 2.0	-0.018
				3200426950656	395.320 ± 0.060	995.693 ± 0.066	33774.9 ± 3.5	-5300.0 ± 2.1	-0.216
				2994265478400	724.620 ± 0.058	948.332 ± 0.064	32910.6 ± 0.7	-22151.0 ± 0.6	-0.143
				2925545995648	999.166 ± 0.059	94.625 ± 0.065	-8971.1 ± 1.1	-39968.9 ± 0.8	-0.133
				2989964110208	774.353 ± 0.058	931.634 ± 0.064	32293.4 ± 0.3	-24735.7 ± 0.4	-0.163
				2994268518784	743.652 ± 0.060	979.499 ± 0.066	34572.5 ± 3.1	-22967.5 ± 2.1	0.059
			od9t03010	2994277277824	467.916 ± 0.058	539.235 ± 0.064	7740.8 ± 1.1	8152.4 ± 1.3	-0.281
				2994268530304	306.095 ± 0.058	398.174 ± 0.064	-1813.0 ± 2.3	13396.3 ± 5.5	0.079
				2994277298816	303.391 ± 0.058	486.952 ± 0.064	2369.5 ± 3.3	15076.9 ± 2.1	0.053
				2994266748800	813.782 ± 0.058	483.950 ± 0.064	11149.4 ± 3.1	-9303.2 ± 1.9	0.050
				2994265535104	203.115 ± 0.058	408.517 ± 0.064	-3115.6 ± 1.3	18480.8 ± 1.1	-0.260
				3097344752000	166.593 ± 0.058	234.421 ± 0.064	-12055.9 ± 0.4	17180.0 ± 0.4	-0.154
				3196128030848	221.638 ± 0.058	569.481 ± 0.064	4876.9 ± 0.4	20412.8 ± 0.4	-0.160
				3097347747712	170.682 ± 0.058	126.993 ± 0.065	-17102.0 ± 1.8	15108.8 ± 1.1	-0.042
				3097344750592	184.705 ± 0.058	91.636 ± 0.064	-18546.0 ± 0.4	13823.7 ± 0.4	-0.143
				3200425179904	734.211 ± 0.058	792.398 ± 0.064	24467.1 ± 1.8	-114.8 ± 1.1	-0.021
				3200426952576	669.829 ± 0.058	815.033 ± 0.064	24416.6 ± 3.2	3347.2 ± 1.8	0.035

Table C1 continued

Table C1 (continued)

Instrument	Date	Filter	Image	<i>Gaia</i> DR2 Source (607290-)	x (px)	y (px)	ξ (mas)	η (mas)	$\rho_{\xi,\eta}$
				3200423956608	481.195 ± 0.058	831.642 ± 0.064	21909.7 ± 0.6	12623.6 ± 0.5	-0.061
				3200426959616	159.493 ± 0.058	678.900 ± 0.064	9012.2 ± 2.7	25287.3 ± 1.9	0.017
				2989964233984	1006.071 ± 0.058	612.706 ± 0.064	20640.3 ± 0.4	-16203.9 ± 0.4	-0.152
				3200423962624	265.915 ± 0.058	780.968 ± 0.064	15733.8 ± 1.7	21995.9 ± 0.6	0.106
				3196122664064	423.709 ± 0.058	867.807 ± 0.064	22626.0 ± 0.7	15993.8 ± 0.6	-0.142
				3200423967616	181.773 ± 0.058	800.811 ± 0.064	15206.3 ± 1.0	26352.4 ± 0.8	-0.134
				3200426953728	441.114 ± 0.058	934.175 ± 0.065	26094.7 ± 2.5	16320.3 ± 1.6	-0.024
				2994268520960	918.017 ± 0.058	852.012 ± 0.065	30516.8 ± 3.3	-7824.2 ± 1.9	0.085
				3200425185664	107.350 ± 0.058	820.354 ± 0.064	14834.4 ± 2.5	30234.9 ± 1.3	-0.062
				3200426950656	893.470 ± 0.058	929.533 ± 0.064	33774.9 ± 3.5	-5300.0 ± 2.1	-0.217
			od9t03020	2994277277824	458.007 ± 0.058	539.307 ± 0.064	7740.8 ± 1.1	8152.4 ± 1.3	-0.282
				2994268530304	296.129 ± 0.058	398.188 ± 0.064	-1813.0 ± 2.3	13396.3 ± 5.5	0.079
				2994277298816	293.462 ± 0.058	487.009 ± 0.065	2369.4 ± 3.3	15077.0 ± 2.1	0.052
				2994266748800	803.929 ± 0.058	484.023 ± 0.065	11149.4 ± 3.1	-9303.2 ± 1.9	0.050
				2994265535104	193.168 ± 0.058	408.528 ± 0.064	-3115.6 ± 1.3	18480.8 ± 1.1	-0.259
				3097344752000	156.624 ± 0.058	234.411 ± 0.064	-12055.9 ± 0.4	17180.0 ± 0.4	-0.156
				3196128030848	211.685 ± 0.058	569.550 ± 0.064	4876.9 ± 0.4	20412.8 ± 0.4	-0.158
				3097347747712	160.706 ± 0.058	126.981 ± 0.065	-17102.0 ± 1.8	15108.7 ± 1.1	-0.042
				3097344750592	174.733 ± 0.058	91.618 ± 0.064	-18546.0 ± 0.4	13823.7 ± 0.4	-0.141
				3200425179904	724.385 ± 0.058	792.512 ± 0.064	24467.1 ± 1.8	-114.8 ± 1.1	-0.025
				3200426952576	659.967 ± 0.058	815.123 ± 0.064	24416.6 ± 3.2	3347.2 ± 1.8	0.036
				3200423956608	471.315 ± 0.058	831.742 ± 0.064	21909.7 ± 0.6	12623.6 ± 0.5	-0.061
				3200426959616	149.540 ± 0.058	678.963 ± 0.064	9012.2 ± 2.7	25287.3 ± 1.9	0.017
				2989964233984	996.247 ± 0.058	612.790 ± 0.064	20640.3 ± 0.4	-16203.9 ± 0.4	-0.153
				3200423962624	255.969 ± 0.058	781.048 ± 0.064	15733.8 ± 1.7	21995.9 ± 0.6	0.106
				3196122664064	413.826 ± 0.058	867.907 ± 0.064	22626.0 ± 0.7	15993.8 ± 0.6	-0.143
				3200423967616	171.838 ± 0.058	800.891 ± 0.064	15206.3 ± 1.0	26352.4 ± 0.8	-0.133
				3200426953728	431.231 ± 0.058	934.319 ± 0.064	26094.7 ± 2.5	16320.3 ± 1.6	-0.023
				2994268520960	908.208 ± 0.058	852.110 ± 0.064	30516.8 ± 3.3	-7824.2 ± 1.9	0.085
				3200425185664	97.388 ± 0.058	820.447 ± 0.064	14834.4 ± 2.5	30234.9 ± 1.3	-0.063
				3200426950656	883.658 ± 0.058	929.644 ± 0.064	33774.9 ± 3.5	-5300.0 ± 2.1	-0.219
			od9t03030	2994277277824	132.812 ± 0.059	541.060 ± 0.065	7740.8 ± 1.1	8152.4 ± 1.3	-0.282
				2994266748800	478.886 ± 0.060	485.669 ± 0.066	11149.4 ± 3.1	-9303.2 ± 1.9	0.052
				3200425179904	399.240 ± 0.059	794.331 ± 0.065	24467.1 ± 1.7	-114.8 ± 1.1	-0.023
				3200423956608	146.155 ± 0.058	833.606 ± 0.064	21909.7 ± 0.6	12623.6 ± 0.5	-0.060
				2994277277312	724.112 ± 0.061	206.423 ± 0.067	2113.1 ± 6.3	-25851.3 ± 7.3	-0.324
				2994266745600	724.766 ± 0.059	472.700 ± 0.064	14816.1 ± 1.5	-21241.3 ± 1.1	-0.077
				2989964233984	671.117 ± 0.058	614.491 ± 0.064	20640.3 ± 0.4	-16203.9 ± 0.4	-0.152
				3196122664064	88.605 ± 0.058	869.735 ± 0.064	22626.0 ± 0.7	15993.8 ± 0.6	-0.142
				3200426953728	106.103 ± 0.060	936.106 ± 0.066	26094.7 ± 2.5	16320.3 ± 1.6	-0.022
				2994268520960	582.916 ± 0.060	853.894 ± 0.066	30516.8 ± 3.3	-7824.2 ± 1.9	0.085
				2925546004992	854.059 ± 0.061	73.307 ± 0.066	-1959.8 ± 5.2	-34368.3 ± 2.0	-0.019
				3200426950656	558.342 ± 0.060	931.400 ± 0.066	33774.9 ± 3.5	-5300.0 ± 2.1	-0.218
				2925557800192	926.219 ± 0.059	139.326 ± 0.065	2449.5 ± 2.3	-36655.5 ± 1.7	-0.051
				2994265478400	864.491 ± 0.058	801.079 ± 0.064	32910.5 ± 0.7	-22151.0 ± 0.6	-0.144
				2989964110208	908.065 ± 0.058	772.179 ± 0.064	32293.3 ± 0.3	-24735.7 ± 0.4	-0.165

Table C1 continued

Table C1 (continued)

Instrument	Date	Filter	Image	<i>Gaia</i> DR2 Source (607290-)	x (px)	y (px)	ξ (mas)	η (mas)	$\rho_{\xi,\eta}$
				2994268518784	890.878 ± 0.060	826.281 ± 0.065	34572.4 ± 3.1	-22967.5 ± 2.1	0.061
			od9t04010	2994277277824	522.607 ± 0.058	558.218 ± 0.064	7740.8 ± 1.1	8152.4 ± 1.3	-0.282
				2994268530304	329.817 ± 0.058	463.881 ± 0.064	-1813.0 ± 2.3	13396.3 ± 5.5	0.079
				2994266748800	842.442 ± 0.058	415.315 ± 0.064	11149.3 ± 3.1	-9303.2 ± 1.9	0.051
				2994265535104	233.008 ± 0.058	500.493 ± 0.064	-3115.6 ± 1.3	18480.8 ± 1.1	-0.257
				3196128030848	292.494 ± 0.058	651.122 ± 0.064	4876.9 ± 0.4	20412.8 ± 0.4	-0.158
				3097347747712	128.700 ± 0.059	236.930 ± 0.065	-17102.0 ± 1.8	15108.8 ± 1.1	-0.043
				3097344750592	133.085 ± 0.058	199.180 ± 0.064	-18546.1 ± 0.4	13823.7 ± 0.4	-0.143
				3200425179904	845.513 ± 0.058	733.914 ± 0.064	24467.1 ± 1.8	-114.8 ± 1.1	-0.024
				3200426952576	789.053 ± 0.058	772.310 ± 0.064	24416.6 ± 3.2	3347.2 ± 1.8	0.036
				3200423956608	611.202 ± 0.058	837.198 ± 0.064	21909.7 ± 0.6	12623.6 ± 0.5	-0.062
				2994277277312	1007.207 ± 0.058	82.134 ± 0.064	2113.1 ± 6.3	-25851.3 ± 7.3	-0.323
				3200426959616	260.816 ± 0.058	772.930 ± 0.064	9012.1 ± 2.7	25287.3 ± 1.9	0.019
				3200423962624	390.059 ± 0.058	843.944 ± 0.065	15733.8 ± 1.7	21995.9 ± 0.6	0.106
				3200435464064	92.189 ± 0.058	625.632 ± 0.064	-2029.4 ± 1.0	27976.8 ± 1.5	-0.328
				3196122664064	565.010 ± 0.058	887.004 ± 0.064	22626.0 ± 0.7	15993.8 ± 0.6	-0.142
				3200423967616	313.869 ± 0.058	884.935 ± 0.064	15206.3 ± 1.0	26352.4 ± 0.8	-0.135
				3200426953728	599.036 ± 0.058	946.613 ± 0.064	26094.7 ± 2.5	16320.3 ± 1.6	-0.021
				3200425185664	247.062 ± 0.058	923.047 ± 0.064	14834.4 ± 2.5	30234.9 ± 1.3	-0.063
				3200426950656	1034.562 ± 0.058	825.072 ± 0.064	33774.9 ± 3.5	-5300.0 ± 2.1	-0.219
				3200423976192	100.971 ± 0.058	883.755 ± 0.064	8940.6 ± 0.9	35150.2 ± 0.8	-0.117
				3196122663808	184.469 ± 0.058	951.454 ± 0.064	14188.0 ± 0.5	33666.8 ± 0.5	-0.153
			od9t04020	2994277277824	512.729 ± 0.058	558.270 ± 0.064	7740.8 ± 1.1	8152.4 ± 1.3	-0.282
				2994268530304	319.860 ± 0.058	463.913 ± 0.064	-1813.0 ± 2.3	13396.3 ± 5.5	0.077
				2994266748800	832.581 ± 0.058	415.352 ± 0.064	11149.3 ± 3.1	-9303.2 ± 1.9	0.050
				2994265535104	223.060 ± 0.058	500.526 ± 0.064	-3115.6 ± 1.3	18480.8 ± 1.1	-0.259
				3196128030848	282.603 ± 0.058	651.179 ± 0.064	4876.9 ± 0.4	20412.8 ± 0.4	-0.156
				3097347747712	118.779 ± 0.058	236.904 ± 0.065	-17102.0 ± 1.8	15108.8 ± 1.1	-0.042
				3097344750592	123.158 ± 0.058	199.169 ± 0.064	-18546.1 ± 0.4	13823.7 ± 0.4	-0.143
				3200425179904	835.725 ± 0.058	733.972 ± 0.064	24467.1 ± 1.8	-114.8 ± 1.1	-0.025
				3200426952576	779.217 ± 0.058	772.377 ± 0.064	24416.6 ± 3.2	3347.2 ± 1.8	0.035
				3200423956608	601.369 ± 0.058	837.282 ± 0.064	21909.7 ± 0.6	12623.6 ± 0.5	-0.063
				2994277277312	997.391 ± 0.058	82.167 ± 0.064	2113.1 ± 6.3	-25851.3 ± 7.3	-0.325
				3200426959616	250.896 ± 0.058	773.009 ± 0.064	9012.1 ± 2.7	25287.3 ± 1.9	0.018
				3200423962624	380.201 ± 0.058	844.039 ± 0.064	15733.8 ± 1.7	21995.9 ± 0.6	0.106
				3200435464064	82.258 ± 0.058	625.692 ± 0.064	-2029.4 ± 1.0	27976.8 ± 1.5	-0.327
				3196122664064	555.154 ± 0.058	887.090 ± 0.064	22626.0 ± 0.7	15993.8 ± 0.6	-0.142
				3200423967616	303.960 ± 0.058	885.012 ± 0.064	15206.3 ± 1.0	26352.4 ± 0.8	-0.134
				3200426953728	589.220 ± 0.058	946.708 ± 0.064	26094.7 ± 2.5	16320.3 ± 1.6	-0.021
				3200425185664	237.194 ± 0.058	923.131 ± 0.064	14834.3 ± 2.5	30234.9 ± 1.3	-0.062
				3200426950656	1024.800 ± 0.058	825.148 ± 0.064	33774.9 ± 3.5	-5300.0 ± 2.1	-0.219
				3200423976192	91.018 ± 0.058	883.821 ± 0.064	8940.6 ± 0.9	35150.2 ± 0.8	-0.117
				3196122663808	174.577 ± 0.058	951.542 ± 0.064	14188.0 ± 0.5	33666.8 ± 0.5	-0.153
			od9t04030	2994277277824	187.515 ± 0.058	559.979 ± 0.064	7740.8 ± 1.1	8152.4 ± 1.3	-0.282
				2994266748800	507.455 ± 0.061	416.956 ± 0.067	11149.3 ± 3.1	-9303.2 ± 1.9	0.052
				2994276656640	436.501 ± 0.058	609.700 ± 0.064	17072.3 ± 0.3	-728.4 ± 0.4	-0.187

Table C1 continued

Table C1 (continued)

Instrument	Date	Filter	Image	<i>Gaia</i> DR2 Source (607290-)	x (px)	y (px)	ξ (mas)	η (mas)	$\rho_{\xi,\eta}$
				3200425179904	510.362 ± 0.059	735.694 ± 0.065	24467.1 ± 1.8	-114.8 ± 1.1	-0.024
				3200426952576	454.011 ± 0.060	774.130 ± 0.066	24416.6 ± 3.2	3347.2 ± 1.8	0.034
				3200423956608	276.073 ± 0.058	839.060 ± 0.064	21909.7 ± 0.6	12623.6 ± 0.5	-0.061
				2994277277312	671.861 ± 0.063	83.760 ± 0.068	2113.1 ± 6.3	-25851.3 ± 7.3	-0.323
				2989964233984	726.371 ± 0.058	491.760 ± 0.064	20640.3 ± 0.4	-16203.9 ± 0.4	-0.154
				3196122664064	229.892 ± 0.058	888.889 ± 0.064	22626.0 ± 0.7	15993.8 ± 0.6	-0.141
				3200426953728	263.952 ± 0.059	948.472 ± 0.065	26094.7 ± 2.5	16320.3 ± 1.6	-0.021
				2994268520960	703.259 ± 0.059	745.632 ± 0.065	30516.7 ± 3.3	-7824.2 ± 1.9	0.083
				3200426950656	699.596 ± 0.059	826.864 ± 0.065	33774.9 ± 3.5	-5300.0 ± 2.1	-0.219
				2994265478400	961.516 ± 0.058	621.969 ± 0.064	32910.5 ± 0.7	-22151.0 ± 0.6	-0.143
				2989964110208	996.158 ± 0.058	582.790 ± 0.064	32293.3 ± 0.3	-24735.7 ± 0.4	-0.165
				2994268518784	993.546 ± 0.059	639.463 ± 0.066	34572.4 ± 3.1	-22967.5 ± 2.1	0.060
WFC3	2016-01-29	f127m	icytb0011	2994277277824	132.055 ± 0.143	94.246 ± 0.112	7783.2 ± 0.6	8138.6 ± 0.7	0.024
				2994268530304	215.507 ± 0.144	77.782 ± 0.111	-1777.3 ± 1.1	13379.5 ± 2.7	0.345
				2994277298816	188.208 ± 0.143	55.432 ± 0.113	2409.6 ± 1.6	15061.1 ± 1.1	0.333
				2994266748800	65.740 ± 0.142	216.281 ± 0.111	11192.5 ± 1.5	-9319.9 ± 1.1	0.281
				2994276656640	41.775 ± 0.143	138.631 ± 0.112	17108.4 ± 0.2	-745.0 ± 0.4	-0.208
				2994265535104	237.121 ± 0.145	42.960 ± 0.111	-3079.2 ± 0.6	18465.5 ± 0.6	-0.002
				3200423956608	37.132 ± 0.145	27.968 ± 0.111	21948.8 ± 0.3	12607.9 ± 0.4	-0.049
			icytb0041	2994277277824	131.993 ± 0.144	94.196 ± 0.111	7783.2 ± 0.6	8138.6 ± 0.7	0.024
				2994268530304	215.404 ± 0.142	77.736 ± 0.113	-1777.3 ± 1.1	13379.5 ± 2.7	0.344
				2994277298816	188.206 ± 0.143	55.400 ± 0.115	2409.6 ± 1.6	15061.1 ± 1.1	0.333
				2994266748800	65.774 ± 0.143	216.184 ± 0.111	11192.5 ± 1.5	-9319.9 ± 1.1	0.281
				2994276656640	41.834 ± 0.144	138.562 ± 0.112	17108.4 ± 0.2	-745.0 ± 0.4	-0.208
				2994265535104	237.074 ± 0.143	42.916 ± 0.111	-3079.2 ± 0.6	18465.5 ± 0.6	-0.001
				3200423956608	37.108 ± 0.144	27.876 ± 0.112	21948.8 ± 0.3	12607.9 ± 0.4	-0.050
			icytb0071	2994277277824	132.096 ± 0.144	94.252 ± 0.111	7783.1 ± 0.6	8138.6 ± 0.7	0.026
				2994268530304	215.441 ± 0.143	77.751 ± 0.112	-1777.3 ± 1.1	13379.5 ± 2.7	0.346
				2994277298816	188.281 ± 0.143	55.457 ± 0.114	2409.6 ± 1.6	15061.1 ± 1.1	0.335
				2994266748800	65.750 ± 0.141	216.255 ± 0.111	11192.5 ± 1.5	-9319.9 ± 1.1	0.279
				2994276656640	41.835 ± 0.144	138.639 ± 0.111	17108.4 ± 0.2	-745.0 ± 0.4	-0.207
				2994265535104	237.119 ± 0.143	42.931 ± 0.112	-3079.2 ± 0.6	18465.5 ± 0.6	-0.000
				3200423956608	37.137 ± 0.142	27.982 ± 0.112	21948.8 ± 0.3	12607.9 ± 0.4	-0.049
			icytb00a1	2994277277824	132.095 ± 0.145	94.174 ± 0.111	7783.1 ± 0.6	8138.6 ± 0.7	0.026
				2994268530304	215.432 ± 0.144	77.779 ± 0.111	-1777.3 ± 1.1	13379.5 ± 2.7	0.345
				2994277298816	188.324 ± 0.146	55.452 ± 0.114	2409.6 ± 1.6	15061.1 ± 1.1	0.334
				2994266748800	65.837 ± 0.144	216.202 ± 0.111	11192.5 ± 1.5	-9319.9 ± 1.1	0.280
				2994276656640	41.869 ± 0.144	138.550 ± 0.111	17108.4 ± 0.2	-745.0 ± 0.4	-0.209
				2994265535104	237.118 ± 0.142	42.963 ± 0.111	-3079.2 ± 0.6	18465.5 ± 0.6	-0.000
				3200423956608	37.158 ± 0.147	27.886 ± 0.112	21948.8 ± 0.3	12607.9 ± 0.4	-0.050
			icytb1011	2994277277824	114.173 ± 0.145	103.732 ± 0.112	7783.1 ± 0.6	8138.6 ± 0.7	0.025
				2994268530304	176.063 ± 0.145	45.287 ± 0.112	-1777.3 ± 1.1	13379.5 ± 2.7	0.344
				2994277298816	141.272 ± 0.144	40.878 ± 0.114	2409.6 ± 1.6	15061.1 ± 1.1	0.333
				2994276656640	61.112 ± 0.143	188.958 ± 0.112	17108.4 ± 0.2	-745.0 ± 0.4	-0.209
				3200435093120	24.913 ± 0.143	6.519 ± 0.112	15755.4 ± 0.2	23059.4 ± 0.4	-0.214
			icytb1041	2994277277824	114.146 ± 0.145	103.728 ± 0.111	7783.1 ± 0.6	8138.6 ± 0.7	0.026

Table C1 continued

Table C1 (continued)

Instrument	Date	Filter	Image	<i>Gaia</i> DR2 Source (607290-)	x (px)	y (px)	ξ (mas)	η (mas)	$\rho_{\xi,\eta}$
				2994268530304	176.052 ± 0.146	45.315 ± 0.113	-1777.3 ± 1.1	13379.5 ± 2.6	0.345
				2994277298816	141.241 ± 0.146	40.922 ± 0.114	2409.6 ± 1.6	15061.1 ± 1.1	0.334
				2994276656640	61.084 ± 0.143	188.947 ± 0.112	17108.4 ± 0.2	-745.0 ± 0.4	-0.210
				3200435093120	24.835 ± 0.143	6.524 ± 0.113	15755.4 ± 0.2	23059.4 ± 0.4	-0.213
			icytb1071	2994277277824	114.190 ± 0.146	103.731 ± 0.111	7783.1 ± 0.6	8138.6 ± 0.7	0.028
				2994268530304	176.086 ± 0.145	45.311 ± 0.112	-1777.3 ± 1.1	13379.5 ± 2.7	0.345
				2994277298816	141.296 ± 0.145	40.902 ± 0.114	2409.6 ± 1.6	15061.1 ± 1.1	0.332
				2994276656640	61.114 ± 0.144	188.952 ± 0.111	17108.4 ± 0.2	-745.0 ± 0.4	-0.207
				3200435093120	24.772 ± 0.141	6.578 ± 0.111	15755.4 ± 0.2	23059.4 ± 0.4	-0.212
			icytb10a1	2994277277824	114.184 ± 0.142	103.736 ± 0.112	7783.1 ± 0.6	8138.6 ± 0.7	0.026
				2994268530304	176.083 ± 0.144	45.332 ± 0.112	-1777.3 ± 1.1	13379.5 ± 2.7	0.345
				2994277298816	141.291 ± 0.143	40.928 ± 0.112	2409.6 ± 1.6	15061.1 ± 1.1	0.333
				2994276656640	61.099 ± 0.145	188.995 ± 0.112	17108.4 ± 0.2	-745.0 ± 0.4	-0.208
				3200435093120	24.719 ± 0.139	6.598 ± 0.110	15755.4 ± 0.2	23059.4 ± 0.4	-0.214
		f139m	icytb0021	2994277277824	132.053 ± 0.123	94.131 ± 0.102	7783.2 ± 0.6	8138.6 ± 0.7	0.025
				2994268530304	215.402 ± 0.122	77.633 ± 0.103	-1777.3 ± 1.1	13379.5 ± 2.6	0.345
				2994277298816	188.227 ± 0.125	55.320 ± 0.104	2409.6 ± 1.6	15061.1 ± 1.1	0.335
				2994266748800	65.825 ± 0.123	216.122 ± 0.102	11192.5 ± 1.5	-9319.9 ± 1.1	0.281
				2994276656640	41.859 ± 0.124	138.456 ± 0.102	17108.4 ± 0.2	-745.0 ± 0.4	-0.207
				2994265535104	237.078 ± 0.126	42.851 ± 0.103	-3079.2 ± 0.6	18465.5 ± 0.6	-0.002
				3200423956608	37.099 ± 0.126	27.746 ± 0.103	21948.8 ± 0.3	12607.9 ± 0.4	-0.051
			icytb0051	2994277277824	132.067 ± 0.125	94.097 ± 0.103	7783.2 ± 0.6	8138.6 ± 0.7	0.026
				2994268530304	215.415 ± 0.125	77.673 ± 0.102	-1777.3 ± 1.1	13379.5 ± 2.7	0.345
				2994277298816	188.266 ± 0.124	55.384 ± 0.104	2409.6 ± 1.6	15061.1 ± 1.1	0.335
				2994266748800	65.799 ± 0.123	216.150 ± 0.103	11192.5 ± 1.5	-9319.9 ± 1.1	0.281
				2994276656640	41.854 ± 0.126	138.358 ± 0.102	17108.4 ± 0.2	-745.0 ± 0.4	-0.210
				2994265535104	237.085 ± 0.126	42.812 ± 0.102	-3079.2 ± 0.6	18465.5 ± 0.6	0.001
				3200423956608	37.141 ± 0.124	27.823 ± 0.102	21948.8 ± 0.3	12607.9 ± 0.4	-0.051
			icytb0081	2994277277824	132.101 ± 0.126	94.147 ± 0.102	7783.1 ± 0.6	8138.6 ± 0.7	0.026
				2994268530304	215.420 ± 0.124	77.682 ± 0.102	-1777.3 ± 1.1	13379.5 ± 2.7	0.344
				2994277298816	188.343 ± 0.125	55.300 ± 0.103	2409.6 ± 1.6	15061.1 ± 1.1	0.333
				2994266748800	65.715 ± 0.123	216.111 ± 0.102	11192.5 ± 1.5	-9319.9 ± 1.1	0.280
				2994276656640	41.942 ± 0.124	138.472 ± 0.103	17108.4 ± 0.2	-745.0 ± 0.4	-0.209
				2994265535104	237.087 ± 0.126	42.768 ± 0.102	-3079.2 ± 0.6	18465.5 ± 0.6	-0.002
				3200423956608	37.081 ± 0.124	27.780 ± 0.102	21948.8 ± 0.3	12607.9 ± 0.4	-0.050
			icytb1021	2994277277824	114.176 ± 0.124	103.679 ± 0.103	7783.1 ± 0.6	8138.6 ± 0.7	0.026
				2994268530304	176.073 ± 0.125	45.258 ± 0.103	-1777.3 ± 1.1	13379.5 ± 2.7	0.343
				2994277298816	141.261 ± 0.126	40.832 ± 0.104	2409.6 ± 1.6	15061.1 ± 1.1	0.333
				2994276656640	61.098 ± 0.124	188.918 ± 0.102	17108.4 ± 0.2	-745.0 ± 0.4	-0.209
				3200435093120	24.905 ± 0.128	6.459 ± 0.104	15755.4 ± 0.2	23059.4 ± 0.4	-0.214
			icytb1051	2994277277824	114.168 ± 0.124	103.683 ± 0.103	7783.1 ± 0.6	8138.6 ± 0.7	0.025
				2994268530304	176.096 ± 0.125	45.261 ± 0.103	-1777.3 ± 1.1	13379.5 ± 2.7	0.345
				2994277298816	141.271 ± 0.126	40.830 ± 0.105	2409.6 ± 1.6	15061.1 ± 1.1	0.333
				2994276656640	61.147 ± 0.123	188.920 ± 0.103	17108.4 ± 0.2	-745.0 ± 0.4	-0.209
				3200435093120	24.854 ± 0.130	6.465 ± 0.103	15755.4 ± 0.2	23059.4 ± 0.4	-0.214
			icytb1081	2994277277824	114.190 ± 0.123	103.662 ± 0.103	7783.1 ± 0.6	8138.6 ± 0.7	0.026

Table C1 continued

Table C1 (continued)

Instrument	Date	Filter	Image	<i>Gaia</i> DR2 Source (607290-)	x (px)	y (px)	ξ (mas)	η (mas)	$\rho_{\xi,\eta}$
				2994268530304	176.105 ± 0.126	45.260 ± 0.102	-1777.3 ± 1.1	13379.5 ± 2.7	0.343
				2994277298816	141.281 ± 0.124	40.832 ± 0.104	2409.6 ± 1.6	15061.1 ± 1.1	0.333
				2994276656640	61.117 ± 0.125	188.935 ± 0.103	17108.4 ± 0.2	-745.0 ± 0.4	-0.207
				3200435093120	24.857 ± 0.125	6.505 ± 0.102	15755.4 ± 0.2	23059.4 ± 0.4	-0.212
		f153m	icytb0031 ^a	2994277277824	132.658 ± 0.092	95.107 ± 0.081	7783.2 ± 0.6	8138.6 ± 0.7	0.023
				2994268530304	215.667 ± 0.093	78.416 ± 0.080	-1777.3 ± 1.1	13379.5 ± 2.6	0.346
				2994277298816	188.335 ± 0.091	56.029 ± 0.084	2409.6 ± 1.6	15061.1 ± 1.1	0.333
				2994266748800	66.849 ± 0.090	217.257 ± 0.080	11192.5 ± 1.5	-9319.9 ± 1.1	0.279
				2994276656640	42.729 ± 0.090	139.080 ± 0.081	17108.4 ± 0.2	-745.0 ± 0.4	-0.209
				2994265535104	237.079 ± 0.091	43.628 ± 0.082	-3079.2 ± 0.6	18465.5 ± 0.6	-0.004
				3200423956608	37.565 ± 0.094	28.327 ± 0.081	21948.8 ± 0.3	12607.9 ± 0.4	-0.051
			icytb0061	2994277277824	132.047 ± 0.092	94.237 ± 0.081	7783.2 ± 0.6	8138.6 ± 0.7	0.026
				2994268530304	215.415 ± 0.093	77.778 ± 0.081	-1777.3 ± 1.1	13379.5 ± 2.7	0.345
				2994277298816	188.062 ± 0.092	55.420 ± 0.083	2409.6 ± 1.6	15061.1 ± 1.1	0.333
				2994266748800	65.833 ± 0.090	216.192 ± 0.081	11192.5 ± 1.5	-9319.9 ± 1.1	0.281
				2994276656640	41.840 ± 0.093	138.594 ± 0.081	17108.4 ± 0.2	-745.0 ± 0.4	-0.207
				2994265535104	237.081 ± 0.089	42.972 ± 0.080	-3079.2 ± 0.6	18465.5 ± 0.6	-0.002
				3200423956608	37.122 ± 0.093	27.934 ± 0.080	21948.8 ± 0.3	12607.9 ± 0.4	-0.050
			icytb0091	2994277277824	132.061 ± 0.091	94.250 ± 0.081	7783.1 ± 0.6	8138.6 ± 0.7	0.025
				2994268530304	215.424 ± 0.090	77.775 ± 0.081	-1777.3 ± 1.1	13379.5 ± 2.7	0.346
				2994277298816	188.295 ± 0.093	55.515 ± 0.082	2409.6 ± 1.6	15061.1 ± 1.1	0.332
				2994266748800	65.821 ± 0.091	216.219 ± 0.080	11192.5 ± 1.5	-9319.9 ± 1.1	0.280
				2994276656640	41.897 ± 0.090	138.659 ± 0.081	17108.4 ± 0.2	-745.0 ± 0.4	-0.209
				2994265535104	237.060 ± 0.094	43.001 ± 0.080	-3079.2 ± 0.6	18465.5 ± 0.6	-0.001
				3200423956608	37.132 ± 0.091	27.921 ± 0.081	21948.8 ± 0.3	12607.9 ± 0.4	-0.049
			icytb1031	2994277277824	114.126 ± 0.093	103.802 ± 0.081	7783.1 ± 0.6	8138.6 ± 0.7	0.026
				2994268530304	176.041 ± 0.095	45.409 ± 0.082	-1777.3 ± 1.1	13379.5 ± 2.6	0.344
				2994277298816	141.167 ± 0.096	41.187 ± 0.087	2409.6 ± 1.6	15061.1 ± 1.1	0.335
				2994276656640	61.135 ± 0.093	189.059 ± 0.081	17108.4 ± 0.2	-745.0 ± 0.4	-0.208
				3200435093120	24.816 ± 0.094	6.666 ± 0.081	15755.4 ± 0.2	23059.4 ± 0.4	-0.213
			icytb1061	2994277277824	114.159 ± 0.093	103.804 ± 0.081	7783.1 ± 0.6	8138.6 ± 0.7	0.023
				2994268530304	176.060 ± 0.093	45.399 ± 0.082	-1777.3 ± 1.1	13379.5 ± 2.7	0.345
				2994277298816	141.261 ± 0.096	41.007 ± 0.085	2409.6 ± 1.6	15061.1 ± 1.1	0.335
				2994276656640	61.092 ± 0.092	189.025 ± 0.081	17108.4 ± 0.2	-745.0 ± 0.4	-0.208
				3200435093120	24.813 ± 0.093	6.636 ± 0.081	15755.4 ± 0.2	23059.4 ± 0.4	-0.214
			icytb1091	2994277277824	114.183 ± 0.093	103.834 ± 0.080	7783.1 ± 0.6	8138.6 ± 0.7	0.023
				2994268530304	176.087 ± 0.091	45.431 ± 0.081	-1777.3 ± 1.1	13379.5 ± 2.7	0.343
				2994277298816	141.253 ± 0.094	41.008 ± 0.083	2409.6 ± 1.6	15061.1 ± 1.1	0.332
				2994276656640	61.163 ± 0.091	189.045 ± 0.080	17108.4 ± 0.2	-745.0 ± 0.4	-0.208
				3200435093120	24.903 ± 0.089	6.622 ± 0.080	15755.4 ± 0.2	23059.4 ± 0.4	-0.214
WFC3	2018-06-07	f127m	icytb2011	2994277277824	131.752 ± 0.142	162.982 ± 0.112	7680.7 ± 1.9	8159.0 ± 2.1	-0.388
				2994268530304	58.043 ± 0.146	120.955 ± 0.111	-1864.1 ± 4.1	13407.7 ± 8.2	-0.175
				2994277298816	63.848 ± 0.144	155.673 ± 0.111	2313.2 ± 5.4	15087.3 ± 4.6	0.037
				2994266748800	261.629 ± 0.143	114.578 ± 0.111	11090.2 ± 5.2	-9291.2 ± 3.4	-0.072
				2994276656640	228.895 ± 0.142	188.923 ± 0.112	17020.1 ± 0.5	-717.9 ± 0.5	-0.173
				3196128030848	38.665 ± 0.145	193.973 ± 0.112	4820.2 ± 0.6	20422.3 ± 0.6	-0.194

Table C1 continued

Table C1 (continued)

Instrument	Date	Filter	Image	<i>Gaia</i> DR2 Source (607290-)	x (px)	y (px)	ξ (mas)	η (mas)	$\rho_{\xi,\eta}$
			icytb2041	2994277277824	131.784 ± 0.143	162.991 ± 0.110	7680.7 ± 1.9	8159.0 ± 2.1	-0.389
				2994268530304	57.961 ± 0.145	120.923 ± 0.112	-1864.1 ± 4.1	13407.7 ± 8.2	-0.176
				2994277298816	63.862 ± 0.145	155.637 ± 0.111	2313.3 ± 5.4	15087.3 ± 4.6	0.037
				2994266748800	261.721 ± 0.143	114.542 ± 0.111	11090.2 ± 5.2	-9291.2 ± 3.4	-0.073
				2994276656640	228.917 ± 0.142	188.804 ± 0.111	17020.1 ± 0.5	-717.9 ± 0.5	-0.170
				3196128030848	38.652 ± 0.142	193.919 ± 0.112	4820.2 ± 0.6	20422.3 ± 0.6	-0.194
			icytb2071	2994277277824	131.721 ± 0.142	162.992 ± 0.110	7680.7 ± 1.9	8159.0 ± 2.1	-0.390
				2994268530304	57.947 ± 0.145	120.931 ± 0.111	-1864.1 ± 4.1	13407.7 ± 8.2	-0.174
				2994277298816	63.905 ± 0.146	155.569 ± 0.113	2313.2 ± 5.4	15087.3 ± 4.6	0.036
				2994266748800	261.666 ± 0.144	114.488 ± 0.110	11090.2 ± 5.2	-9291.2 ± 3.4	-0.072
				2994276656640	228.845 ± 0.144	189.120 ± 0.112	17020.1 ± 0.5	-717.9 ± 0.5	-0.170
				3196128030848	38.629 ± 0.144	193.947 ± 0.111	4820.2 ± 0.6	20422.3 ± 0.6	-0.195
			icytb20a1	2994277277824	131.702 ± 0.142	162.963 ± 0.110	7680.7 ± 1.9	8159.0 ± 2.1	-0.389
				2994268530304	57.811 ± 0.145	120.929 ± 0.113	-1864.1 ± 4.1	13407.7 ± 8.2	-0.177
				2994277298816	63.828 ± 0.147	155.592 ± 0.112	2313.3 ± 5.4	15087.3 ± 4.6	0.037
				2994266748800	261.360 ± 0.145	114.474 ± 0.111	11090.2 ± 5.2	-9291.2 ± 3.4	-0.074
				2994276656640	228.835 ± 0.143	188.804 ± 0.111	17020.1 ± 0.5	-717.9 ± 0.5	-0.171
				3196128030848	38.618 ± 0.142	193.815 ± 0.112	4820.2 ± 0.6	20422.3 ± 0.6	-0.197
			icytb3011	2994277277824	148.150 ± 0.144	162.015 ± 0.112	7680.7 ± 1.9	8159.0 ± 2.1	-0.388
				2994268530304	63.317 ± 0.146	155.145 ± 0.114	-1864.1 ± 4.1	13407.7 ± 8.2	-0.176
				2994277298816	83.217 ± 0.144	184.006 ± 0.112	2313.2 ± 5.4	15087.3 ± 4.6	0.035
				2994266748800	245.100 ± 0.146	63.181 ± 0.111	11090.2 ± 5.2	-9291.2 ± 3.4	-0.073
				2994276656640	246.927 ± 0.143	144.456 ± 0.112	17020.1 ± 0.5	-717.9 ± 0.5	-0.170
				2994265535104	33.068 ± 0.142	182.475 ± 0.113	-3167.9 ± 2.2	18490.1 ± 2.1	-0.346
			icytb3041	3196128030848	76.781 ± 0.145	229.572 ± 0.112	4820.2 ± 0.6	20422.3 ± 0.6	-0.196
				2994277277824	148.036 ± 0.146	162.037 ± 0.112	7680.7 ± 1.9	8159.0 ± 2.1	-0.390
				2994268530304	63.346 ± 0.144	155.114 ± 0.113	-1864.1 ± 4.1	13407.7 ± 8.2	-0.175
				2994277298816	83.232 ± 0.144	183.986 ± 0.112	2313.3 ± 5.4	15087.3 ± 4.6	0.034
				2994266748800	245.121 ± 0.143	63.150 ± 0.112	11090.2 ± 5.2	-9291.2 ± 3.4	-0.074
				2994276656640	246.924 ± 0.144	144.504 ± 0.112	17020.1 ± 0.5	-717.9 ± 0.5	-0.172
			icytb3071	2994265535104	32.983 ± 0.144	182.555 ± 0.113	-3167.9 ± 2.2	18490.1 ± 2.1	-0.345
				3196128030848	76.791 ± 0.144	229.574 ± 0.111	4820.2 ± 0.6	20422.3 ± 0.6	-0.196
				2994277277824	148.039 ± 0.142	162.033 ± 0.112	7680.7 ± 1.9	8159.0 ± 2.1	-0.389
				2994268530304	63.371 ± 0.145	155.107 ± 0.113	-1864.1 ± 4.1	13407.7 ± 8.2	-0.176
				2994277298816	83.202 ± 0.144	184.005 ± 0.112	2313.2 ± 5.4	15087.3 ± 4.6	0.034
				2994266748800	245.112 ± 0.143	63.095 ± 0.112	11090.2 ± 5.2	-9291.2 ± 3.4	-0.073
			icytb30a1	2994276656640	246.887 ± 0.143	144.460 ± 0.112	17020.1 ± 0.5	-717.9 ± 0.5	-0.170
				2994265535104	32.985 ± 0.141	182.488 ± 0.112	-3167.9 ± 2.2	18490.1 ± 2.1	-0.346
				3196128030848	76.798 ± 0.145	229.565 ± 0.112	4820.2 ± 0.6	20422.3 ± 0.6	-0.195
				2994277277824	148.067 ± 0.144	161.988 ± 0.112	7680.7 ± 1.9	8159.0 ± 2.1	-0.390
				2994268530304	63.319 ± 0.144	155.047 ± 0.113	-1864.1 ± 4.1	13407.7 ± 8.2	-0.175
				2994277298816	83.194 ± 0.145	183.966 ± 0.112	2313.2 ± 5.4	15087.3 ± 4.6	0.035
			icytb30a1	2994266748800	245.107 ± 0.144	63.063 ± 0.111	11090.2 ± 5.2	-9291.2 ± 3.4	-0.073
				2994276656640	246.856 ± 0.145	144.310 ± 0.111	17020.1 ± 0.5	-717.9 ± 0.5	-0.172
				2994265535104	33.043 ± 0.145	182.415 ± 0.112	-3167.9 ± 2.2	18490.1 ± 2.1	-0.345
				3196128030848	76.779 ± 0.142	229.461 ± 0.110	4820.2 ± 0.6	20422.3 ± 0.6	-0.195

Table C1 continued

Table C1 (continued)

Instrument	Date	Filter	Image	<i>Gaia</i> DR2 Source (607290-)	x (px)	y (px)	ξ (mas)	η (mas)	$\rho_{\xi,\eta}$
			icytb4011	2994277277824	131.463 ± 0.142	162.659 ± 0.110	7680.7 ± 1.9	8159.0 ± 2.1	-0.389
				2994268530304	57.473 ± 0.145	120.636 ± 0.112	-1864.1 ± 4.1	13407.6 ± 8.2	-0.176
				2994277298816	63.633 ± 0.145	155.181 ± 0.113	2313.3 ± 5.4	15087.3 ± 4.6	0.035
				2994266748800	261.135 ± 0.144	114.066 ± 0.111	11090.2 ± 5.2	-9291.2 ± 3.4	-0.074
				2994276656640	228.581 ± 0.143	188.386 ± 0.111	17020.1 ± 0.5	-717.9 ± 0.5	-0.170
				3196128030848	38.264 ± 0.143	193.629 ± 0.111	4820.2 ± 0.6	20422.3 ± 0.6	-0.194
			icytb4041	2994277277824	131.637 ± 0.143	162.349 ± 0.110	7680.7 ± 1.9	8159.0 ± 2.1	-0.389
				2994268530304	57.819 ± 0.143	120.650 ± 0.112	-1864.1 ± 4.1	13407.7 ± 8.2	-0.176
				2994277298816	63.786 ± 0.144	155.060 ± 0.113	2313.3 ± 5.4	15087.3 ± 4.6	0.035
				2994266748800	261.030 ± 0.145	113.794 ± 0.111	11090.2 ± 5.2	-9291.2 ± 3.4	-0.074
				2994276656640	228.396 ± 0.144	188.026 ± 0.112	17020.1 ± 0.5	-717.9 ± 0.5	-0.171
				3196128030848	38.709 ± 0.142	193.275 ± 0.112	4820.2 ± 0.6	20422.3 ± 0.6	-0.196
			icytb4071	2994277277824	131.472 ± 0.144	162.496 ± 0.110	7680.7 ± 1.9	8159.0 ± 2.1	-0.388
				2994268530304	57.476 ± 0.143	120.528 ± 0.113	-1864.1 ± 4.1	13407.7 ± 8.2	-0.175
				2994277298816	63.530 ± 0.146	155.163 ± 0.114	2313.2 ± 5.4	15087.3 ± 4.6	0.036
				2994266748800	261.121 ± 0.143	114.090 ± 0.111	11090.2 ± 5.2	-9291.2 ± 3.4	-0.072
				2994276656640	228.456 ± 0.143	188.455 ± 0.112	17020.1 ± 0.5	-717.9 ± 0.5	-0.172
				3196128030848	38.293 ± 0.143	193.645 ± 0.112	4820.2 ± 0.6	20422.3 ± 0.6	-0.194
			icytb40a1	2994277277824	131.555 ± 0.141	162.342 ± 0.110	7680.7 ± 1.9	8159.0 ± 2.1	-0.389
				2994268530304	57.762 ± 0.145	120.509 ± 0.113	-1864.1 ± 4.1	13407.6 ± 8.2	-0.177
				2994277298816	63.629 ± 0.144	155.035 ± 0.114	2313.2 ± 5.4	15087.3 ± 4.6	0.037
				2994266748800	261.162 ± 0.144	113.915 ± 0.111	11090.2 ± 5.2	-9291.2 ± 3.4	-0.072
				2994276656640	228.285 ± 0.144	188.117 ± 0.110	17020.1 ± 0.5	-717.9 ± 0.5	-0.171
				3196128030848	38.265 ± 0.146	193.445 ± 0.111	4820.2 ± 0.6	20422.3 ± 0.6	-0.193
			icytb5011	2994277277824	147.668 ± 0.145	162.179 ± 0.112	7680.7 ± 1.9	8159.0 ± 2.1	-0.390
				2994268530304	63.058 ± 0.144	155.286 ± 0.112	-1864.1 ± 4.1	13407.6 ± 8.2	-0.176
				2994277298816	83.068 ± 0.145	184.150 ± 0.112	2313.2 ± 5.4	15087.3 ± 4.6	0.035
				2994266748800	244.939 ± 0.146	63.512 ± 0.111	11090.2 ± 5.2	-9291.2 ± 3.4	-0.073
				2994276656640	246.722 ± 0.144	144.793 ± 0.111	17020.1 ± 0.5	-717.9 ± 0.5	-0.170
				2994265535104	32.655 ± 0.144	182.782 ± 0.113	-3167.9 ± 2.2	18490.1 ± 2.1	-0.347
				3196128030848	76.462 ± 0.144	229.717 ± 0.111	4820.2 ± 0.6	20422.3 ± 0.6	-0.193
			icytb5041	2994277277824	147.740 ± 0.144	162.185 ± 0.113	7680.7 ± 1.9	8159.0 ± 2.1	-0.389
				2994268530304	63.071 ± 0.142	155.313 ± 0.114	-1864.1 ± 4.1	13407.7 ± 8.2	-0.176
				2994277298816	83.081 ± 0.145	184.153 ± 0.111	2313.3 ± 5.4	15087.3 ± 4.6	0.036
				2994266748800	244.952 ± 0.146	63.428 ± 0.112	11090.2 ± 5.2	-9291.2 ± 3.4	-0.073
				2994276656640	246.671 ± 0.146	144.782 ± 0.111	17020.1 ± 0.5	-717.9 ± 0.5	-0.171
				2994265535104	32.621 ± 0.142	182.778 ± 0.112	-3167.9 ± 2.2	18490.1 ± 2.1	-0.346
				3196128030848	76.519 ± 0.145	229.761 ± 0.111	4820.2 ± 0.6	20422.3 ± 0.6	-0.194
			icytb5071	2994277277824	147.789 ± 0.144	162.150 ± 0.111	7680.7 ± 1.9	8159.0 ± 2.1	-0.391
				2994268530304	63.051 ± 0.145	155.274 ± 0.112	-1864.1 ± 4.1	13407.7 ± 8.2	-0.175
				2994277298816	83.079 ± 0.146	184.132 ± 0.111	2313.3 ± 5.4	15087.3 ± 4.6	0.036
				2994266748800	244.949 ± 0.143	63.357 ± 0.112	11090.2 ± 5.2	-9291.2 ± 3.4	-0.072
				2994276656640	246.685 ± 0.142	144.730 ± 0.113	17020.1 ± 0.5	-717.9 ± 0.5	-0.173
				2994265535104	32.721 ± 0.145	182.777 ± 0.113	-3167.9 ± 2.2	18490.1 ± 2.1	-0.346
				3196128030848	76.576 ± 0.143	229.713 ± 0.112	4820.2 ± 0.6	20422.3 ± 0.6	-0.196
			icytb50a1	2994277277824	147.721 ± 0.143	162.128 ± 0.113	7680.7 ± 1.9	8159.0 ± 2.1	-0.391

Table C1 continued

Table C1 (continued)

Instrument	Date	Filter	Image	<i>Gaia</i> DR2 Source (607290-)	x (px)	y (px)	ξ (mas)	η (mas)	$\rho_{\xi,\eta}$
				2994268530304	63.050 ± 0.145	155.173 ± 0.114	-1864.1 ± 4.1	13407.7 ± 8.2	-0.175
				2994277298816	83.042 ± 0.145	184.139 ± 0.112	2313.3 ± 5.4	15087.3 ± 4.6	0.034
				2994266748800	244.901 ± 0.144	63.233 ± 0.111	11090.2 ± 5.2	-9291.2 ± 3.4	-0.074
				2994276656640	246.647 ± 0.144	144.775 ± 0.112	17020.1 ± 0.5	-717.9 ± 0.5	-0.170
				2994265535104	32.672 ± 0.144	182.676 ± 0.113	-3167.9 ± 2.2	18490.1 ± 2.1	-0.346
				3196128030848	76.571 ± 0.143	229.710 ± 0.112	4820.2 ± 0.6	20422.3 ± 0.6	-0.194
			icytb6011	2994277277824	131.779 ± 0.145	163.012 ± 0.111	7680.7 ± 1.9	8159.0 ± 2.1	-0.390
				2994268530304	57.925 ± 0.146	121.009 ± 0.114	-1864.1 ± 4.1	13407.7 ± 8.2	-0.176
				2994277298816	63.821 ± 0.147	155.681 ± 0.114	2313.3 ± 5.4	15087.3 ± 4.6	0.035
				2994266748800	261.520 ± 0.143	114.560 ± 0.111	11090.2 ± 5.2	-9291.2 ± 3.4	-0.072
				2994276656640	228.858 ± 0.143	189.073 ± 0.112	17020.1 ± 0.5	-717.9 ± 0.5	-0.172
				3196128030848	38.620 ± 0.145	193.867 ± 0.111	4820.2 ± 0.6	20422.3 ± 0.6	-0.195
			icytb6041	2994277277824	131.780 ± 0.143	162.966 ± 0.111	7680.7 ± 1.9	8159.0 ± 2.1	-0.389
				2994268530304	57.978 ± 0.141	120.972 ± 0.112	-1864.1 ± 4.1	13407.7 ± 8.2	-0.175
				2994277298816	63.879 ± 0.140	155.668 ± 0.113	2313.2 ± 5.4	15087.3 ± 4.6	0.034
				2994266748800	261.568 ± 0.145	114.508 ± 0.111	11090.2 ± 5.2	-9291.2 ± 3.4	-0.073
				2994276656640	228.900 ± 0.145	188.856 ± 0.112	17020.1 ± 0.5	-717.9 ± 0.5	-0.171
				3196128030848	38.621 ± 0.141	193.942 ± 0.111	4820.2 ± 0.6	20422.3 ± 0.6	-0.196
			icytb6071	2994277277824	131.742 ± 0.143	162.968 ± 0.110	7680.7 ± 1.9	8159.0 ± 2.1	-0.390
				2994268530304	58.059 ± 0.143	120.932 ± 0.113	-1864.1 ± 4.1	13407.7 ± 8.2	-0.177
				2994277298816	63.880 ± 0.145	155.622 ± 0.113	2313.2 ± 5.4	15087.3 ± 4.6	0.034
				2994266748800	261.570 ± 0.142	114.511 ± 0.112	11090.2 ± 5.2	-9291.2 ± 3.4	-0.073
				2994276656640	228.896 ± 0.144	188.761 ± 0.111	17020.1 ± 0.5	-717.9 ± 0.5	-0.170
				3196128030848	38.607 ± 0.146	193.894 ± 0.112	4820.2 ± 0.6	20422.3 ± 0.6	-0.195
			icytb60a1	2994277277824	131.839 ± 0.140	162.961 ± 0.110	7680.7 ± 1.9	8159.0 ± 2.1	-0.389
				2994268530304	57.807 ± 0.144	120.966 ± 0.112	-1864.1 ± 4.1	13407.7 ± 8.2	-0.176
				2994277298816	63.874 ± 0.145	155.614 ± 0.113	2313.2 ± 5.4	15087.3 ± 4.6	0.034
				2994266748800	261.696 ± 0.144	114.492 ± 0.112	11090.2 ± 5.2	-9291.2 ± 3.4	-0.073
				2994276656640	228.887 ± 0.144	188.823 ± 0.110	17020.1 ± 0.5	-717.9 ± 0.5	-0.168
				3196128030848	38.608 ± 0.145	193.904 ± 0.112	4820.2 ± 0.6	20422.3 ± 0.6	-0.195
			icytb7011	2994277277824	147.680 ± 0.146	162.233 ± 0.111	7680.7 ± 1.9	8159.0 ± 2.1	-0.389
				2994268530304	63.109 ± 0.144	155.512 ± 0.112	-1864.1 ± 4.1	13407.7 ± 8.2	-0.176
				2994277298816	83.052 ± 0.145	184.262 ± 0.112	2313.3 ± 5.4	15087.3 ± 4.6	0.037
				2994266748800	244.924 ± 0.145	63.607 ± 0.112	11090.2 ± 5.2	-9291.2 ± 3.4	-0.073
				2994276656640	246.674 ± 0.144	144.863 ± 0.111	17020.1 ± 0.5	-717.9 ± 0.5	-0.172
				2994265535104	32.662 ± 0.145	182.914 ± 0.113	-3167.9 ± 2.2	18490.1 ± 2.1	-0.346
				3196128030848	76.448 ± 0.145	229.845 ± 0.110	4820.2 ± 0.6	20422.3 ± 0.6	-0.194
			icytb7041	2994277277824	147.696 ± 0.146	162.236 ± 0.113	7680.7 ± 1.9	8159.0 ± 2.1	-0.390
				2994268530304	63.107 ± 0.146	155.489 ± 0.113	-1864.1 ± 4.1	13407.7 ± 8.2	-0.176
				2994277298816	83.063 ± 0.146	184.234 ± 0.111	2313.3 ± 5.4	15087.3 ± 4.6	0.035
				2994266748800	244.965 ± 0.144	63.535 ± 0.112	11090.2 ± 5.2	-9291.2 ± 3.4	-0.075
				2994276656640	246.692 ± 0.144	144.870 ± 0.112	17020.1 ± 0.5	-717.9 ± 0.5	-0.171
				2994265535104	32.690 ± 0.145	182.872 ± 0.114	-3167.9 ± 2.2	18490.1 ± 2.1	-0.347
				3196128030848	76.492 ± 0.142	229.770 ± 0.111	4820.2 ± 0.6	20422.3 ± 0.6	-0.195
			icytb7071	2994277277824	147.684 ± 0.145	162.211 ± 0.112	7680.7 ± 1.9	8159.0 ± 2.1	-0.389
				2994268530304	63.128 ± 0.144	155.398 ± 0.113	-1864.1 ± 4.1	13407.7 ± 8.2	-0.174

Table C1 continued

Table C1 (continued)

Instrument	Date	Filter	Image	<i>Gaia</i> DR2 Source (607290-)	x (px)	y (px)	ξ (mas)	η (mas)	$\rho_{\xi,\eta}$
				2994277298816	83.080 ± 0.145	184.189 ± 0.112	2313.3 ± 5.4	15087.3 ± 4.6	0.036
				2994266748800	244.968 ± 0.145	63.508 ± 0.111	11090.2 ± 5.2	-9291.2 ± 3.4	-0.073
				2994276656640	246.693 ± 0.144	144.850 ± 0.112	17020.1 ± 0.5	-717.9 ± 0.5	-0.171
				2994265535104	32.715 ± 0.146	182.850 ± 0.115	-3167.9 ± 2.2	18490.1 ± 2.1	-0.346
				3196128030848	76.555 ± 0.143	229.794 ± 0.111	4820.2 ± 0.6	20422.3 ± 0.6	-0.195
			icytb70a1	2994277277824	147.745 ± 0.144	162.223 ± 0.112	7680.7 ± 1.9	8159.0 ± 2.1	-0.391
				2994268530304	63.039 ± 0.145	155.405 ± 0.112	-1864.1 ± 4.1	13407.7 ± 8.2	-0.178
				2994277298816	83.043 ± 0.143	184.188 ± 0.111	2313.2 ± 5.4	15087.3 ± 4.6	0.037
				2994266748800	244.911 ± 0.143	63.557 ± 0.111	11090.2 ± 5.3	-9291.2 ± 3.4	-0.072
				2994276656640	246.738 ± 0.145	144.813 ± 0.111	17020.1 ± 0.5	-717.9 ± 0.5	-0.171
				2994265535104	32.680 ± 0.145	182.764 ± 0.112	-3167.9 ± 2.2	18490.1 ± 2.1	-0.346
				3196128030848	76.340 ± 0.142	229.781 ± 0.112	4820.2 ± 0.6	20422.3 ± 0.6	-0.197
			icytb8011	2994277277824	131.653 ± 0.142	162.883 ± 0.111	7680.7 ± 1.9	8159.0 ± 2.1	-0.389
				2994268530304	57.828 ± 0.142	120.867 ± 0.112	-1864.1 ± 4.1	13407.7 ± 8.2	-0.176
				2994277298816	63.820 ± 0.147	155.496 ± 0.113	2313.2 ± 5.4	15087.3 ± 4.6	0.035
				2994266748800	261.423 ± 0.144	114.421 ± 0.111	11090.2 ± 5.2	-9291.2 ± 3.4	-0.073
				2994276656640	228.863 ± 0.144	188.606 ± 0.112	17020.1 ± 0.5	-717.9 ± 0.5	-0.170
				3196128030848	38.549 ± 0.144	193.853 ± 0.111	4820.2 ± 0.6	20422.3 ± 0.6	-0.196
			icytb8041	2994277277824	131.653 ± 0.143	162.911 ± 0.111	7680.7 ± 1.9	8159.0 ± 2.1	-0.389
				2994268530304	57.710 ± 0.144	120.851 ± 0.113	-1864.1 ± 4.1	13407.7 ± 8.2	-0.175
				2994277298816	63.825 ± 0.145	155.486 ± 0.113	2313.3 ± 5.4	15087.3 ± 4.6	0.035
				2994266748800	261.482 ± 0.142	114.346 ± 0.111	11090.2 ± 5.2	-9291.2 ± 3.4	-0.073
				2994276656640	228.814 ± 0.144	188.565 ± 0.111	17020.1 ± 0.5	-717.9 ± 0.5	-0.170
				3196128030848	38.572 ± 0.144	193.841 ± 0.111	4820.2 ± 0.6	20422.3 ± 0.6	-0.195
			icytb8071	2994277277824	131.652 ± 0.142	162.879 ± 0.110	7680.7 ± 1.9	8159.0 ± 2.1	-0.390
				2994268530304	57.821 ± 0.144	120.850 ± 0.113	-1864.1 ± 4.1	13407.7 ± 8.2	-0.176
				2994277298816	63.787 ± 0.147	155.451 ± 0.114	2313.2 ± 5.4	15087.3 ± 4.6	0.034
				2994266748800	261.385 ± 0.144	114.379 ± 0.112	11090.2 ± 5.3	-9291.2 ± 3.4	-0.072
				2994276656640	228.756 ± 0.144	188.636 ± 0.112	17020.1 ± 0.5	-717.9 ± 0.5	-0.171
				3196128030848	38.528 ± 0.143	193.840 ± 0.112	4820.2 ± 0.6	20422.3 ± 0.6	-0.195
			icytb80a1	2994277277824	131.656 ± 0.144	162.925 ± 0.111	7680.7 ± 1.9	8159.0 ± 2.1	-0.390
				2994268530304	57.669 ± 0.147	120.797 ± 0.112	-1864.1 ± 4.1	13407.6 ± 8.2	-0.175
				2994277298816	63.793 ± 0.143	155.532 ± 0.112	2313.2 ± 5.4	15087.3 ± 4.6	0.036
				2994266748800	261.374 ± 0.144	114.306 ± 0.111	11090.2 ± 5.2	-9291.2 ± 3.4	-0.070
				2994276656640	228.695 ± 0.146	188.586 ± 0.111	17020.1 ± 0.5	-717.9 ± 0.5	-0.169
				3196128030848	38.476 ± 0.142	193.788 ± 0.112	4820.2 ± 0.6	20422.3 ± 0.6	-0.195
		f139m	icytb2021	2994277277824	131.761 ± 0.125	162.930 ± 0.102	7680.7 ± 1.9	8159.0 ± 2.1	-0.390
				2994268530304	57.941 ± 0.123	120.924 ± 0.102	-1864.1 ± 4.1	13407.6 ± 8.2	-0.176
				2994277298816	63.885 ± 0.124	155.620 ± 0.103	2313.2 ± 5.4	15087.3 ± 4.6	0.035
				2994266748800	261.627 ± 0.124	114.430 ± 0.102	11090.2 ± 5.2	-9291.2 ± 3.4	-0.073
				2994276656640	228.896 ± 0.124	188.862 ± 0.103	17020.1 ± 0.5	-717.9 ± 0.5	-0.172
				3196128030848	38.552 ± 0.124	193.926 ± 0.102	4820.2 ± 0.6	20422.3 ± 0.6	-0.193
			icytb2051	2994277277824	131.786 ± 0.125	162.916 ± 0.101	7680.7 ± 1.9	8159.0 ± 2.1	-0.390
				2994268530304	57.999 ± 0.123	120.881 ± 0.102	-1864.1 ± 4.1	13407.7 ± 8.2	-0.176
				2994277298816	63.859 ± 0.124	155.566 ± 0.104	2313.2 ± 5.4	15087.3 ± 4.6	0.036
				2994266748800	261.656 ± 0.126	114.454 ± 0.102	11090.2 ± 5.2	-9291.2 ± 3.4	-0.072

Table C1 continued

Table C1 (continued)

Instrument	Date	Filter	Image	<i>Gaia</i> DR2 Source (607290-)	x (px)	y (px)	ξ (mas)	η (mas)	$\rho_{\xi,\eta}$
				2994276656640	228.904 ± 0.124	188.827 ± 0.103	17020.1 ± 0.5	-717.9 ± 0.5	-0.171
				3196128030848	38.628 ± 0.124	193.924 ± 0.102	4820.2 ± 0.6	20422.3 ± 0.6	-0.194
			icytb2081	2994277277824	131.830 ± 0.125	162.810 ± 0.102	7680.7 ± 1.9	8159.0 ± 2.1	-0.390
				2994268530304	57.857 ± 0.125	120.880 ± 0.102	-1864.1 ± 4.1	13407.7 ± 8.2	-0.175
				2994277298816	63.871 ± 0.125	155.533 ± 0.103	2313.3 ± 5.4	15087.3 ± 4.6	0.034
				2994266748800	261.643 ± 0.125	114.399 ± 0.104	11090.2 ± 5.2	-9291.2 ± 3.4	-0.073
				2994276656640	228.882 ± 0.125	188.708 ± 0.102	17020.1 ± 0.5	-717.9 ± 0.5	-0.171
				3196128030848	38.671 ± 0.124	193.868 ± 0.103	4820.2 ± 0.6	20422.3 ± 0.6	-0.196
			icytb3021	2994277277824	148.123 ± 0.127	161.980 ± 0.103	7680.7 ± 1.9	8159.0 ± 2.1	-0.390
				2994268530304	63.433 ± 0.125	155.045 ± 0.103	-1864.1 ± 4.1	13407.7 ± 8.2	-0.176
				2994277298816	83.236 ± 0.126	183.958 ± 0.103	2313.2 ± 5.4	15087.3 ± 4.6	0.037
				2994266748800	245.201 ± 0.126	63.077 ± 0.102	11090.2 ± 5.2	-9291.2 ± 3.4	-0.073
				2994276656640	246.952 ± 0.126	144.342 ± 0.102	17020.1 ± 0.5	-717.9 ± 0.5	-0.170
				2994265535104	33.060 ± 0.123	182.443 ± 0.102	-3167.9 ± 2.2	18490.1 ± 2.1	-0.345
				3196128030848	76.796 ± 0.126	229.498 ± 0.102	4820.2 ± 0.6	20422.3 ± 0.6	-0.195
			icytb3051	2994277277824	148.078 ± 0.126	161.965 ± 0.104	7680.7 ± 1.9	8159.0 ± 2.1	-0.389
				2994268530304	63.390 ± 0.124	155.060 ± 0.103	-1864.1 ± 4.1	13407.7 ± 8.2	-0.175
				2994277298816	83.229 ± 0.124	183.971 ± 0.103	2313.3 ± 5.4	15087.3 ± 4.6	0.036
				2994266748800	245.179 ± 0.124	63.106 ± 0.102	11090.2 ± 5.2	-9291.2 ± 3.4	-0.073
				2994276656640	246.926 ± 0.127	144.329 ± 0.102	17020.1 ± 0.5	-717.9 ± 0.5	-0.170
				2994265535104	33.075 ± 0.125	182.427 ± 0.102	-3167.9 ± 2.2	18490.1 ± 2.1	-0.345
				3196128030848	76.803 ± 0.123	229.466 ± 0.103	4820.2 ± 0.6	20422.3 ± 0.6	-0.194
			icytb3081	2994277277824	148.101 ± 0.124	161.947 ± 0.102	7680.7 ± 1.9	8159.0 ± 2.1	-0.388
				2994268530304	63.365 ± 0.126	155.020 ± 0.103	-1864.1 ± 4.1	13407.7 ± 8.2	-0.176
				2994277298816	83.226 ± 0.125	183.942 ± 0.102	2313.3 ± 5.4	15087.3 ± 4.6	0.036
				2994266748800	245.155 ± 0.125	63.070 ± 0.103	11090.2 ± 5.2	-9291.2 ± 3.4	-0.070
				2994276656640	246.987 ± 0.124	144.306 ± 0.102	17020.1 ± 0.5	-717.9 ± 0.5	-0.169
				2994265535104	33.056 ± 0.126	182.417 ± 0.102	-3167.9 ± 2.2	18490.1 ± 2.1	-0.344
				3196128030848	76.788 ± 0.125	229.444 ± 0.103	4820.2 ± 0.6	20422.3 ± 0.6	-0.194
			icytb4021	2994277277824	131.477 ± 0.124	162.347 ± 0.101	7680.7 ± 1.9	8159.0 ± 2.1	-0.388
				2994268530304	57.555 ± 0.124	120.471 ± 0.102	-1864.1 ± 4.1	13407.7 ± 8.2	-0.175
				2994277298816	63.636 ± 0.126	155.046 ± 0.104	2313.3 ± 5.4	15087.3 ± 4.6	0.036
				2994266748800	261.156 ± 0.125	113.917 ± 0.102	11090.2 ± 5.3	-9291.2 ± 3.4	-0.074
				2994276656640	228.501 ± 0.127	188.374 ± 0.103	17020.1 ± 0.5	-717.9 ± 0.5	-0.171
				3196128030848	38.405 ± 0.124	193.620 ± 0.102	4820.2 ± 0.6	20422.3 ± 0.6	-0.194
			icytb4051	2994277277824	131.467 ± 0.123	162.438 ± 0.100	7680.7 ± 1.9	8159.0 ± 2.1	-0.388
				2994268530304	57.510 ± 0.127	120.474 ± 0.103	-1864.1 ± 4.1	13407.6 ± 8.2	-0.177
				2994277298816	63.632 ± 0.126	155.057 ± 0.103	2313.3 ± 5.4	15087.3 ± 4.6	0.035
				2994266748800	261.150 ± 0.125	113.883 ± 0.102	11090.2 ± 5.2	-9291.2 ± 3.4	-0.073
				2994276656640	228.513 ± 0.126	188.313 ± 0.102	17020.1 ± 0.5	-717.9 ± 0.5	-0.170
				3196128030848	38.192 ± 0.127	193.541 ± 0.103	4820.2 ± 0.6	20422.3 ± 0.6	-0.195
			icytb4081	2994277277824	131.479 ± 0.125	162.403 ± 0.102	7680.7 ± 1.9	8159.0 ± 2.1	-0.387
				2994268530304	57.476 ± 0.126	120.464 ± 0.104	-1864.1 ± 4.1	13407.7 ± 8.2	-0.175
				2994277298816	63.611 ± 0.125	155.065 ± 0.102	2313.3 ± 5.4	15087.3 ± 4.6	0.037
				2994266748800	261.169 ± 0.124	113.934 ± 0.102	11090.2 ± 5.2	-9291.2 ± 3.4	-0.071
				2994276656640	228.400 ± 0.125	188.430 ± 0.102	17020.1 ± 0.5	-717.9 ± 0.5	-0.171

Table C1 continued

Table C1 (continued)

Instrument	Date	Filter	Image	<i>Gaia</i> DR2 Source (607290-)	x (px)	y (px)	ξ (mas)	η (mas)	$\rho_{\xi,\eta}$
				3196128030848	38.212 ± 0.125	193.535 ± 0.103	4820.2 ± 0.6	20422.3 ± 0.6	-0.196
			icytb5021	2994277277824	147.714 ± 0.126	162.122 ± 0.102	7680.7 ± 1.9	8159.0 ± 2.1	-0.390
				2994268530304	63.111 ± 0.126	155.211 ± 0.102	-1864.1 ± 4.1	13407.7 ± 8.2	-0.177
				2994277298816	83.095 ± 0.124	184.102 ± 0.103	2313.3 ± 5.4	15087.3 ± 4.6	0.035
				2994266748800	244.918 ± 0.125	63.307 ± 0.103	11090.2 ± 5.2	-9291.2 ± 3.4	-0.072
				2994276656640	246.776 ± 0.126	144.669 ± 0.102	17020.1 ± 0.5	-717.9 ± 0.5	-0.172
				2994265535104	32.599 ± 0.125	182.687 ± 0.103	-3167.9 ± 2.2	18490.1 ± 2.1	-0.344
				3196128030848	76.444 ± 0.126	229.641 ± 0.103	4820.2 ± 0.6	20422.3 ± 0.6	-0.195
			icytb5051	2994277277824	147.726 ± 0.125	162.107 ± 0.101	7680.7 ± 1.9	8159.0 ± 2.1	-0.391
				2994268530304	63.103 ± 0.128	155.164 ± 0.102	-1864.1 ± 4.1	13407.7 ± 8.2	-0.175
				2994277298816	83.080 ± 0.126	184.094 ± 0.102	2313.3 ± 5.4	15087.3 ± 4.6	0.036
				2994266748800	244.947 ± 0.124	63.348 ± 0.101	11090.2 ± 5.2	-9291.2 ± 3.4	-0.072
				2994276656640	246.755 ± 0.124	144.682 ± 0.103	17020.1 ± 0.5	-717.9 ± 0.5	-0.171
				2994265535104	32.606 ± 0.123	182.708 ± 0.104	-3167.9 ± 2.2	18490.1 ± 2.1	-0.345
				3196128030848	76.545 ± 0.122	229.639 ± 0.102	4820.2 ± 0.6	20422.3 ± 0.6	-0.194
			icytb5081	2994277277824	147.664 ± 0.126	162.094 ± 0.103	7680.7 ± 1.9	8159.0 ± 2.1	-0.391
				2994268530304	62.931 ± 0.127	155.215 ± 0.103	-1864.1 ± 4.1	13407.6 ± 8.2	-0.175
				2994277298816	83.103 ± 0.125	184.081 ± 0.103	2313.3 ± 5.4	15087.3 ± 4.6	0.037
				2994266748800	244.962 ± 0.124	63.300 ± 0.101	11090.2 ± 5.2	-9291.2 ± 3.4	-0.073
				2994276656640	246.735 ± 0.126	144.596 ± 0.102	17020.1 ± 0.5	-717.9 ± 0.5	-0.171
				2994265535104	32.568 ± 0.125	182.621 ± 0.104	-3167.9 ± 2.2	18490.1 ± 2.1	-0.346
				3196128030848	76.401 ± 0.124	229.641 ± 0.103	4820.2 ± 0.6	20422.3 ± 0.6	-0.195
			icytb6021	2994277277824	131.739 ± 0.127	162.936 ± 0.102	7680.7 ± 1.9	8159.0 ± 2.1	-0.390
				2994268530304	58.029 ± 0.124	120.937 ± 0.102	-1864.1 ± 4.1	13407.7 ± 8.2	-0.177
				2994277298816	63.891 ± 0.123	155.553 ± 0.102	2313.2 ± 5.4	15087.3 ± 4.6	0.034
				2994266748800	261.606 ± 0.125	114.462 ± 0.102	11090.2 ± 5.2	-9291.2 ± 3.4	-0.073
				2994276656640	228.877 ± 0.122	188.760 ± 0.102	17020.1 ± 0.5	-717.9 ± 0.5	-0.170
				3196128030848	38.692 ± 0.123	193.861 ± 0.101	4820.2 ± 0.6	20422.3 ± 0.6	-0.194
			icytb6051	2994277277824	132.131 ± 0.123	162.410 ± 0.102	7680.7 ± 1.9	8159.0 ± 2.1	-0.388
				2994268530304	58.788 ± 0.125	120.144 ± 0.103	-1864.1 ± 4.1	13407.7 ± 8.2	-0.175
				2994277298816	64.457 ± 0.135	154.857 ± 0.115	2313.3 ± 5.4	15087.3 ± 4.6	0.035
				2994266748800	261.596 ± 0.124	114.102 ± 0.102	11090.2 ± 5.2	-9291.2 ± 3.4	-0.071
				2994276656640	229.009 ± 0.123	188.247 ± 0.103	17020.1 ± 0.5	-717.9 ± 0.5	-0.170
			icytb6081	2994277277824	131.730 ± 0.123	162.893 ± 0.102	7680.7 ± 1.9	8159.0 ± 2.1	-0.389
				2994268530304	57.919 ± 0.124	120.883 ± 0.103	-1864.1 ± 4.1	13407.7 ± 8.2	-0.177
				2994277298816	63.892 ± 0.125	155.540 ± 0.104	2313.3 ± 5.4	15087.3 ± 4.6	0.034
				2994266748800	261.644 ± 0.123	114.442 ± 0.102	11090.2 ± 5.2	-9291.2 ± 3.4	-0.074
				2994276656640	228.888 ± 0.124	188.713 ± 0.102	17020.1 ± 0.5	-717.9 ± 0.5	-0.170
				3196128030848	38.614 ± 0.123	193.879 ± 0.103	4820.2 ± 0.6	20422.3 ± 0.6	-0.195
			icytb7021	2994277277824	147.828 ± 0.125	162.211 ± 0.103	7680.7 ± 1.9	8159.0 ± 2.1	-0.389
				2994268530304	63.118 ± 0.125	155.279 ± 0.103	-1864.1 ± 4.1	13407.7 ± 8.2	-0.174
				2994277298816	83.073 ± 0.126	184.201 ± 0.103	2313.3 ± 5.4	15087.3 ± 4.6	0.037
				2994266748800	244.950 ± 0.125	63.500 ± 0.102	11090.2 ± 5.3	-9291.2 ± 3.4	-0.072
				2994276656640	246.758 ± 0.123	144.763 ± 0.103	17020.1 ± 0.5	-717.9 ± 0.5	-0.172
				2994265535104	32.700 ± 0.124	182.826 ± 0.103	-3167.9 ± 2.2	18490.1 ± 2.1	-0.346
				3196128030848	76.495 ± 0.126	229.806 ± 0.102	4820.2 ± 0.6	20422.3 ± 0.6	-0.194

Table C1 continued

Table C1 (continued)

Instrument	Date	Filter	Image	<i>Gaia</i> DR2 Source (607290-)	x (px)	y (px)	ξ (mas)	η (mas)	$\rho_{\xi,\eta}$	
			icytb7051	2994277277824	147.640 ± 0.124	162.188 ± 0.103	7680.7 ± 1.9	8159.0 ± 2.1	-0.391	
				2994268530304	63.036 ± 0.126	155.408 ± 0.102	-1864.1 ± 4.1	13407.7 ± 8.2	-0.174	
				2994277298816	83.056 ± 0.124	184.189 ± 0.102	2313.2 ± 5.4	15087.3 ± 4.6	0.034	
				2994266748800	244.974 ± 0.123	63.532 ± 0.102	11090.2 ± 5.2	-9291.2 ± 3.4	-0.072	
				2994276656640	246.714 ± 0.125	144.801 ± 0.102	17020.1 ± 0.5	-717.9 ± 0.5	-0.170	
				2994265535104	32.686 ± 0.126	182.766 ± 0.102	-3167.9 ± 2.2	18490.1 ± 2.1	-0.345	
			3196128030848	76.508 ± 0.123	229.773 ± 0.102	4820.2 ± 0.6	20422.3 ± 0.6	-0.195		
			icytb7081	2994277277824	147.800 ± 0.127	162.193 ± 0.102	7680.7 ± 1.9	8159.0 ± 2.1	-0.388	
				2994268530304	63.069 ± 0.124	155.305 ± 0.103	-1864.1 ± 4.1	13407.7 ± 8.2	-0.176	
				2994277298816	83.061 ± 0.124	184.151 ± 0.102	2313.3 ± 5.4	15087.3 ± 4.6	0.034	
				2994266748800	244.937 ± 0.125	63.507 ± 0.103	11090.2 ± 5.2	-9291.2 ± 3.4	-0.072	
				2994276656640	246.736 ± 0.125	144.794 ± 0.102	17020.1 ± 0.5	-717.9 ± 0.5	-0.171	
				2994265535104	32.721 ± 0.124	182.748 ± 0.103	-3167.9 ± 2.2	18490.1 ± 2.1	-0.345	
			3196128030848	76.517 ± 0.124	229.715 ± 0.102	4820.2 ± 0.6	20422.3 ± 0.6	-0.195		
			icytb8021	2994277277824	132.013 ± 0.123	162.833 ± 0.102	7680.7 ± 1.9	8159.0 ± 2.1	-0.389	
				2994268530304	58.265 ± 0.125	120.727 ± 0.102	-1864.1 ± 4.1	13407.7 ± 8.2	-0.178	
				2994277298816	64.171 ± 0.127	155.378 ± 0.104	2313.3 ± 5.4	15087.3 ± 4.6	0.036	
				2994266748800	261.627 ± 0.123	114.530 ± 0.103	11090.2 ± 5.2	-9291.2 ± 3.4	-0.073	
				2994276656640	229.118 ± 0.126	188.997 ± 0.101	17020.1 ± 0.5	-717.9 ± 0.5	-0.171	
				3196128030848	38.796 ± 0.124	193.694 ± 0.102	4820.2 ± 0.6	20422.3 ± 0.6	-0.195	
			icytb8051	2994277277824	131.679 ± 0.123	162.743 ± 0.101	7680.7 ± 1.9	8159.0 ± 2.1	-0.390	
				2994268530304	57.790 ± 0.125	120.766 ± 0.102	-1864.1 ± 4.1	13407.7 ± 8.2	-0.176	
				2994277298816	63.838 ± 0.125	155.398 ± 0.104	2313.3 ± 5.4	15087.3 ± 4.6	0.034	
				2994266748800	261.447 ± 0.125	114.250 ± 0.101	11090.2 ± 5.2	-9291.2 ± 3.4	-0.073	
				2994276656640	228.840 ± 0.122	188.514 ± 0.102	17020.1 ± 0.5	-717.9 ± 0.5	-0.171	
				3196128030848	38.591 ± 0.123	193.772 ± 0.102	4820.2 ± 0.6	20422.3 ± 0.6	-0.195	
			icytb8081	2994277277824	131.608 ± 0.125	162.772 ± 0.102	7680.7 ± 1.9	8159.0 ± 2.1	-0.390	
				2994268530304	57.794 ± 0.125	120.747 ± 0.105	-1864.1 ± 4.1	13407.7 ± 8.2	-0.175	
				2994277298816	63.791 ± 0.125	155.202 ± 0.103	2313.3 ± 5.4	15087.3 ± 4.6	0.036	
				2994266748800	261.476 ± 0.127	114.209 ± 0.101	11090.2 ± 5.2	-9291.2 ± 3.4	-0.072	
				2994276656640	228.763 ± 0.124	188.612 ± 0.103	17020.1 ± 0.5	-717.9 ± 0.5	-0.171	
				3196128030848	38.536 ± 0.125	193.756 ± 0.103	4820.2 ± 0.6	20422.3 ± 0.6	-0.194	
		f153m	icytb2031	2994277277824	131.707 ± 0.090	163.016 ± 0.078	7680.7 ± 1.9	8159.0 ± 2.1	-0.388	
					2994268530304	57.904 ± 0.092	121.019 ± 0.080	-1864.1 ± 4.1	13407.7 ± 8.2	-0.175
					2994277298816	63.864 ± 0.093	155.620 ± 0.080	2313.2 ± 5.4	15087.3 ± 4.6	0.035
					2994266748800	261.571 ± 0.092	114.547 ± 0.080	11090.2 ± 5.2	-9291.2 ± 3.4	-0.073
					2994276656640	228.870 ± 0.092	188.988 ± 0.080	17020.1 ± 0.5	-717.9 ± 0.5	-0.172
					3196128030848	38.616 ± 0.093	193.997 ± 0.079	4820.2 ± 0.6	20422.3 ± 0.6	-0.198
			icytb2061	2994277277824	131.712 ± 0.091	162.881 ± 0.080	7680.7 ± 1.9	8159.0 ± 2.1	-0.388	
				2994268530304	57.849 ± 0.090	120.844 ± 0.082	-1864.1 ± 4.1	13407.7 ± 8.2	-0.176	
				2994277298816	63.742 ± 0.095	155.450 ± 0.084	2313.3 ± 5.4	15087.3 ± 4.6	0.035	
			2994276656640	228.947 ± 0.092	188.822 ± 0.080	17020.1 ± 0.5	-717.9 ± 0.5	-0.170		
			icytb2091	2994277277824	131.699 ± 0.091	162.996 ± 0.080	7680.7 ± 1.9	8159.0 ± 2.1	-0.388	
				2994268530304	57.784 ± 0.093	120.951 ± 0.082	-1864.1 ± 4.1	13407.7 ± 8.2	-0.175	
				2994277298816	63.833 ± 0.093	155.654 ± 0.081	2313.2 ± 5.4	15087.3 ± 4.6	0.037	
			2994266748800	261.475 ± 0.091	114.523 ± 0.081	11090.2 ± 5.2	-9291.2 ± 3.4	-0.073		

Table C1 continued

Table C1 (continued)

Instrument	Date	Filter	Image	<i>Gaia</i> DR2 Source (607290-)	x (px)	y (px)	ξ (mas)	η (mas)	$\rho_{\xi,\eta}$
				2994276656640	228.846 ± 0.090	188.796 ± 0.080	17020.1 ± 0.5	-717.9 ± 0.5	-0.171
				3196128030848	38.538 ± 0.092	193.993 ± 0.081	4820.2 ± 0.6	20422.3 ± 0.6	-0.194
			icytb3031	2994277277824	147.988 ± 0.091	162.096 ± 0.080	7680.7 ± 1.9	8159.0 ± 2.1	-0.391
				2994268530304	63.350 ± 0.094	155.214 ± 0.082	-1864.1 ± 4.1	13407.6 ± 8.2	-0.175
				2994277298816	83.194 ± 0.092	184.056 ± 0.081	2313.2 ± 5.4	15087.3 ± 4.6	0.035
				2994266748800	245.197 ± 0.094	63.264 ± 0.081	11090.2 ± 5.2	-9291.2 ± 3.4	-0.074
				2994276656640	246.922 ± 0.093	144.586 ± 0.080	17020.1 ± 0.5	-717.9 ± 0.5	-0.171
				2994265535104	32.898 ± 0.092	182.657 ± 0.082	-3167.9 ± 2.2	18490.1 ± 2.1	-0.344
				3196128030848	76.761 ± 0.092	229.624 ± 0.079	4820.2 ± 0.6	20422.3 ± 0.6	-0.196
			icytb3061	2994277277824	148.016 ± 0.093	162.056 ± 0.080	7680.7 ± 1.9	8159.0 ± 2.1	-0.392
				2994268530304	63.325 ± 0.093	155.196 ± 0.082	-1864.1 ± 4.1	13407.7 ± 8.2	-0.176
				2994277298816	83.229 ± 0.091	184.039 ± 0.081	2313.2 ± 5.4	15087.3 ± 4.6	0.033
				2994266748800	245.140 ± 0.091	63.244 ± 0.081	11090.2 ± 5.2	-9291.2 ± 3.4	-0.072
				2994276656640	246.829 ± 0.093	144.524 ± 0.081	17020.1 ± 0.5	-717.9 ± 0.5	-0.172
				2994265535104	32.868 ± 0.093	182.670 ± 0.082	-3167.9 ± 2.2	18490.1 ± 2.1	-0.346
				3196128030848	76.760 ± 0.092	229.589 ± 0.080	4820.2 ± 0.6	20422.3 ± 0.6	-0.195
			icytb3091	2994277277824	148.063 ± 0.093	162.015 ± 0.081	7680.7 ± 1.9	8159.0 ± 2.1	-0.388
				2994268530304	63.340 ± 0.098	155.205 ± 0.085	-1864.1 ± 4.1	13407.7 ± 8.2	-0.177
				2994277298816	83.215 ± 0.092	183.990 ± 0.082	2313.2 ± 5.4	15087.3 ± 4.6	0.035
				2994266748800	245.125 ± 0.093	63.137 ± 0.081	11090.2 ± 5.2	-9291.2 ± 3.4	-0.073
				2994276656640	246.894 ± 0.092	144.406 ± 0.080	17020.1 ± 0.5	-717.9 ± 0.5	-0.172
				2994265535104	32.948 ± 0.092	182.520 ± 0.082	-3167.9 ± 2.2	18490.1 ± 2.1	-0.346
				3196128030848	76.754 ± 0.094	229.429 ± 0.080	4820.2 ± 0.6	20422.3 ± 0.6	-0.195
			icytb4031	2994277277824	131.479 ± 0.091	162.564 ± 0.080	7680.7 ± 1.9	8159.0 ± 2.1	-0.390
				2994268530304	57.468 ± 0.094	120.578 ± 0.082	-1864.1 ± 4.1	13407.7 ± 8.2	-0.175
				2994277298816	63.378 ± 0.102	155.113 ± 0.095	2313.2 ± 5.4	15087.3 ± 4.6	0.036
				2994266748800	261.447 ± 0.094	114.310 ± 0.082	11090.2 ± 5.3	-9291.2 ± 3.4	-0.073
				2994276656640	228.546 ± 0.092	188.252 ± 0.080	17020.1 ± 0.5	-717.9 ± 0.5	-0.170
				3196128030848	37.893 ± 0.091	193.324 ± 0.080	4820.2 ± 0.6	20422.3 ± 0.6	-0.194
			icytb4061	2994277277824	131.418 ± 0.092	162.735 ± 0.079	7680.7 ± 1.9	8159.0 ± 2.1	-0.389
				2994268530304	57.394 ± 0.093	120.713 ± 0.080	-1864.1 ± 4.1	13407.7 ± 8.2	-0.176
				2994277298816	63.596 ± 0.096	155.274 ± 0.083	2313.3 ± 5.4	15087.3 ± 4.6	0.037
				2994266748800	261.142 ± 0.093	114.169 ± 0.079	11090.2 ± 5.2	-9291.2 ± 3.4	-0.071
				2994276656640	228.278 ± 0.093	188.530 ± 0.081	17020.1 ± 0.5	-717.9 ± 0.5	-0.171
				3196128030848	38.232 ± 0.094	193.730 ± 0.081	4820.2 ± 0.6	20422.3 ± 0.6	-0.193
			icytb4091 ^a	2994277277824	132.854 ± 0.092	162.562 ± 0.080	7680.7 ± 1.9	8159.0 ± 2.1	-0.389
				2994268530304	58.500 ± 0.093	120.498 ± 0.083	-1864.1 ± 4.1	13407.7 ± 8.2	-0.176
				2994277298816	64.554 ± 0.096	154.976 ± 0.088	2313.2 ± 5.4	15087.3 ± 4.6	0.035
				2994266748800	263.131 ± 0.091	114.172 ± 0.081	11090.2 ± 5.2	-9291.2 ± 3.4	-0.073
				2994276656640	230.456 ± 0.093	188.457 ± 0.080	17020.1 ± 0.5	-717.9 ± 0.5	-0.170
				3196128030848	39.454 ± 0.093	193.370 ± 0.081	4820.2 ± 0.6	20422.3 ± 0.6	-0.194
			icytb5031	2994277277824	147.742 ± 0.092	162.257 ± 0.081	7680.7 ± 1.9	8159.0 ± 2.1	-0.388
				2994268530304	63.088 ± 0.094	155.381 ± 0.083	-1864.1 ± 4.1	13407.6 ± 8.2	-0.177
				2994277298816	83.072 ± 0.091	184.221 ± 0.081	2313.2 ± 5.4	15087.3 ± 4.6	0.036
				2994266748800	244.966 ± 0.092	63.485 ± 0.080	11090.2 ± 5.2	-9291.2 ± 3.4	-0.073
				2994276656640	246.703 ± 0.091	144.806 ± 0.081	17020.1 ± 0.5	-717.9 ± 0.5	-0.171

Table C1 continued

Table C1 (continued)

Instrument	Date	Filter	Image	<i>Gaia</i> DR2 Source (607290-)	x (px)	y (px)	ξ (mas)	η (mas)	$\rho_{\xi,\eta}$
				2994265535104	32.748 ± 0.095	182.775 ± 0.081	-3167.9 ± 2.2	18490.1 ± 2.1	-0.344
				3196128030848	76.416 ± 0.090	229.802 ± 0.081	4820.2 ± 0.6	20422.3 ± 0.6	-0.195
			icytb5061	2994277277824	147.739 ± 0.092	162.233 ± 0.082	7680.7 ± 1.9	8159.0 ± 2.1	-0.391
				2994268530304	63.129 ± 0.096	155.356 ± 0.084	-1864.1 ± 4.1	13407.6 ± 8.2	-0.175
				2994277298816	83.063 ± 0.093	184.217 ± 0.081	2313.2 ± 5.4	15087.3 ± 4.6	0.038
				2994266748800	244.970 ± 0.092	63.416 ± 0.081	11090.2 ± 5.2	-9291.2 ± 3.4	-0.074
				2994276656640	246.693 ± 0.093	144.784 ± 0.080	17020.1 ± 0.5	-717.9 ± 0.5	-0.171
				2994265535104	32.630 ± 0.092	182.792 ± 0.082	-3167.9 ± 2.2	18490.1 ± 2.1	-0.346
				3196128030848	76.426 ± 0.092	229.774 ± 0.081	4820.2 ± 0.6	20422.3 ± 0.6	-0.195
			icytb5091	2994277277824	147.625 ± 0.094	162.156 ± 0.081	7680.7 ± 1.9	8159.0 ± 2.1	-0.389
				2994268530304	63.036 ± 0.096	155.314 ± 0.086	-1864.1 ± 4.1	13407.7 ± 8.2	-0.175
				2994277298816	83.030 ± 0.093	184.190 ± 0.081	2313.3 ± 5.4	15087.3 ± 4.6	0.035
				2994266748800	244.992 ± 0.092	63.446 ± 0.081	11090.2 ± 5.2	-9291.2 ± 3.4	-0.073
				2994276656640	246.690 ± 0.091	144.811 ± 0.080	17020.1 ± 0.5	-717.9 ± 0.5	-0.169
				2994265535104	32.593 ± 0.094	182.805 ± 0.083	-3167.9 ± 2.2	18490.1 ± 2.1	-0.345
				3196128030848	76.416 ± 0.091	229.743 ± 0.080	4820.2 ± 0.6	20422.3 ± 0.6	-0.195
			icytb6031 ^a	2994277277824	132.279 ± 0.091	163.268 ± 0.080	7680.7 ± 1.9	8159.0 ± 2.1	-0.389
				2994268530304	58.476 ± 0.094	121.064 ± 0.084	-1864.1 ± 4.1	13407.6 ± 8.2	-0.175
				2994277298816	64.020 ± 0.099	155.927 ± 0.087	2313.3 ± 5.4	15087.3 ± 4.6	0.036
				2994266748800	262.496 ± 0.093	115.009 ± 0.082	11090.2 ± 5.3	-9291.2 ± 3.4	-0.072
				2994276656640	229.503 ± 0.092	189.506 ± 0.080	17020.1 ± 0.5	-717.9 ± 0.5	-0.171
				3196128030848	39.089 ± 0.094	194.097 ± 0.079	4820.2 ± 0.6	20422.3 ± 0.6	-0.195
			icytb6061	2994277277824	131.758 ± 0.090	163.000 ± 0.080	7680.7 ± 1.9	8159.0 ± 2.1	-0.390
				2994268530304	57.967 ± 0.093	121.005 ± 0.081	-1864.1 ± 4.1	13407.6 ± 8.2	-0.174
				2994277298816	63.874 ± 0.092	155.630 ± 0.081	2313.3 ± 5.4	15087.3 ± 4.6	0.035
				2994266748800	261.625 ± 0.089	114.499 ± 0.079	11090.2 ± 5.2	-9291.2 ± 3.4	-0.072
				2994276656640	228.875 ± 0.092	188.911 ± 0.081	17020.1 ± 0.5	-717.9 ± 0.5	-0.171
				3196128030848	38.549 ± 0.093	194.018 ± 0.081	4820.2 ± 0.6	20422.3 ± 0.6	-0.194
			icytb6091 ^a	2994277277824	131.784 ± 0.091	162.999 ± 0.080	7680.7 ± 1.9	8159.0 ± 2.1	-0.391
				2994268530304	58.009 ± 0.095	121.356 ± 0.082	-1864.1 ± 4.1	13407.7 ± 8.2	-0.177
				2994277298816	63.961 ± 0.093	155.793 ± 0.082	2313.2 ± 5.4	15087.3 ± 4.6	0.036
				2994266748800	261.372 ± 0.093	114.216 ± 0.081	11090.2 ± 5.2	-9291.2 ± 3.4	-0.074
				2994276656640	228.969 ± 0.093	188.336 ± 0.080	17020.1 ± 0.5	-717.9 ± 0.5	-0.170
				3196128030848	38.686 ± 0.092	194.263 ± 0.080	4820.2 ± 0.6	20422.3 ± 0.6	-0.194
			icytb7031	2994277277824	147.684 ± 0.090	162.298 ± 0.080	7680.7 ± 1.9	8159.0 ± 2.1	-0.387
				2994268530304	63.164 ± 0.094	155.505 ± 0.083	-1864.1 ± 4.1	13407.7 ± 8.2	-0.175
				2994277298816	83.060 ± 0.093	184.324 ± 0.081	2313.2 ± 5.4	15087.3 ± 4.6	0.036
				2994266748800	244.955 ± 0.093	63.618 ± 0.080	11090.2 ± 5.2	-9291.2 ± 3.4	-0.073
				2994276656640	246.640 ± 0.092	144.906 ± 0.080	17020.1 ± 0.5	-717.9 ± 0.5	-0.171
				2994265535104	32.723 ± 0.092	182.886 ± 0.082	-3167.9 ± 2.2	18490.1 ± 2.1	-0.345
				3196128030848	76.476 ± 0.091	229.948 ± 0.080	4820.2 ± 0.6	20422.3 ± 0.6	-0.195
			icytb7061	2994277277824	147.724 ± 0.091	162.370 ± 0.081	7680.7 ± 1.9	8159.0 ± 2.1	-0.389
				2994268530304	63.044 ± 0.092	155.573 ± 0.081	-1864.1 ± 4.1	13407.6 ± 8.2	-0.178
				2994277298816	83.045 ± 0.093	184.340 ± 0.081	2313.3 ± 5.4	15087.3 ± 4.6	0.033
				2994266748800	244.954 ± 0.092	63.660 ± 0.080	11090.2 ± 5.2	-9291.2 ± 3.4	-0.072
				2994276656640	246.607 ± 0.092	144.871 ± 0.080	17020.1 ± 0.5	-717.9 ± 0.5	-0.170

Table C1 continued

Table C1 (continued)

Instrument	Date	Filter	Image	<i>Gaia</i> DR2 Source (607290-)	x (px)	y (px)	ξ (mas)	η (mas)	$\rho_{\xi,\eta}$
				2994265535104	32.692 ± 0.091	182.987 ± 0.081	-3167.9 ± 2.2	18490.1 ± 2.1	-0.346
				3196128030848	76.372 ± 0.093	229.898 ± 0.081	4820.2 ± 0.6	20422.3 ± 0.6	-0.194
			icytb7091	2994277277824	147.635 ± 0.093	162.274 ± 0.081	7680.7 ± 1.9	8159.0 ± 2.1	-0.388
				2994268530304	62.963 ± 0.093	155.540 ± 0.082	-1864.1 ± 4.1	13407.7 ± 8.2	-0.177
				2994277298816	83.019 ± 0.095	184.343 ± 0.082	2313.2 ± 5.4	15087.3 ± 4.6	0.036
				2994266748800	244.900 ± 0.093	63.635 ± 0.081	11090.2 ± 5.2	-9291.2 ± 3.4	-0.073
				2994276656640	246.603 ± 0.094	144.882 ± 0.079	17020.1 ± 0.5	-717.9 ± 0.5	-0.172
				2994265535104	32.625 ± 0.092	182.924 ± 0.082	-3167.9 ± 2.2	18490.1 ± 2.1	-0.346
				3196128030848	76.351 ± 0.093	229.939 ± 0.081	4820.2 ± 0.6	20422.3 ± 0.6	-0.195
			icytb8031	2994277277824	131.582 ± 0.093	162.919 ± 0.080	7680.7 ± 1.9	8159.0 ± 2.1	-0.389
				2994268530304	57.774 ± 0.092	120.875 ± 0.080	-1864.1 ± 4.1	13407.7 ± 8.2	-0.175
				2994277298816	63.814 ± 0.094	155.486 ± 0.082	2313.3 ± 5.4	15087.3 ± 4.6	0.036
				2994266748800	261.462 ± 0.092	114.380 ± 0.080	11090.2 ± 5.2	-9291.2 ± 3.4	-0.072
				2994276656640	228.806 ± 0.095	188.743 ± 0.080	17020.1 ± 0.5	-717.9 ± 0.5	-0.170
				3196128030848	38.596 ± 0.092	193.874 ± 0.081	4820.2 ± 0.6	20422.3 ± 0.6	-0.195
			icytb8061	2994277277824	131.619 ± 0.093	162.833 ± 0.079	7680.7 ± 1.9	8159.0 ± 2.1	-0.389
				2994268530304	57.807 ± 0.094	120.862 ± 0.081	-1864.1 ± 4.1	13407.7 ± 8.2	-0.175
				2994277298816	63.774 ± 0.093	155.464 ± 0.083	2313.2 ± 5.4	15087.3 ± 4.6	0.037
				2994266748800	261.409 ± 0.091	114.359 ± 0.081	11090.2 ± 5.2	-9291.2 ± 3.4	-0.074
				2994276656640	228.772 ± 0.093	188.800 ± 0.080	17020.1 ± 0.5	-717.9 ± 0.5	-0.170
				3196128030848	38.534 ± 0.092	193.837 ± 0.081	4820.2 ± 0.6	20422.3 ± 0.6	-0.196
			icytb8091	2994277277824	131.578 ± 0.090	162.902 ± 0.080	7680.7 ± 1.9	8159.0 ± 2.1	-0.390
				2994268530304	57.688 ± 0.092	120.848 ± 0.082	-1864.1 ± 4.1	13407.7 ± 8.2	-0.176
				2994277298816	63.755 ± 0.091	155.470 ± 0.082	2313.3 ± 5.4	15087.3 ± 4.6	0.036
				2994266748800	261.284 ± 0.092	114.440 ± 0.081	11090.2 ± 5.2	-9291.2 ± 3.4	-0.075
				2994276656640	228.741 ± 0.093	188.631 ± 0.081	17020.1 ± 0.5	-717.9 ± 0.5	-0.171
				3196128030848	38.453 ± 0.093	193.843 ± 0.081	4820.2 ± 0.6	20422.3 ± 0.6	-0.196

^a Image removed from analysis due to poor data quality.

Table C2. Fit parameters for the ACS epoch.

Property	Unit	No prior	With prior
x_0^{acq}	px	$570.25^{+0.23}_{-0.24}$	$569.91^{+0.20}_{-0.20}$
y_0^{acq}	px	$592.24^{+0.25}_{-0.25}$	$592.20^{+0.20}_{-0.20}$
θ_N	deg	$\equiv -80.95$	$\equiv -80.95$
p_x	mas px ⁻¹	$\equiv 25.00$	$\equiv 25.00$
p_y	mas px ⁻¹	$\equiv 25.00$	$\equiv 25.00$
Δx	px	$54.375^{+0.017}_{-0.017}$	$54.375^{+0.017}_{-0.017}$
Δy	px	$-69.194^{+0.034}_{-0.034}$	$-69.194^{+0.034}_{-0.034}$
$\Delta\theta$	deg	$0.0037^{+0.0020}_{-0.0020}$	$0.0037^{+0.0020}_{-0.0020}$
χ_{gaia}^2	...	2.84	...
χ_{align}^2	...	14.92	14.92
x_0^{coro}	px	$624.59^{+0.23}_{-0.24}$	$624.25^{+0.20}_{-0.20}$
y_0^{coro}	px	$523.08^{+0.25}_{-0.25}$	$523.04^{+0.20}_{-0.20}$
$\rho_{x_0 y_0}$...	0.30	0.00
Δx_{106b}	px	$205.34^{+0.25}_{-0.25}$	$205.68^{+0.22}_{-0.22}$
Δy_{106b}	px	$-197.73^{+0.26}_{-0.26}$	$-197.70^{+0.22}_{-0.21}$
$\Delta\alpha_{106b}^*$	mas	$-5689.9^{+6.3}_{-6.3}$	$-5690.3^{+5.4}_{-5.3}$
$\Delta\delta_{106b}$	mas	$4291.2^{+6.6}_{-6.5}$	$4299.7^{+5.4}_{-5.4}$
ρ_{106b}	mas	$7126.6^{+5.5}_{-5.5}$	$7132.1^{+5.4}_{-5.4}$
θ_{106b}	deg	$307.023^{+0.058}_{-0.057}$	$307.076^{+0.043}_{-0.043}$
$\rho_{x_{106b} y_{106b}}$...	0.27	-0.00
$\rho_{\rho_{106b} \theta_{106b}}$...	-0.04	0.01

Table C3. Fit parameters for the STIS epoch.

Image	x_0 (px)	y_0 (px)	θ_N (deg)	p_x (mas px ⁻¹)	p_y (mas px ⁻¹)	χ^2_{ν}
od9t01010	565.74 ± 0.02	340.84 ± 0.03	84.769 ± 0.002	50.738 ± 0.002	50.766 ± 0.003	0.95
od9t01020	555.90 ± 0.02	340.85 ± 0.03	84.770 ± 0.002	50.732 ± 0.003	50.757 ± 0.003	0.91
od9t01030	230.61 ± 0.03	342.50 ± 0.03	84.764 ± 0.002	50.727 ± 0.003	50.757 ± 0.003	0.98
od9t03010	566.19 ± 0.02	340.85 ± 0.02	69.866 ± 0.003	50.745 ± 0.003	50.767 ± 0.003	1.05
od9t03020	556.30 ± 0.02	340.87 ± 0.02	69.865 ± 0.002	50.737 ± 0.003	50.759 ± 0.003	0.95
od9t03030	231.09 ± 0.03	342.61 ± 0.04	69.863 ± 0.003	50.724 ± 0.003	50.755 ± 0.004	0.84
od9t04010	566.15 ± 0.02	341.16 ± 0.03	54.865 ± 0.003	50.742 ± 0.003	50.763 ± 0.003	0.90
od9t04020	556.28 ± 0.02	341.17 ± 0.03	54.864 ± 0.002	50.735 ± 0.003	50.757 ± 0.003	0.86
od9t04030	231.04 ± 0.04	342.83 ± 0.05	54.866 ± 0.003	50.730 ± 0.003	50.751 ± 0.005	0.88

Table C4. Fit parameters for the WFC3 2016 epoch.

Image	x_0 (px)	y_0 (px)	χ^2_ν
icytb0011	170.84 ± 0.05	173.12 ± 0.04	0.30
icytb0041	170.82 ± 0.05	173.06 ± 0.04	0.15
icytb0071	170.86 ± 0.05	173.12 ± 0.04	0.27
icytb00a1	170.88 ± 0.06	173.08 ± 0.04	0.19
icytb1011	188.82 ± 0.06	149.87 ± 0.05	0.26
icytb1041	188.79 ± 0.07	149.89 ± 0.05	0.18
icytb1071	188.81 ± 0.06	149.89 ± 0.05	0.23
icytb10a1	188.79 ± 0.06	149.91 ± 0.05	0.27
icytb0021	170.84 ± 0.05	172.98 ± 0.04	0.17
icytb0051	170.85 ± 0.05	172.98 ± 0.04	0.29
icytb0081	170.86 ± 0.05	172.97 ± 0.04	0.34
icytb1021	188.82 ± 0.06	149.83 ± 0.05	0.27
icytb1051	188.83 ± 0.06	149.83 ± 0.05	0.25
icytb1081	188.83 ± 0.06	149.84 ± 0.05	0.22
icytb0031	171.32 ± 0.03	173.78 ± 0.03	10.88 ^a
icytb0061	170.82 ± 0.04	173.10 ± 0.03	0.53
icytb0091	170.86 ± 0.04	173.13 ± 0.03	0.36
icytb1031	188.78 ± 0.04	150.02 ± 0.04	0.69
icytb1061	188.79 ± 0.04	149.97 ± 0.04	0.32
icytb1091	188.84 ± 0.04	149.99 ± 0.04	0.32

^aImage removed from analysis due to poor data quality.

Table C5. Fit parameters for the WFC3 2018 epoch.

Image	x_0 (px)	y_0 (px)	χ^2_ν
icytb2011	154.74 ± 0.06	78.72 ± 0.05	0.14
icytb2041	154.76 ± 0.06	78.68 ± 0.05	0.18
icytb2071	154.73 ± 0.06	78.72 ± 0.05	0.32
icytb20a1	154.64 ± 0.06	78.64 ± 0.05	0.50
icytb3011	133.19 ± 0.06	75.93 ± 0.04	0.42
icytb3041	133.17 ± 0.06	75.94 ± 0.04	0.31
icytb3071	133.17 ± 0.06	75.92 ± 0.05	0.42
icytb30a1	133.17 ± 0.05	75.84 ± 0.04	0.45
icytb4011	154.37 ± 0.06	78.30 ± 0.05	0.70
icytb4041	154.51 ± 0.06	78.06 ± 0.05	3.01
icytb4071	154.33 ± 0.06	78.27 ± 0.05	0.45
icytb40a1	154.38 ± 0.06	78.10 ± 0.05	1.13
icytb5011	132.91 ± 0.06	76.15 ± 0.04	0.21
icytb5041	132.92 ± 0.05	76.16 ± 0.04	0.26
icytb5071	132.94 ± 0.06	76.12 ± 0.04	0.29
icytb50a1	132.91 ± 0.06	76.08 ± 0.04	0.52
icytb6011	154.69 ± 0.06	78.74 ± 0.05	0.35
icytb6041	154.73 ± 0.06	78.69 ± 0.05	0.24
icytb6071	154.73 ± 0.06	78.66 ± 0.05	0.29
icytb60a1	154.73 ± 0.06	78.66 ± 0.05	0.29
icytb7011	132.91 ± 0.06	76.27 ± 0.04	0.28
icytb7041	132.93 ± 0.05	76.24 ± 0.04	0.24
icytb7071	132.94 ± 0.05	76.21 ± 0.04	0.29
icytb70a1	132.90 ± 0.05	76.20 ± 0.04	0.17
icytb8011	154.63 ± 0.06	78.56 ± 0.05	0.53
icytb8041	154.62 ± 0.06	78.54 ± 0.05	0.68
icytb8071	154.59 ± 0.06	78.55 ± 0.05	0.37
icytb80a1	154.55 ± 0.06	78.53 ± 0.05	0.70
icytb2021	154.72 ± 0.05	78.66 ± 0.04	0.25
icytb2051	154.75 ± 0.05	78.64 ± 0.04	0.13
icytb2081	154.74 ± 0.05	78.57 ± 0.04	0.42
icytb3021	133.23 ± 0.05	75.86 ± 0.04	0.42
icytb3051	133.21 ± 0.05	75.85 ± 0.04	0.41
icytb3081	133.21 ± 0.05	75.83 ± 0.04	0.42
icytb4021	154.40 ± 0.05	78.17 ± 0.04	1.04
icytb4051	154.36 ± 0.05	78.16 ± 0.04	0.75
icytb4081	154.33 ± 0.05	78.18 ± 0.04	0.60
icytb5021	132.92 ± 0.05	76.06 ± 0.04	0.31

Table C5 (continued)

Image	x_0 (px)	y_0 (px)	χ^2_ν
icytb5051	132.93 ± 0.05	76.06 ± 0.04	0.39
icytb5081	132.88 ± 0.05	76.03 ± 0.04	0.35
icytb6021	154.75 ± 0.05	78.63 ± 0.04	0.28
icytb6051	155.14 ± 0.05	78.02 ± 0.04	3.92
icytb6081	154.72 ± 0.05	78.60 ± 0.04	0.27
icytb7021	132.96 ± 0.05	76.18 ± 0.04	0.27
icytb7051	132.91 ± 0.05	76.19 ± 0.04	0.33
icytb7081	132.95 ± 0.05	76.16 ± 0.04	0.23
icytb8021	154.93 ± 0.05	78.58 ± 0.04	1.00
icytb8051	154.64 ± 0.05	78.45 ± 0.04	0.70
icytb8081	154.61 ± 0.05	78.43 ± 0.04	0.36
icytb2031	154.70 ± 0.04	78.74 ± 0.04	0.27
icytb2061	154.68 ± 0.04	78.55 ± 0.03	5.02
icytb2091	154.64 ± 0.04	78.69 ± 0.03	0.78
icytb3031	133.16 ± 0.04	76.03 ± 0.03	0.48
icytb3061	133.14 ± 0.04	76.00 ± 0.03	0.67
icytb3091	133.16 ± 0.04	75.90 ± 0.03	0.68
icytb4031	154.31 ± 0.04	78.22 ± 0.03	2.84
icytb4061	154.29 ± 0.04	78.40 ± 0.03	1.22
icytb4091	155.80 ± 0.04	78.21 ± 0.04	8.01 ^a
icytb5031	132.93 ± 0.04	76.20 ± 0.03	0.16
icytb5061	132.92 ± 0.04	76.18 ± 0.03	0.32
icytb5091	132.88 ± 0.04	76.16 ± 0.03	0.52
icytb6031	155.26 ± 0.04	79.02 ± 0.03	3.63 ^a
icytb6061	154.72 ± 0.04	78.72 ± 0.03	0.30
icytb6091	154.75 ± 0.04	78.69 ± 0.03	10.82 ^a
icytb7031	132.92 ± 0.04	76.31 ± 0.03	0.52
icytb7061	132.89 ± 0.04	76.34 ± 0.03	0.25
icytb7091	132.84 ± 0.04	76.31 ± 0.03	0.48
icytb8031	154.62 ± 0.04	78.59 ± 0.03	0.71
icytb8061	154.60 ± 0.04	78.57 ± 0.03	0.48
icytb8091	154.53 ± 0.04	78.56 ± 0.03	1.07

^aImage removed from analysis due to poor data quality.**Table C5** continued